A Thesis

On

TOOL PATH GENERATION AND FINITE ELEMENT ANALYSIS OF SINGLE POINT INCREMENTAL SHEET FORMING FOR COMPONENT GEOMETRIC ACCURACY

Submitted in partial fulfillment of the requirement for the award of

Degree of

Master of Engineering

IN

CAD/CAM & Robotics

Submitted By

GHANSHAM GOYAL

Roll No. 801081010

Under the Guidance of

ANIRBAN BHATTACHARYA

Assistant Professor

Department of Mechanical Engineering

Thapar University, Patiala

DEPARTMENT OF MECHANICAL ENGINEERING

THAPAR UNIVERSITY

PATIALA-147004, INDIA

June-2012

DECLARATION

I hereby declare that the thesis entitled **"TOOL PATH GENERATION AND FINITE ELEMENT ANALYSIS OF SINGLE POINT INCREMENTAL SHEET FORMING FOR COMPONENT GEOMETRIC ACCURACY"** is an authentic record of my study carried out as requirement for the award of the degree of **Master of Engineering (CAD/CAM & Robotics)** at **Thapar University, Patiala** under the guidance of **ANIRBAN BHATTACHARYA,** Assistant Professor, Department of Mechanical Engineering, Thapar University, Patiala during July 2011 to June 2012. The matter embodied in this report has not been submitted in part or full to any other university or institute for the award of any other degree.

ghansham goyal

(Ghansham Goyal)

Reg. No. 801081010

This is to certify that above declaration made by the student concerned is correct to the best of my knowledge & belief.

Anirban Bhattacharya 15/07/2012

(Mr. ANIRBAN BHATTACHARYA)
Assistant professor,
Department of Mechanical Engineering,
Thapar University, Patiala

Countersigned by:

(Dr. AJAY BATISH)
Professor and Head,
Department of Mechanical Engineering,
Thapar University,
Patiala-147004

(Prof. S.K.MOHAPATRA)
Dean, Academic Affairs,
Thapar University,
Patiala-147004

ACKNOWLEDGEMENT

I would like to express a deep sense of gratitude and thank profusely to my guide **Mr. Anirban Bhattacharya** for his sincere & invaluable guidance, suggestions and attitude, which inspired me to submit thesis in the present form. His dynamism and diligent enthusiasm have been highly instrumental in keeping my spirits high. His flawless and forthright suggestions blended with an innate intelligent application have crowned my task with success.

I am also thankful to **Dr. AJAY BATISH,** Professor and Head, Department of Mechanical Engineering for his encouragement and inspiration for execution of the thesis work.

I am also thankful to the Civil Engineering Department of Thapar University for the help regarding the finite element simulation used for the present study.

Dated: 09/07/2012

ghansham goyal

GHANSHAM GOYAL

Registration No.: 801081010

ABSTRACT

Single point incremental forming is a flexible process for the production of low volume customized sheet metal parts. A final component is obtained by the localized deformation induced by the forming tool. Toolpaths for different axisymmetric shapes have been generated using MATLAB. It is well known that geometrical accuracy is one major problem in single point incremental forming process due to the bending of the sheet. Finite element analyses have been used to study the geometric accuracies and other features in the present work. The output of simulation is given in terms of final geometric profile, thickness distribution to the component, stress, strain and the tool reaction forces. The geometrical discrepancies are determined by comparing the desired geometry with obtained geometry after finite element analysis. Use of top fillet at the major base of component and height compensation to eliminate over travel has been used to quantify the improvements in accuracy.

The single pass deformation strategy shows inhomogeneous thickness distribution in the final deformed component due to left out undeformed portion at the central region of the formed component. A two-step deformation strategy (first outer-to-inner followed by inner-to-outer) has been used to achieve a more uniform distribution of thickness in single point incremental forming.

The strain history (strain path and strain increment) is analyzed in single pass deformation for three different geometry shapes (pyramid, cone, other axisymmetric shape) and two steps deformation cone. The three components of force are studied throughout the forming process in the single pass and two pass deformation strategy. It was focused on the influence of four process parameters (draw angle, incremental step size, tool diameter and blank thickness) on the forming forces.

LIST OF FIGURES

LIST OF TABLES

ABBREVIATIONS

ANOVA	Analysis of variance
CAD	Computer Aided design
CNC	Computer numerical control
CPU	Central processing time
$h_{obtained}$	Height obtained after radius compensation
h_{reqd}	Required height of component
a	Distance between required height and component height obtained without *HC*
ac	Angle for top fillet curvature w.r.t x-axis
DD	Down-down
DDDU	Down-down-down-up
DF	Downward force
DU	Down-up
DUDD	Down-up-down-down
dr	Total decrement in x-direction
dz	Incremental Step size in z-direction
dxx	x-coordinate on last contour of component
dxtc	Step decrement in x-direction for *OAS* when viewed from top
dyfc	Step increment in y-direction for *OAS* when viewed from top
FEA	Finite element analysis
FEM	Finite element method
H	x-coordinate of centre of first curvature of top fillet parabola
HC	Height Compensation
H_b	Horizontal bending
h	Component height
h_f	x-coordinate of centre of second curvature of *OAS*
h_o	Height of intermediate profile
ht	x-coordinate of Centre point of top fillet curvature

h_{rc}	Component height used to apply radius compensation
hc1	x-coordinate of centre of edge curvature of pyramid
I-to-O	Inner-to-outer
K	y-coordinate of centre of first curvature of top fillet parabola
k_f	y-coordinate of centre of second curvature of *OAS*
kt	y-coordinate of centre point of top fillet curvature
kc1	y-coordinate of centre of edge curvature of pyramid
MSPIF	multi-pass single point incremental forming
m	Slope of top fillet curvature
n	Total no. of points in each contour
nse	Number of points from start to maximum opening when viewed from top
nsf	Number of points in between maximum opening of *OAS* when viewed from top
OAS	Other axisymmetric shape
OD	Opening Diameter of component
O-to-I	Outer-to-inner
R	Component opening radius
RC	Radius compensation
RF	Radial force
RP	Tool reference point
R_b	Radius of first curvature of top fillet parabola
R_c	Top fillet radius
R_{2c}	Radius of second curvature of flower
Rn	Offset radius of *OAS* when viewed from top
R_o	Opening radius of intermediate profile
r	Tool Radius
r_c	Edge radius of pyramid
SBS	Sheet blank size
SPIF	Single Point incremental forming

TD	Tool diameter
TF	Tangential force
$TPIF$	Two Point incremental forming
TRF	Tool reaction force
T_{AB}	Sheet thickness of part AB
T_{BC}	Sheet thickness of part BC
t_o	Blank initial thickness
$u(i,j)$	j number of x-coordinate for i number of contours with helix
V_b	Vertical bending
$v(i,j)$	j number of y-coordinate for i number of contours with helix
$w(i,j)$	j number of z-coordinate for i number of contours with helix
X	Intermediate x-point on first curvature of top fillet parabola
xc	Number of intermediate x-coordinate of top fillet curvature without RC
xce	x-coordinate of End point of top fillet curvature
xcs	x-coordinate of Start point of top fillet curvature
x_p	x-coordinate along parabola profile
$x1$	x-coordinates on cone profile without radius compensation
$x11$	x-coordinates on cone profile after radius compensation
$x11c$	x-coordinate on top fillet curvature after radius compensation
$xc1$	Start x-coordinate of edge curvature of pyramid
$xc2$	End x-coordinate of edge curvature of pyramid
$x(i,j)$	j number of x-coordinate for i number of contours without helix
Y	Intermediate y-point on first curvature of top fillet parabola
yc	Number of intermediate y-coordinate of top fillet curvature without RC
yce	y-coordinate of End point of top fillet curvature
ycs	y-coordinate of Start point of top fillet curvature
y_p	y-coordinate along parabola profile
$y1$	y-coordinates on cone profile without radius compensation
$y11$	y-coordinates on cone profile after radius compensation

$y11c$	y-coordinate on top fillet curvature after radius compensation
$yc1$	Start y-coordinate of edge curvature of pyramid
$yc2$	End y-coordinate of edge curvature of pyramid
$y(i, j)$	j number of y-coordinate for i number of contours without helix
$z(i, j)$	j number of z-coordinate for i number of contours without helix
Δx	Radius compensation in x-direction
Δxc	Radius compensation in x-direction for top fillet curvature
Δy	Radius compensation in y-direction
Δyc	Radius compensation in y-direction for top fillet curvature
α	Draw angle
α_o	Draw angle of intermediate profile
$\alpha_{\max}$	Maximum draw angle
∂	Manufactured part having maximum deviation from reference drawing
θ	Angle between any two points on a contour
σ_{eq}	Equivalent stress
ε_{eq}	Equivalent Plastic strain
a1 to *a8*	Centre and corner points of pyramid in x-direction
a_p, b_p, c_p	Parabola constants
b1 to *b8*	Centre and corner points of pyramid in y-direction
N1 to *N6*	Node numbers from 1 to 6
$xcf1$ to $xcf4$	x-coordinates of offset centre point of *OAS* when viewed from top
$xfc1, yfc1, zfc1$	x, y, z-coordinates of OAS from start to maximum opening curvature when viewed from top
$xsc1, ysc1, zsc1$	x, y, z-coordinates of OAS for maximum opening curvature when viewed from top
$xtc1, ytc1, ztc1$	x, y, z-coordinates of OAS from maximum opening curvature to x=0, when viewed from top
$ycf1$ to $ycf4$	y-coordinates of offset centre point of *OAS* when viewed from top

INDEX

CHAPTER 1

INTRODUCTION TO INCREMENTAL FORMING

1.1 PREAMBLE OF INCREMENTAL FORMING

Incremental forming processes have an origin in conventional spinning and shear spinning. These conventional processes are constrained as far as achievable part geometry is concerned and it required dedicated tooling and dies.

The new forming method is invented as Incremental forming used to capable of producing any type of surfaces including complex shaped surfaces without the need of any dies. The main achievement of this process is dieless forming process.

Incremental forming sheet metal methods are now at a stage where it is possible to make either custom manufactured parts or to manufacture small batch production quantities with very short turn around times from design to manufacture [1].

1.2 CLASSIFICATION OF INCREMENTAL FORMING PROCESSES

Incremental sheet forming is defined as a family of sheet forming processes where the deformation is highly localized, without drawing in of material from a surrounding area and using a fully clamped blank, where the final shape is determined by the *xyz* movement of some tool part without the need for a die.

Incremental sheet metal forming processes can be broadly classified into two categories:

1. Symmetric incremental sheet metal forming processes
2. Asymmetric incremental sheet metal forming processes

1.2.1 Symmetric incremental sheet metal forming processes

Symmetric incremental sheet metal forming processes includes:

1.2.1.1 Spinning

In spinning, a work piece is clamped onto a rotating mandrel while the spinning tools approach the work piece and deform it into the required shape. The tool may make several passes to complete the required shape of the sheet.

1.2.1.2 Shear Spinning

The process of shear spinning is almost same as the conventional spinning except, in case of conventional spinning, the roller tool pushes against the blank until it conforms to the contour of the mandrel. The resulting spun part will have a diameter smaller than the blank, but will maintain a constant thickness. But in case of shear spinning, the roller not only bends the blank

against the mandrel, it also applies a downward force while it moves, stretching the material over the mandrel. By doing so, the outer diameter of the spun part will remain equal to the original blank diameter, but the thickness of the part walls will be thinner as shown in Figure 1.1.

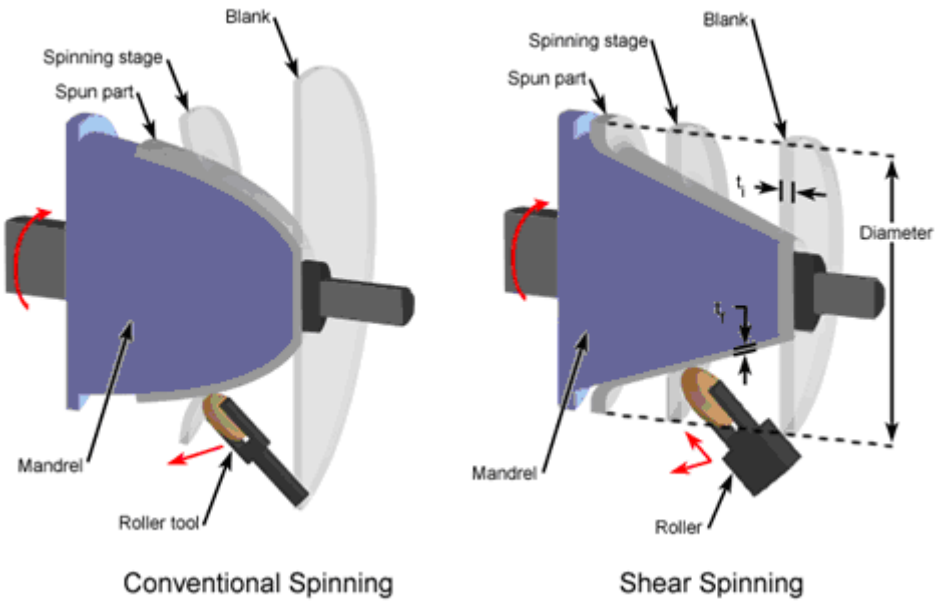

Figure 1.1: Spinning and Shear spinning [2]

1.2.1.3 Symmetric Incremental Forming

The Symmetric incremental forming process is a shear spinning without a rotating mandrel with a single point forming tool. The rotating mandrel showed dies in spinning are unnecessary in symmetric incremental forming.

In incremental sheet forming, the blank edge is clamped and does not move inwards, the sheet is formed by having a tool moves under control in 3 dimensional space, mostly by a succession of 'planar' contours or a single 'spiral' contour.

1.2.2 Asymmetric incremental sheet metal forming processes

Asymmetric incremental sheet metal forming process is the further extension of Symmetric incremental forming process, where asymmetric sheet metal shapes can be produced. While remaining characteristics like dieless process, requirement of solid small sized forming tool etc is same as in symmetric incremental forming process.

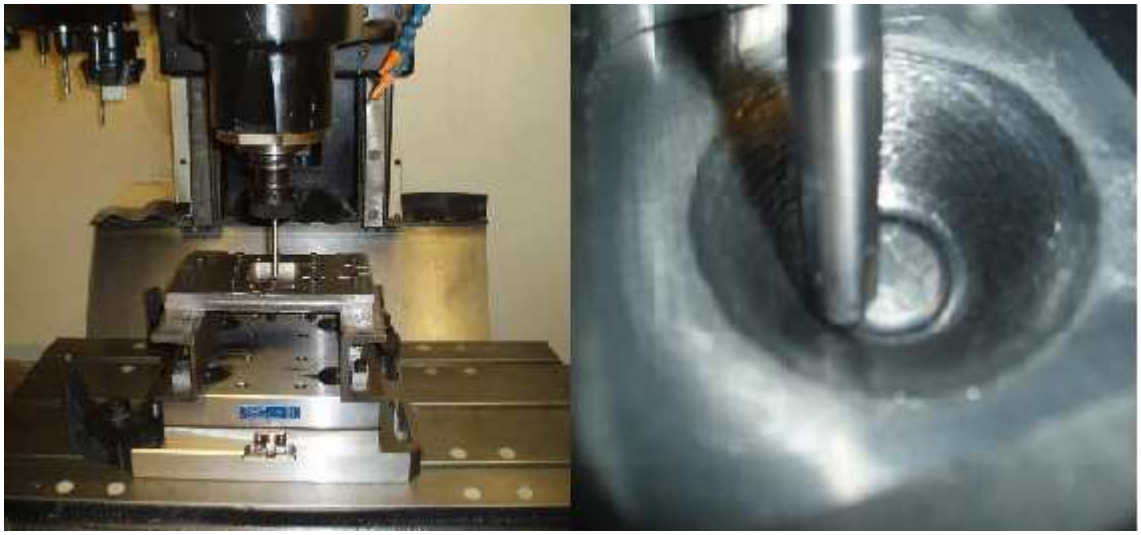

Figure 1.2: Incremental Forming [3]

Table 1: Comparison between Spinning and Incremental forming

	Spinning	Shear spinning	Incremental Forming
Blank edge	moves inwards	remains constant	Clamped
Wall thickness	remains constant	reduces, has to follow the *sine law*	reduces, determined by the process
Shape basically determined by	movement of roller, or by mandrel	Mandrel	movement of forming tool
Die/mandrel required	yes	Yes	No
Asymmetric shapes possible	No	No	Yes

1.3 TYPES OF ASYMMETRIC INCREMENTAL SHEET FORMING

1. Single Point incremental forming (*SPIF*)
2. Two Point incremental forming (*TPIF*)

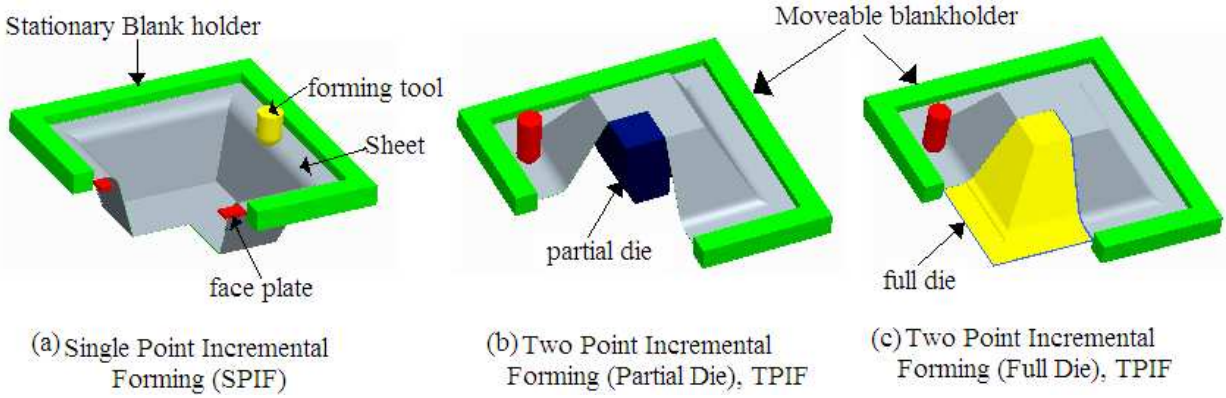

Figure 1.3: Single Point Incremental Forming and Two Point Incremental Forming

Table 2: Comparison between Single Point Incremental Forming (*SPIF*) and Two Point Incremental Forming (*TPIF*)

	Single Point Incremental Forming (*SPIF*)	Two Point Incremental Forming (*TPIF*)
Definition	This process has only one point where sheet metal is pressed or forced.	This process has two points where sheet metal is pressed simultaneously.
Die	No need of partial and full die, so back surface of sheet being deformed is a free unsupported surface.	Partial or full die used as a static support that creates upward counter force on the sheet.
Motion of Blankholder	There is no motion of blankholder i.e. blankholder remains stationary.	Blankholder moves vertically downward with toolpath increments in the z-axis direction.
Flexibility	This process has high degree of flexibility; because changes in part design sizes can be easily and quickly accommodated.	This process has less degree of flexibility, because changes in part design sizes are difficult due to the requirement of dies.
Number of products	This process is limited to small size batch production.	This process can be used for large lot because die has to be made for particular type of production.
Manufacturing Operation	Manufacturing starts from the outer diameter towards the centre of desired geometry.	Manufacturing starts from the centre of desired geometry.

1.4 MERITS OF INCREMENTAL FORMING

1. Parts can be formed directly from CAD data with minimum of specialized tooling.
2. Changes in part design sizes can be easily and quickly accommodated gives a high degree of flexibility.
3. The process does not require any component specific tooling, die and it is a dieless process.
4. A simple CNC control machine can be used for this process.
5. This process is useful for small scale customized products.
6. This process increases formability due to localized thinning and incremental nature of the process.
7. Low cost mainly due to low tooling cost.
8. Increase turnaround time for low production run because need to manufacture a die is eliminated.
9. The operation is quiet and relatively noise free.

1.5 DEMERITS OF INCREMENTAL FORMING

1. Forming time is more as compared to other sheet metal processes such as deep drawing.
2. Time consumption is same either to manufacture first component or n^{th} component of lot.
3. There is a limitation on the maximum draw angle that can be formed in one pass, hence multi pass methodologies are preferred for the forming of large angles.
4.

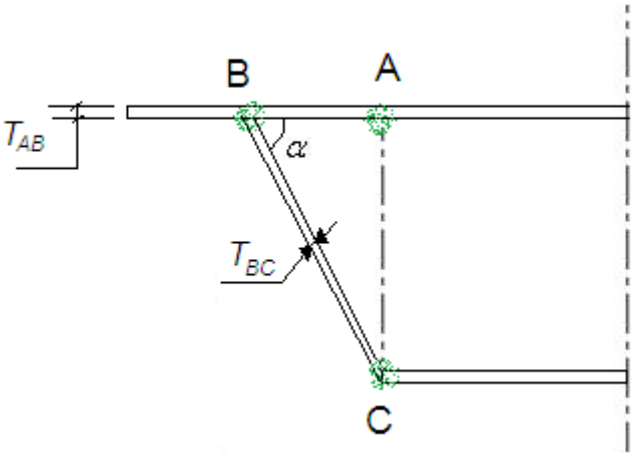

Figure 1.4: Illustration of *Sine Law*

Sine Law to determine thickness:

$$T_{BC} = T_{AB} \times Sin(90 - \alpha)$$

1.6 APPLICATIONS OF INCREMENTAL SHEET FORMING

The major advantage of asymmetric incremental forming is that it can be used to make asymmetric parts, quickly and economically, without using expensive dies. Incremental forming has the following application areas:

1. Automotive industry: Vehicle headlight, motorbike seat, motorbike tank etc
2. Solar oven cavity
3. Medical Applications like manufacture of ankle support, dental crown etc
4. Aerospace industry :different housings of plane etc

Motor bike seat [1]

Motor bike tank [1]

1/8 model of Bullet train [17]

Solar oven cavity [1]

Figure 1.5: Applications of Incremental Forming

1.7 BASIC ELEMENTS OF ASYMMETRIC INCREMENTAL SHEET FORMING

Asymmetric incremental sheet forming has four basic elements are given as:

1. Single point forming tool
2. Blankholder and platform
3. Sheet metal blank
4. Forming machinery

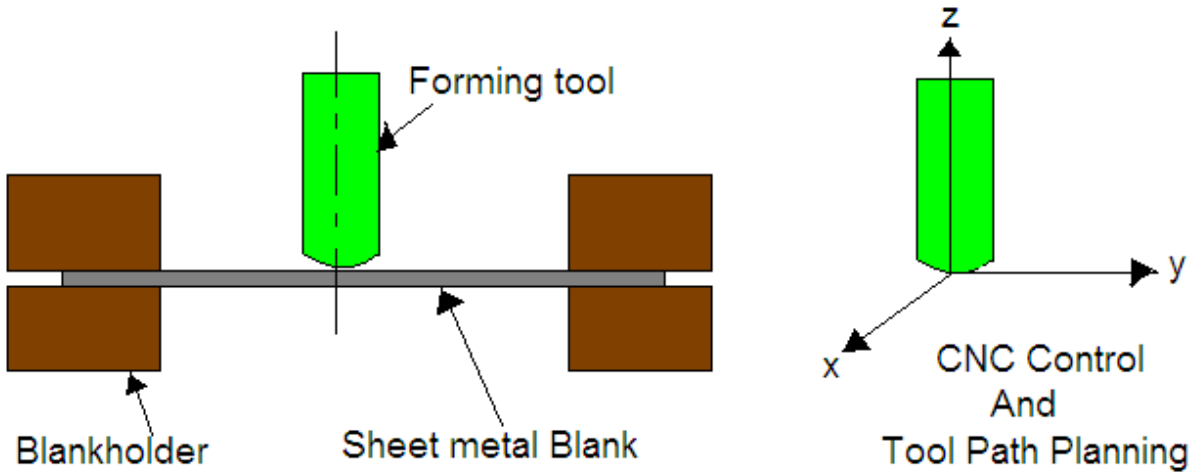

Figure 1.6: Basic elements of Asymmetric incremental sheet forming

1.7.1 Single Point Forming tool

The main element of incremental sheet forming is the single point forming tool. Solid hemispherical tools are usually used for plastically incremental deformation of sheet metal. This assures a continuous point contact between sheet and forming tool.

The tool diameters are varied from 6 mm to 100 mm depending upon small and large manufacturing parts. The effects of tool diameter selection:

Table: 3 Effect of variation in tool diameter on various parameters in incremental forming

Parameter	Effect
Surface roughness	Decrease with increase in tool diameter.
Manufacturing time	Decreases with increase in tool diameter.
Power consumption	Increases with increase in tool diameter, because for large angle of contact involved.

The tool ball head are usually made of tool steel, but sometimes plastic tools are used to avoid chemical reaction and to increase the surface quality.

Sometimes steel tools are coated with cemented carbide to reduce the friction and to reduce wear, lubrication is used.

1.7.2 Blank holder and platform

Blankholder are used to clamp the sheet. Blankholder may be rigid or may be movable depending upon the single point and two point incremental forming.

For single point incremental forming, blankholder is rigid apparatus consisting of metal plate on four posts to which sheet can be clamped.

For two point incremental forming, blankholder moves vertically along z-axis with either partial or full dies to enable asymmetric two point incremental forming.

1.7.3 Sheet metal blank

It is a blank sheet that is mounted or clamped into the blankholder and undergoes a deformation due to tool movement as per stored coordinates in CNC machine.

1.7.4 Forming machinery

Three axis CNC machines are preferable to perform incremental forming. The selection of CNC machine depends upon its high or less speeds, small or large working area, stiffness, maximum feed rate, maximum load and its cost. High speeds, large working volumes and sufficient stiffness CNC machines are favorable for incremental forming.

The following types of machines are available for incremental forming [1].

1. CNC milling machines
    a. Gantry milling machine
    b. Gateway milling machine
    c. Bedplate type milling machine
    d. Console milling machine
2. Purpose built machines
3. Robots

1.8 TOOLPATH GENERATION FOR INCREMENTAL SHEET FORMING

Effective toolpath generation is very important for incremental forming. Normally two types of toolpath trajectory used in incremental sheet forming. These are:

1. Contour toolpath
2. Spiral toolpath

1.8.1 Contour toolpath

Contour toolpath is defined by fixed step size increments (*dz*) between consecutive contours.

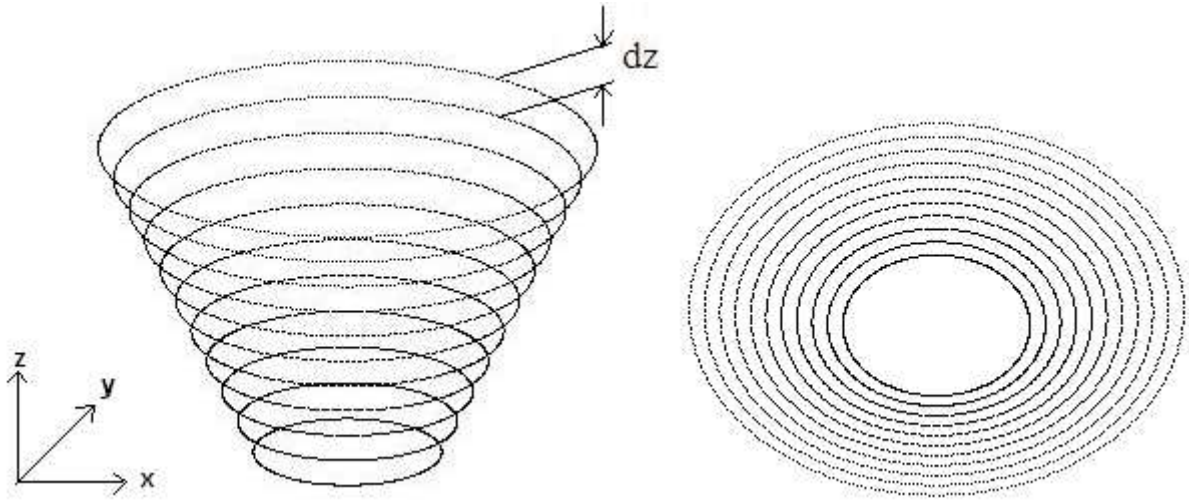

Figure 1.7: Contour toolpath used in incremental sheet forming

1.8.2 Spiral toolpath

Spiral toolpath is continuous with incremental drop of the tool distributed over the complete contour of the part.

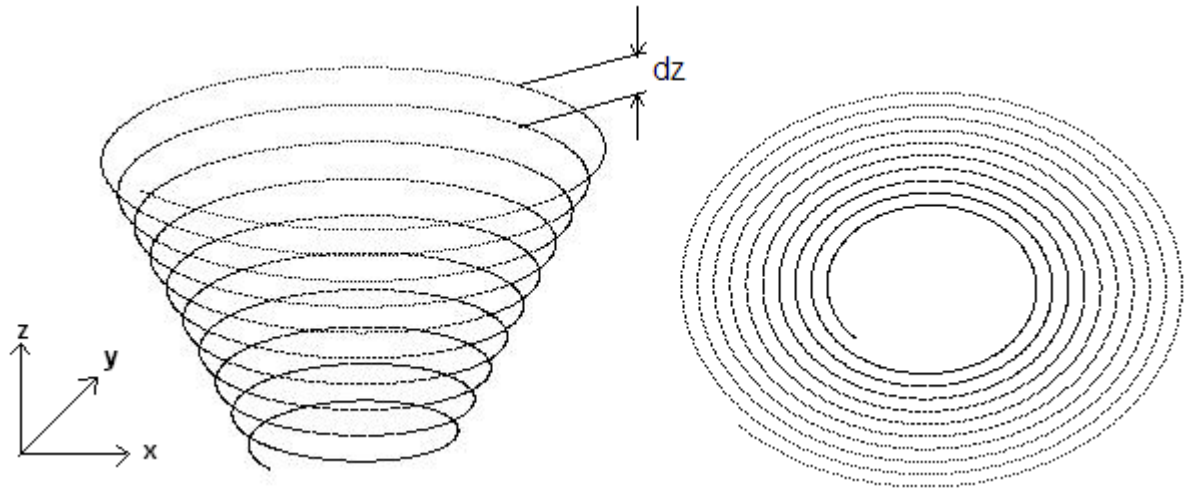

Figure 1.8: Spiral toolpath used in incremental sheet forming

Table: 4 Comparison between Contour toolpath and Spiral toolpath

Parameter	Contour toolpath	Spiral toolpath
Generation of marks	Leave marks at the transition point between discrete layers.	No marks occur at the step down.
Surface Roughness	More surface roughness as compared to Spiral toolpath.	Less surface roughness as compared to Contour toolpath.
Forces	Create peak forces.	Create less force.
Number of contours	Number or contours more than one, depending upon the incremental step size.	Only one contour.

1.9 SELECTION OF METHOD OF INCREMENTAL FORMING

There are two methods of incremental forming.

1. Single pass incremental forming
2. Multi pass incremental forming

Selection of method of incremental forming depends upon material process parameters. Material process parameters include its thickness and maximum draw angle (α_{max}) has been investigated experimentally for a particular material. (See Table: 5)

Table: 5 Materials with initial thickness and Maximum draw angle (α_{max}) [1]

Material	(α_{max})	Initial thickness (*mm*)
AA 1050-O	67.1	1.21
AA 6114-T4	60	1
Al 3003-O	78.1	2.1
Al 3003-O	72.1	1.3
Al 3003-O	71	1.21
Al 3003-O	67	0.93
Al 5754-O	78.1	2.1
Al 5182-O	78.1	2.1
AA 6111-T4P	53	0.93
Mild steel	65	1
HSS	65	1
Copper	65	1
Brass	40	1

For the selection of method of incremental forming, first check and compare the design draw angle (α) proposed in CAD drawing with standard maximum draw angle (α_{max}) determined experimentally corresponding to particular material, if design draw angle less than maximum draw angle of material, then go with single pass incremental forming otherwise go with multi pass incremental forming.

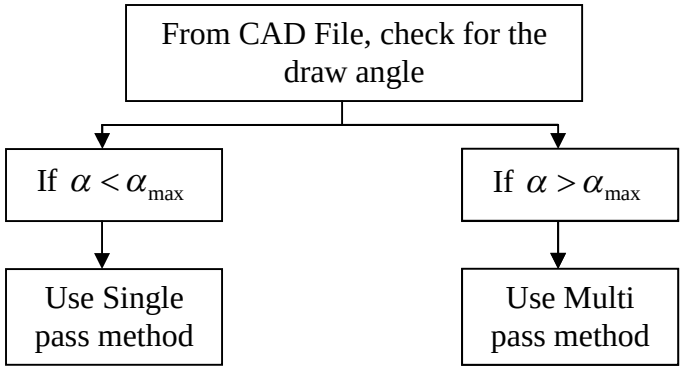

Flow Chart 1: Procedure followed for making a part

CHAPTER 2
LITERATURE REVIEW

2.1 INTRODUCTION

Incremental forming is a sheet metal process which has played consistently an important role in sheet Metal manufacturing industry from early times. Because of increasing need of manufacturing complex components with strict geometrical dimensions and tolerances, there are many advancements have been done so far in Incremental forming process to improve the quality of components being manufactured. Some of the Literature review is presented here.

2.2 LITERATURE REVIEW

Jeswiet et al. **[1]** describes the modifications in traditional forming methods such as conventional spinning and shear forming and introduce the use of new forming method is incremental forming (Single point incremental forming and two point incremental forming) in which deformation is localized. It was predicted to forming a asymmetric complicated shapes using CNC milling machine, without the use of any die. This paper also describe the effect of various design parameters like incremental step size, diameter of forming tool, maximum draw angle, speed of forming tool and sheet thickness on the final shape of the object. It was found that, with increase in spindle rotation speed, formability increases due to local heating of a sheet and it also increases with thicker sheets, smaller tool diameter and smaller incremental step size. Forces in incremental forming increases with increase in draw angle, increase in tool diameter and with increase in incremental step size. Surface quality of final object is increases with decrease in forming speed of tool, decrease in incremental step size, increase in tool diameter and increase in draw angle.

Ham and Jeswiet **[4]** have studied the dimensional accuracy of single point incremental forming by comparing the manufactured parts with the part drawings used to create the manufacturing tool paths. They analyzed the effect of forming parameters like material type, material thickness, forming tool size, incremental step size, and shape of part on the dimensional accuracy of parts manufactured using single point incremental forming. The cone and pyramid shape object having maximum deviation from the reference drawing is at the start of deformation and at the tip of the cone $(\partial > 1)$ and rest of the object having deviation $(0.25 \le \partial \le 1)$. The dome shaped object having maximum deviation is very less as compared to cone and pyramid and it is at start

and tip is $(\partial < 1)$ and rest of object is $(0.15 \leq \partial \leq 0.4)$.Finally it was found that all parts of mean error is less than one so SPIF parts to be drawing accurately because comparison shows most of the deviations between 0 and 1 *mm*.

Verbert et al. **[5]** predict that single step incremental forming process is not able to manufacture workpiece geometries whose required draw angle is greater than the maximum draw angle of sheet material. For this they have to suggest multi step approach for incremental forming. Maximum wall angle for commonly used material is a function of thickness of sheet and diameter of forming tool. They target for material redistribution by shifting material from lower strain zones to the higher strain zones in the part. Mainly it led to a shift of material from the bottom, which would remained unprocessed, to the side wall of the part. This allows producing vertical walls without leading to part failure.

Skjoedt et al. **[6]** present a four stage forming strategy for single point incremental forming of a circular cylindrical cup. They present four stage forming strategy with two different strategy i.e. Down-down-down-up (*DDDU*) and Down-up-down-down (*DUDD*). It is determined that distribution of strains is not only depending on the geometry of the tool path but also the direction i.e. upwards or downwards. It is noticed that, in Down-down (*DD*) strategy, not all of the geometry is formed during the second stage i.e. there leaves some residual cone in the centre. And in Down-up (*DU*) strategy, there is no residual cone after the second stage but material build in the front of the tool which changes the point contact to a line contact therefore process forces increase in the *XY* plane. Finally, *DDDU* strategy can be performed without fracture whereas *DUDD* strategy results in fracture in stage fourth at the transition zone between vertical and horizontal of the part. But finally both strategies increase the maximum draw angle up to 90 degree which has not been possible with single pass incremental forming.

Bhattacharya et al. **[7]** predict that steps formed on the base of deformed component during multi-pass single point incremental forming (*MSPIF*). There have been attempts made to improve the geometric control and accuracy of formed component during multi-pass single point incremental forming (*MSPIF*). There is proposed new toolpath strategy using a combination of In-to-Out and Out-to-In toolpath for each intermediate shape so that desired component base geometry can be achieved. By doing this, residual steps formed at the base centre of deformed component can be eliminated.

Bambach **[8]** investigate that *sine law* does not hold good to determine the sheet thickness, mainly in the region where sheet bending or necking occurs, in single point incremental forming. It also predicts that in the shear zone, thickness of deformed sheet is also less than the thickness estimated by *sine law* due to overspinning and strains are determined parallel to tool direction, which would reduce sheet thickness below the level predicted by *sine law*. They show that trajectories of points on the surface of sheet metal do not follow the straight projection. It was considered that Sheet metal is treated as an infinitely thin surface, whose deformation is followed from the undeformed initial state through a number of intermediate stages to the final geometry. It is also computed the membrane strains for any arbitrary shapes as a function of tool radius and step down of the forming tool.

Durante et al. **[9]** analyze the effect of tool rotation on an incremental forming process. The effect of tool rotation (i.e. speed and direction of tool rotation) has been explained in terms of forming forces, surface roughness and temperature. Temperature and surface roughness is measured using thermocouple and rugosimeter respectively. It is shown that friction coefficient is maximum when tool slides (i.e. tool rotation speed is zero) on workpiece and it decreases as tool rotation speed increases. Tool rotation direction does not have any significance variation on vertical component of force but horizontal component of force changes significantly with change in direction of rotation of tool. Temperature increases as the speed of tool rotation increases. Surface roughness depending on the tool is rotating or not and it is more with non rotating tools.

Silva et al. **[10]** investigate the formability limits of Single point incremental forming in terms of ductile damage mechanics and membrane analysis. Three basic modes of deformation are plane strain stretching at flat surfaces, plane strain stretching at rotationally symmetric surfaces and biaxial stretching at corners in single point incremental forming occurs. Analytical expressions have been derived for stresses and strains in circumferential direction, meridionial direction and thickness direction. It was found that circumferential straight and zigzag crack propagates due to the rotation of the tool. The model is built upon membrane analysis and ductile damage mechanics and observed that fracture is not preceded by localized necking and that the crack propagates under tensile meridional stresses acting under stretching modes of deformation.

The theoretical model like *sine law* does not provide the satisfactory results of sheet thickness after deformation expressed by Ambrogio et al. **[11]**. The numerical simulation is a suitable tool to predict the sheet thickness. With increase in geometrical complexity of the process, very high number of elements is considered for accuracy, thus computational time and cost will increase. This paper refers to use implicit approach based on Lagrangian formulation rather than explicit approach to get better and more accurate results. The main limitation of numerical simulation is CPU processing time.

Ambrogio et al. **[12]** has aimed to evaluate the geometrical errors that occur when single point incremental forming process has been run. For the measurement of geometrical errors, they compare the analytical results with experimental results and *FEA* results with experimental results. During analytical and experimental results comparison, there was found very high discrepancy between actual geometry and the desired one at the base and at the intersection of oblique walls due to the absence of rigid support. There are some geometrical errors along the walls due to elastic spring back. A very good overlapping was observed between the *FEA* results and the experimental results, so it confirms that the numerical simulation is a suitable design tool for the single point incremental forming processes. To reduce geometrical errors at transition zone between horizontal and vertical wall, two different geometric paths were introduced. In the first path, tool moves tangentially to the desired surface and in the second path, tool trajectory is modified by introducing an increased initial slope which is connected to the first one.

The double pass single point incremental forming technique has been proposed by Young and Jeswiet **[13]** as a way to modify the final thickness profile of steep geometry. Double-pass single point incremental forming can allow the production of parts that thin to failure with single-pass techniques. It has been shown that single-pass SPIF does not follows the *sine law* for the prediction of sheet thickness due to the overspinning and bending occurs. It was also predicted that by using double pass single point incremental forming, there is increase in thickness will only occur in the area of part that is affected by the bending in comparison of the single pass incremental forming.

Taleb et al. **[14]** analyzed the three problems exist in asymmetrical incremental forming process are material thickness, geometric accuracy and process duration. A new hybrid process is proposed which is the combination of asymmetrical incremental forming process and stretch

forming process. Stretch forming is used to create a pre-form in the first forming step by stretch the sheet using a particular die and stretch forming machine set up and final geometry is formed using asymmetrical incremental forming. The production time and simulation time is reduced in hybrid process in comparison to the asymmetrical incremental forming process. There is also more uniform thickness distribution is obtained due to stretch forming in hybrid process. This process does not hold good for any arbitrary shape i.e. this process is dedicated for particular component geometry due to use of dies in stretch forming.

Cerro et al. **[15]** predict that incremental sheet forming is a slow process suitable for low series production in comparison with the traditional stamping and drawing process. The process needs a further optimization to the reliability required for the industrial application. This paper shows results obtained with simple *FEA* model and experimental tests give accurate prediction of some characteristics of the formed parts. The effect of process parameters like forming speed, forming force and forming strategy in the characteristics of the parts i.e. thickness, geometrical accuracy, surface roughness etc has been studied, showing the possibility to optimize the quality of the formed parts by an accurate control of the process parameters.

Micari et al. **[16]** has investigated some relevant drawbacks of single point incremental forming process as concerns the level of shape and dimensional accuracy. Sheet is simply clamped in a frame thus it is free to bend during the process and when the punch action is relaxed, the blank “lifts up” and the final depth of the part is lower than the design value. It determines undesired rigid movements and elastic spring back which affects the final accuracy. Several process parameters like tool diameter, tool rotation speed, material properties, incremental step size and design parameters like blank thickness, geometry and steepness of the component surface also affects the accuracy of the component. There are some suitable strategies are suggested like use of flexible support, use of counter pressure, multipoint incremental forming, backdrawing incremental forming and use of optimised trajectories to improve the dimensional accuracy of final component.

The mechanics behind the multi-step forming approach to contribute to a better understanding of the material relocation mechanism underlying the enlarged process window determined by the Duflou et al. **[18]**. It was suggested to choose intermediate shapes in well-defined order to eliminate folding over between successive steps. If the angle increment between two consecutive steps is too large, the horizontal distance between two steps at a certain depth will become too

big compared to the tool diameter, and folding over, resulting in failure, will occur. It was also observed that the larger the horizontal distance between two consecutive step sections closer to the bottom of part results in more rotational motion transforms into the downward translation. The requirement of intermediate steps depends on the desired height of object and diameter of tool used. There are maximum strains in both radial and tangential directions occur at the lower wall edge in the final stage of the vertical wall forming. The bottom of the work piece in multipath strategy cannot predicted accurately as compared with the bottom of a single-step cone is predicted.

Ambrogio et al. **[19]** has studied the problem of spring back effect and reduced material stiffness during single point incremental forming process which results in undesired distorted profiles of desired component. A new strategy is pursued by integrating an on-line measuring system, composed of a digital inspector and a computer numerically controlled (CNC) open program , is based on the modification of the tool path at a given step based on the distance from the present coordinates relative to the previously deformed step. The steps of this methodology are retraction of the punch then reading of the reference points and calculation of modified geometry and finally restarting of the process.

Ambrogio et al. **[20]** has developed the methodology for detecting the approach of failure in incremental forming and this approach is based on the analysis of the trend of the forming force in order to assess whether the process can be run safely. This work is based on forming force measurement and analysis. The vertical component of the forming force between the tool and the sheet was measured utilizing a piezoelectric dynamometer placed below the sheet clamping frame. The instantaneous measured value of force depends on the sheet thickness, wall inclination angle, tool diameter and incremental step size. An effective process parameters correction is set up by measuring forces and able to move towards safer process conditions.

The largest part of the material is unconstrained during the process and the final geometry may be very different with respect to the desired CAD model, Therefore, Ambrogio et al. **[21]** has investigated the influence of the process parameters on component geometric accuracy through a reliable statistical analysis. The ANOVA analysis allowed identifying a quadratic model as the most suitable solution to describe the experimental results. They describe the geometrical error measured at the corner of the component is due to the sheet thickness and the total part depth,

and the geometrical discrepancy at the Centre of component (pillow effect) due to the tool diameter and product height.

Filice et al. **[22]** has performed several tests for the achievement of different straining conditions in the material and consequently to determine the forming limit diagrams for forming operations. These tests were designed in order to cover a set of straining conditions ranging from uni-axial stretching to bi-axial stretching. It was obtained pure uni-axial stretching condition occur along the straight edge of the shell and this type of stretching condition depends on the ratio of punch depth for each loop to the horizontal displacement imposed to the punch between two subsequent loops. The pure bi-axial stretching condition occurs at the centre or corner of the component. Finally it was observed that forming limit curve has a linear shape with a negative slope in the positive minor strain side of the forming limit diagram.

Filice **[23]** has studied an analytical model to predict the thickness distribution in the produced part is proposed. The given analytical expression for thickness determination is valid only for constant wall angle inclination. For simplicity any contribution of the elastic behavior is neglected. The back-drawing incremental forming process was analyzed in this study with the aim of manufacturing cylindrical parts. In particular, the model is applied taking into account the most critical zone and determining a correlation between the desired geometry and a very common material formability index.

Henrard et al. **[24]** has investigated the influence of some crucial computational parameters on the simulation. The influence of several parameters such as mesh size and friction coefficient will be discussed by using the *FEA* code like Abaqus or Lagamine. The output is given in terms of final geometry which depends on the spring back, strain history and distribution during the deformation, and reaction forces. The influence of the mesh density is small as far as the shape is concerned, but with greater stiffness in the mesh, which prevents the plate from bending enough under the tool. The force depends to a great extent on the mesh and on the boundary conditions. In order to get accurate and stable results for the force, fine mesh should be used, which is not feasible in a reasonable computation time. The total force is slightly increased with larger friction coefficient.

The effect of process parameters like tool type, tool size, and feed rate, friction at the interface between tool and sheet, and plane-anisotropy of sheet on the formability was investigated by experiments and *FEA* analyses by Kim and Park **[25]**. The formability of sheet metal in incremental forming is different from that in conventional forming. It was found that the formability is improved when a ball tool of a particular size with a small feed rate and a little friction is used in comparison of hemispherical head tool. Due to the plane-anisotropy, the formability differs according to the direction of the tool movement.

Hirt et al. **[26]** has discussed the limitation on the maximum achievable wall angle that restricts the potential scope of shapes and applications and inhomogeneous thickness distributions in the final part and second limitation on the occurrence of geometric deviations due to the elastic parts of the deformation entail a local spring back of the sheet when the tool moves on. To overcome these limitations it was suggested to use multistage forming strategy to produce steep walls and correction algorithm to enhance the geometric accuracy. It was determined that higher forming limits can be achieved with smaller forming heads and larger values for the vertical pitch.

Fundamental investigations of the incremental sheet metal forming technique were performed by Park and Kim **[27]**. It was determined that the incremental forming technique, especially with the positive forming method, is better than conventional techniques because forming capability increases as the plane-strain mode of deformation is more introduced. With the negative forming method, it is difficult to form sharp corners or edges because cracks easily occur due to the biaxial mode of deformation while with the positive forming method, it is possible to form complicated shapes with sharp corners or edges because the plane-strain mode of deformation becomes quite dominant. The support column of the jig should be properly designed in the positive forming method depending upon complexity of the shape to be formed.

2.3 LITERATURE GAP

After doing detailed study of literature on incremental forming process, it is summarized that many experimentations have been done to improve incremental forming with *CNC* milling machine, by varying sheet material, sheet thickness, maximum draw angle, spindle speed and work piece geometry. During the comparison of results between actual formed geometry and ideal geometry a deviation is reported at the major base of the components due to bending of the sheet. This may be reduced to an extent by the use of proper sized component specific backup plate. The need of a detailed analysis to quantify the amount of bending for different backup plate sizes, or tool diameter and wall angle of the component is felt. Also, for the components with truncated geometry variation in thickness between deformed and undeformed central region is observed. To reduce the variation, a two stage deformation strategy can be used and the effect can be studied.

2.4 OBJECTIVE OF PRESENT STUDY

The objective of the present study were to study/investigate the following

- Generation of toolpath that compensates the over travel at the end of deformation for better dimensional accuracy.
- Quantification of bending for different sheet dimensions and component wall angle for different geometries.
- Comparison of profiles in *SPIF* between components with and without fillet & height compensation.
- Using two-steps deformation strategy to achieve better thickness distribution in the final component.
- Study of tool reaction forces, strain history and few other related issues for components formed with *SPIF*.

CHAPTER 3
METHODOLOGY

After doing detailed study of Literature on Incremental forming process, it is summarized that many experimentations have been done to improve incremental forming with CNC milling machine, by varying sheet material, sheet thickness, maximum draw angle, spindle speed and work piece geometry. *FEM* package ABAQUS is used for simulation and analysis the result for different geometries like cone, pyramid and parabola etc. A new tool path generation for two step deformation strategy and geometric modifications has been proposed for better dimensional accuracy and thickness distribution. MATLAB is used to generate the tool path coordinate to deform the work piece and these coordinates are directly used in ABAQUS to simulate the tool on the sheet.

3.1 TOOL PATH GENERATION:

In single point incremental forming process, different object shapes like cone, pyramid, parabola etc has been formed. To generate different shapes, it need to determine the tool path coordinates depending on geometry type, incremental step size, opening diameter (*OD*), tool size, draw angle and height of component.

3.1.1 Tool path generation for cone:

Initially discussing the methodology of cone by deriving its mathematical formulation and code it in Matlab to generate the tool path coordinates moving on the sheet in 3-axis.

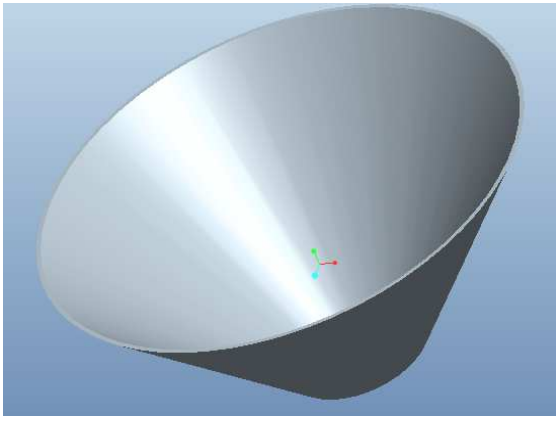

Figure 3.1: Solid model of cone

3.1.1.1 Input Parameters:

1.	Component opening radius	(R)	*mm*
2.	Draw angle	(α)	*degree*
3.	Component height	(h)	*mm*
4.	Tool Radius	(r)	*mm*
5.	Incremental Step size in z-direction	(dz)	*mm*
6.	Total no. of points in each contour	(n)	---

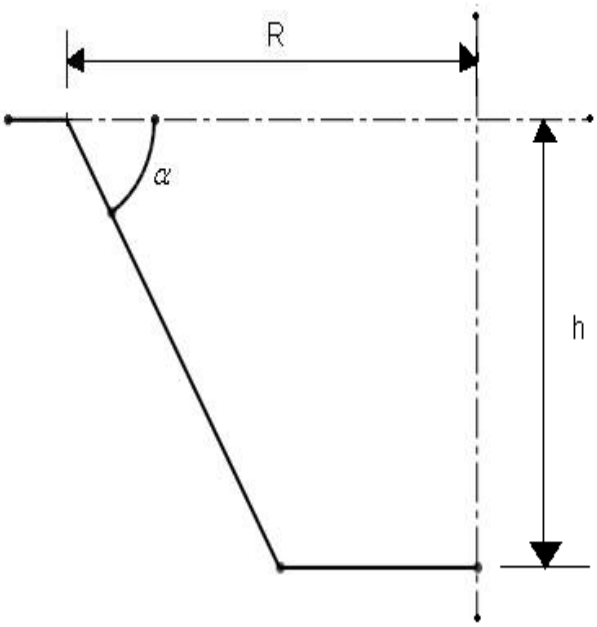

Figure 3.2: Sectional view of cone

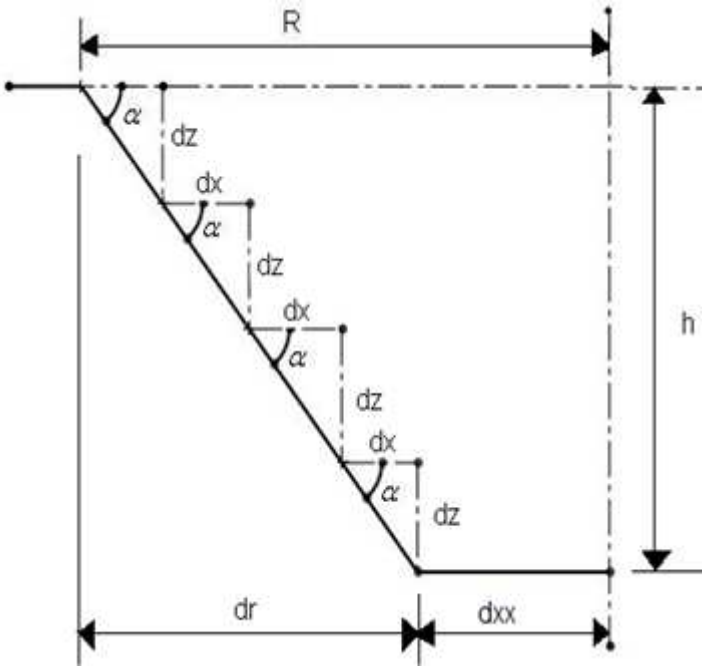

Figure 3.3: Sectional view of cone to determine decrement in *x*-direction

3.1.1.2 Calculation Steps:

3.1.1.2.1 Calculation for total decrement in *x*-direction *(dr)*

$$dr = \frac{h}{tan\alpha}$$

3.1.1.2.2 Calculation for *x*-coordinate on last contour *(dxx)*

$$dxx = -R + dr$$

3.1.1.2.3 Calculation for *x-y* coordinates on cone profile without radius compensation (*RC*)

$$y1 = 0 : -dz : -h$$

$$x1 = \frac{\left((y1) \times (dxx + R)\right)}{-h} - R$$

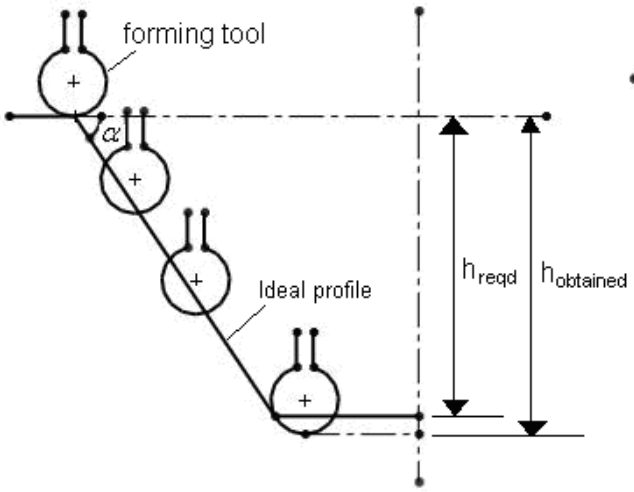

Figure 3.4: Sectional view of cone to determine *x, y* coordinate without *RC*

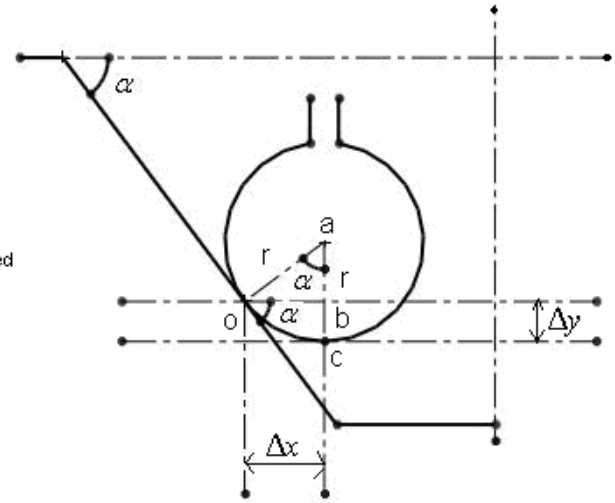

Figure 3.5: Sectional view of cone to determine *x, y* coordinate with *RC*

3.1.1.2.4 Calculation for each *x-y* coordinate on cone profile with radius compensation

$$\Delta x = r \times \sin\alpha$$

$$\Delta y = r \times (1 - \cos\alpha)$$

First calculate radius compensation in *x* & *y* direction i.e. Δx & Δy, after that calculate final *x-y* coordinate on cone profile with radius compensation and is given by

$$x11 = x1 + \Delta x$$

$$y11 = y1 - \Delta y$$

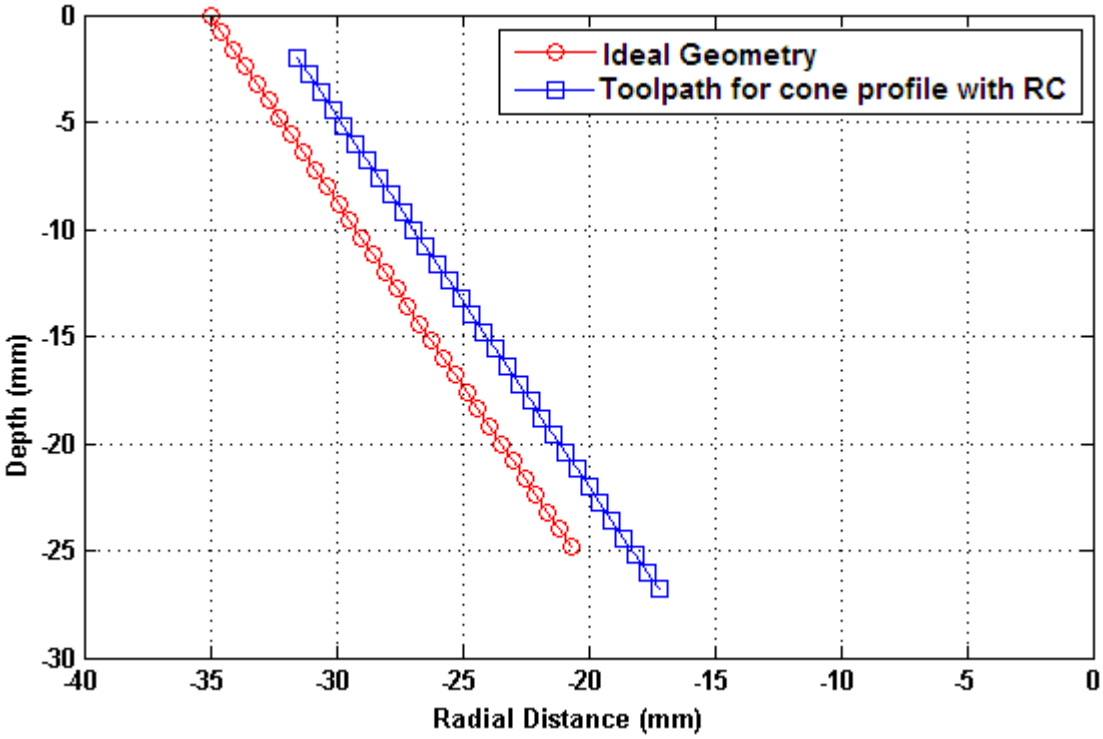

Figure 3.6: Comparison of Toolpath for cone profile without and with radius compensation for *OD*=70 *mm*, Tool diameter (*TD)* =8 *mm*, α =60°, *h*=25 *mm*, and *dz* =0.8 *mm*

3.1.1.2.5 Calculation of angle between any two points on a contour *(θ)*

$$\theta = \frac{360}{n}$$

3.1.1.2.6 Contour toolpath for a cone

Total number of contours = Length of $x1$

Two "for loops" are used to determine the no. of points on each contour corresponding to calculated angle (θ).

First loop used for increment in number of contour and second loop used for increment in number of points on contour as given in input parameters.

So, final *x, y, z* coordinate is given by

$$i = 1{:}1{:}length(x1)$$
$$j = 1{:}1{:}n$$
$$x(i,j) = x11(i) \times \cos\left(\theta \times (j-1)\right)$$
$$y(i,j) = x11(i) \times \sin\left(\theta \times (j-1)\right)$$
$$z(i,j) = y11(i)$$

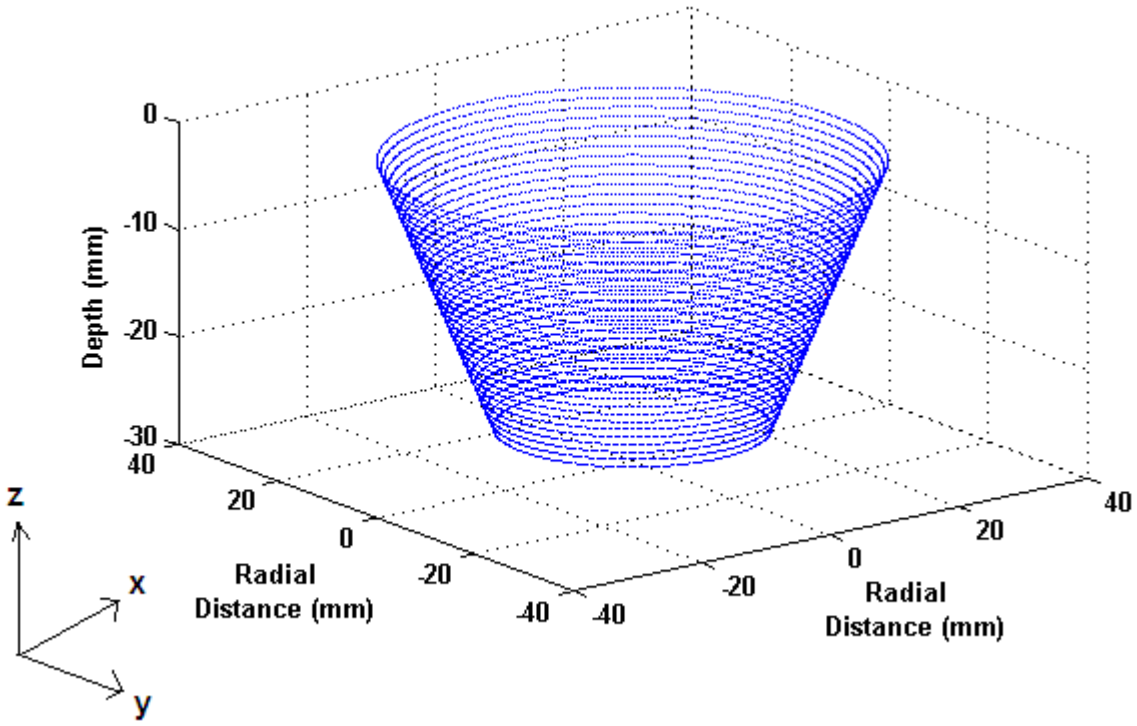

Figure 3.7: Contour toolpath for a Cone with *OD*=70 *mm*, *TD*=8 *mm*, α =60°, *h*=25 *mm*, and *dz* =0.8 *mm*

3.1.1.2.7 Spiral Toolpath for a cone

In case of spiral, Total number of turns will be reduced by one.

$$i = 1{:}1{:}length(x1) - 1$$
$$j = 1{:}1{:}n$$

Points in spiral form are calculated by using section formula as given below:

$$u(i,j) = \frac{((j-1)\times x(i+1,j)) + ((n-j)\times x(i,j))}{n-1}$$

$$v(i,j) = \frac{((j-1)\times y(i+1,j)) + ((n-j)\times y(i,j))}{n-1}$$

$$w(i,j) = \frac{((j-1)\times z(i+1,j)) + ((n-j)\times z(i,j))}{n-1}$$

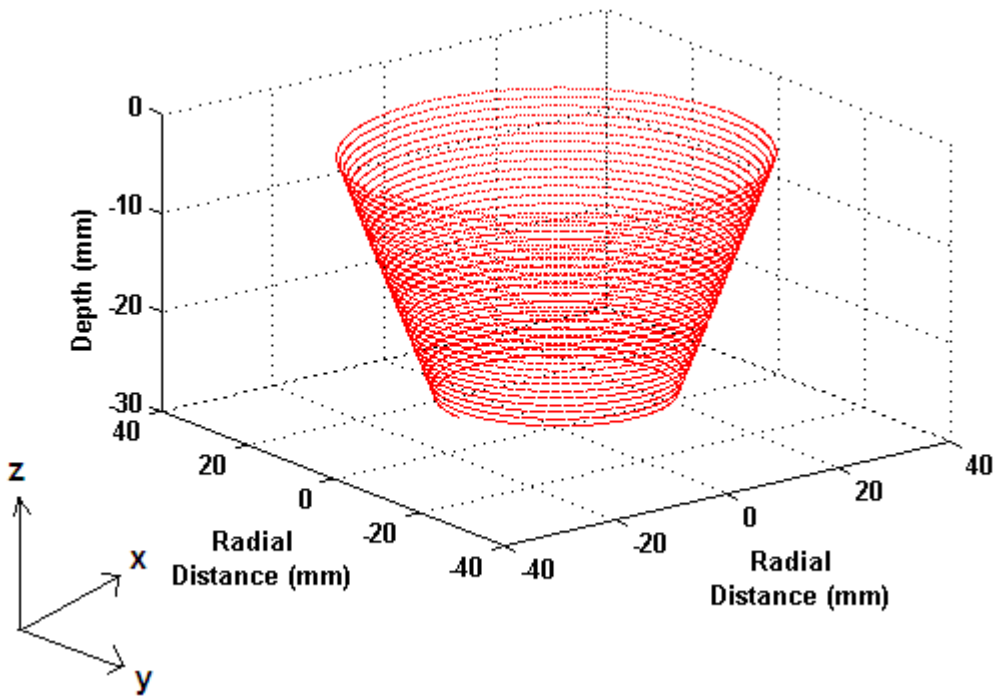

Figure 3.8: Spiral toolpath for a Cone with *OD*=70 *mm*, *TD*=8 *mm*, α =60°, *h*=25 *mm*, and *dz* =0.8 *mm*

3.1.1.3 Problems in cone formulation and its solutions:

3.1.1.3.1 Height compensation (*HC*)

First problem is related to required height of object (cone). Height of object is always comes greater that the required height because of radius compensation of tool as shown in (Figure 3.4) and (Figure 3.9).

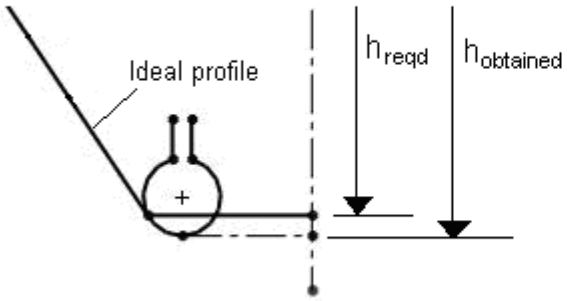

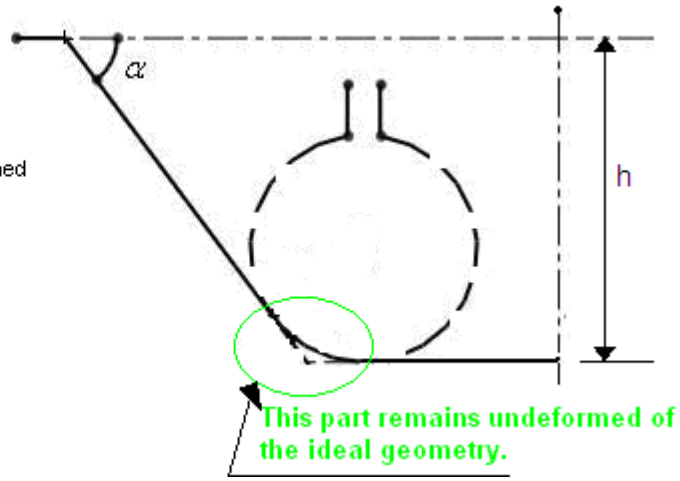

Figure 3.9: Sectional view of cone for *HC*

Figure 3.10: Sectional view of cone after *HC* and *RC*

Radius compensation at last contour is calculated as

$$\Delta y = r \times (1 - \cos \alpha)$$

Apply radius compensation to the height less than the required height, and height of component used to apply radius compensation (h_{rc}) becomes

$$h_{rc} = h - \Delta y$$

After applying height compensation and radius compensation it is possible to achieve required ideal geometry except the corner of component base because spherical or ball ended forming tool is used as shown in Figure 3.10.

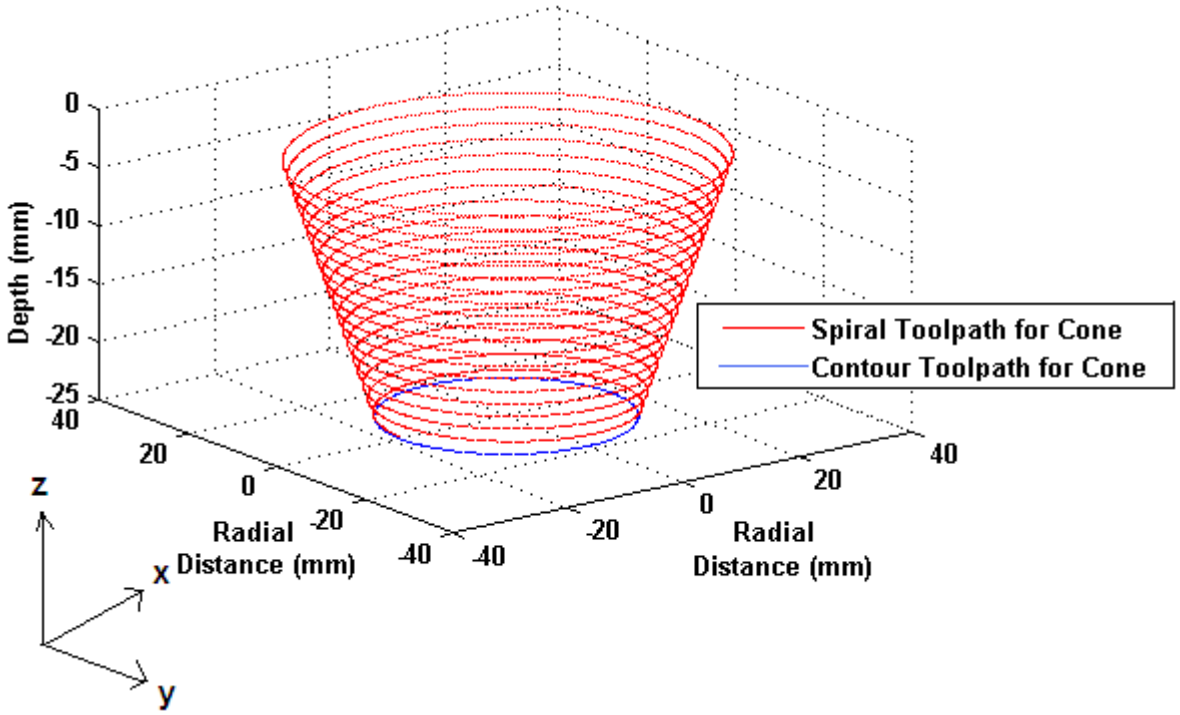

Figure 3.11: Toolpath for a Cone with height compensation for *OD*=70 *mm*, *TD*=8 *mm*, α =60°, *h*=25 *mm*, and *dz* =0.8 *mm*

3.1.1.3.2 Occurrence of higher indentation and bending at start of deformation

Due to radius compensation, starting point of sheet deformation shifts to distance (Δy) in negative *z*-direction as shown in Figure 3.6 and Figure 3.12. The shifting distance (Δy) mainly depends upon the draw angle, for large draw angle the shifting distance (Δy) is more. When tool moves more distance in one step, then higher indentation will occur and chance to occurrence of fracture at this location. This problem can be solved by giving top fillet. With using top fillet, draw angle increases gradually from zero to the required draw angle. Hence this problem can be solved.

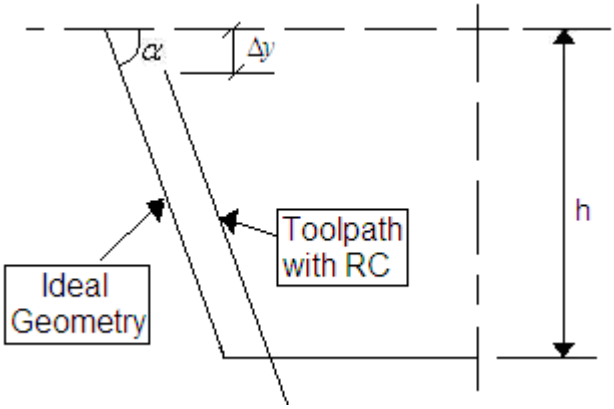

Figure 3.12: Sectional view of cone profile without and with radius compensation

The another problem is related to bending occurs at the start of deformation. If used backing plate, then bending at start can be minimized, but use of backing plate is not an optimized solution because of size of sheet and opening diameter of object changes every time, then required size of backing plate will also change. So it is difficult to manage different size of backing plates for different size of sheets and objects so it becomes expensive process.

3.1.1.3.2.1 Top Fillet Cone

Figure 3.13: Solid model of Fillet cone

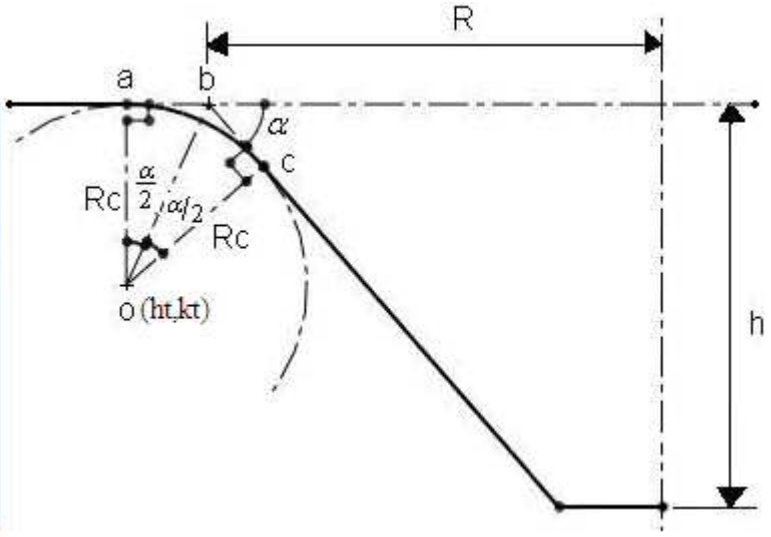

Figure 3.14: Sectional view of Top fillet cone

To prevent higher indentation and bending at the start of deformation of an object, giving some top fillet as shown in Figure 3.14. By doing this, draw angle (α) starts from zero and increases gradually along the curve up to the required draw angle until curve and line both is tangent to each other.

3.1.1.3.2.1.1 Calculation for start point of fillet (*a*):

In $\Delta\, oab$

$$ab = R_c \times tan\left(\frac{\alpha}{2}\right)$$

$$a = (xcs, ycs) = \left(-(R + ab), 0\right)$$

Where,

R_c =Top fillet Radius

3.1.1.3.2.1.2 Calculation for centre point of fillet (*o*):

$$o = (ht, kt) = \left(xcs, -Rc\right)$$

3.1.1.3.2.1.3 Calculation for end point of fillet (*c*):

In $\Delta\, obc$

$$bc = R_c \times tan\left(\frac{\alpha}{2}\right)$$

Here, the coordinates of point *b* is given as:

$$b = (-R, 0)$$

Assume the coordinates of point *c* as

$$c = (xce, yce)$$

By using distance formula on line oc and bc, and obtain two equations in the form of two variables (xce, yce) are given as

$$bc^2 = \sqrt{\left(xce - (-R)\right)^2 + \left(yce\right)^2}$$

$$oc^2 = \sqrt{\left(xce - ht\right)^2 + \left(yce - kt\right)^2}$$

.The coordinate of end point of curvature $c(xce, yce)$ are obtained by solving above two equations.

3.1.1.3.2.1.4 Calculation for intermediate points of curvature:

Intermediate points can be calculated by using general equation of circle.

Here need to calculate only *x*-coordinate of intermediate points by knowing y-coordinate start from zero and increases depending upon incremental step size (dz) in *z*-direction.

$$yc = ycs : dz : yce$$

$$xc = ht + \sqrt{R_c{}^2 - (yc - kt)^2}$$

3.1.1.3.2.1.5 Calculation for slope and radius compensation for curvature:

After that calculate the slope and angle between successive points and then calculate radius compensation of tool for all points on curvature.

$$m = \frac{yc(2) - yc(1)}{xc(2) - xc(1)}$$

$$ac = -\tan(m)$$

$$\Delta xc = r \times \sin(ac)$$

$$\Delta yc = r \times (1 - \cos(ac))$$

3.1.1.3.2.1.6 Calculation for final *x*-*y* coordinates on curvature:

Final coordinates on curvature after radius compensation is

$$x11c = xc + \Delta xc$$

$$y11c = yc - \Delta yc$$

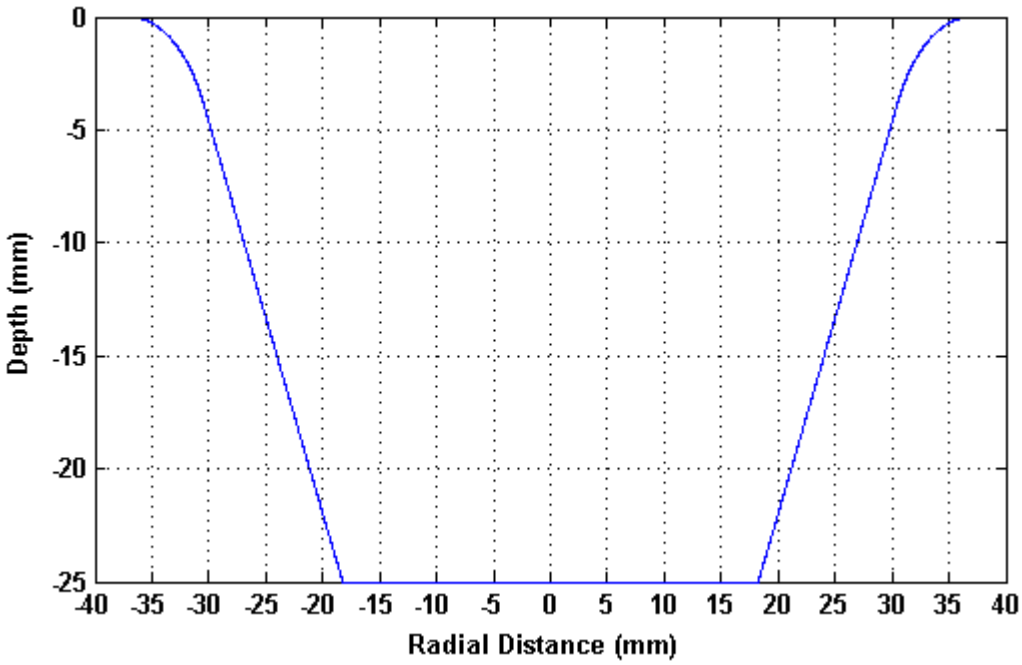

Figure 3.15: Toolpath for cone profile with fillet at top for *OD*=70 *mm*, *TD*=8 *mm*, α =60°, *h*=25 *mm*, and *dz* =0.8 *mm*

Finally need to merge these points on curvature with points on straight line as discussed earlier. The only change in calculation of basic code of cone is in its start point. Now end point of curvature (xce, yce) becomes the start point of straight line and other things are same.

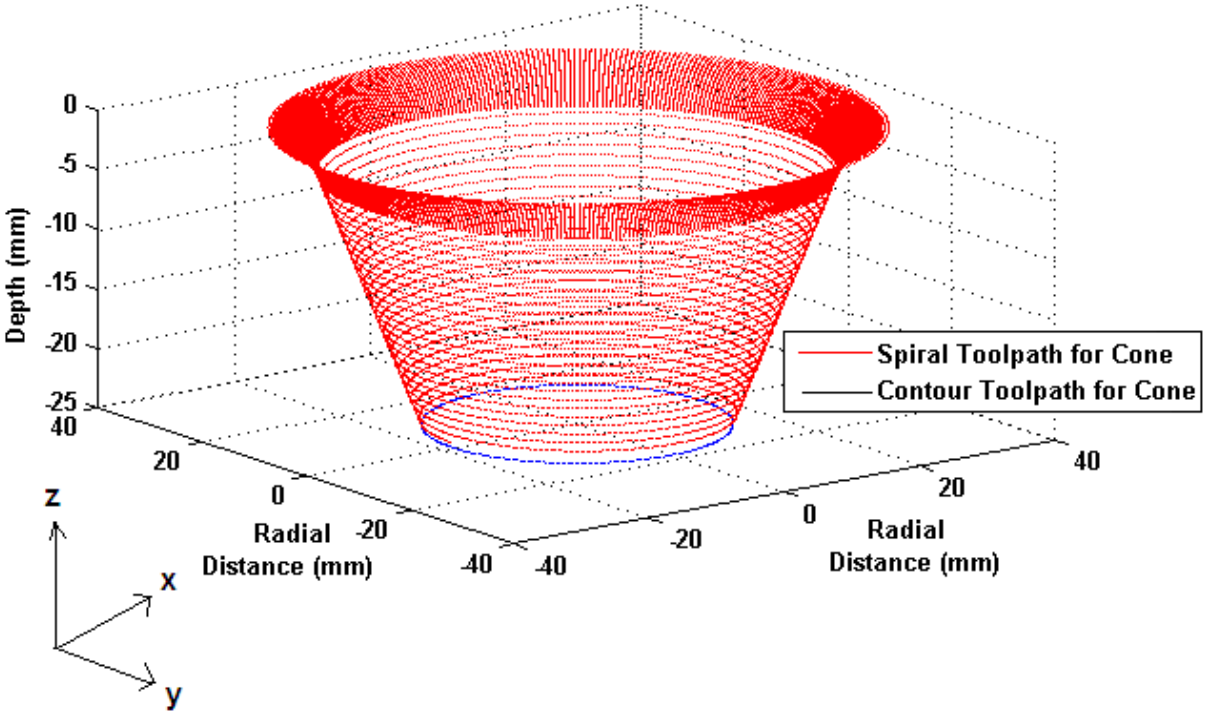

Figure 3.16: Toolpath for Top Fillet Cone for *OD*=70 *mm*, *TD*=8 *mm*, α =60°, *h*=25 *mm*, *dz* =0.8 *mm* and R_c =3.75 mm

3.1.2 Tool path generation for pyramid:

Now deriving the methodology of Pyramid and then code it in Matlab to generate the tool coordinates moving on the blank sheet in 3-axis. Side view of pyramid will be same as in the case of cone shown in Figure 3.14. There is only change in the top view of pyramid.

Figure 3.17: Solid model of pyramid

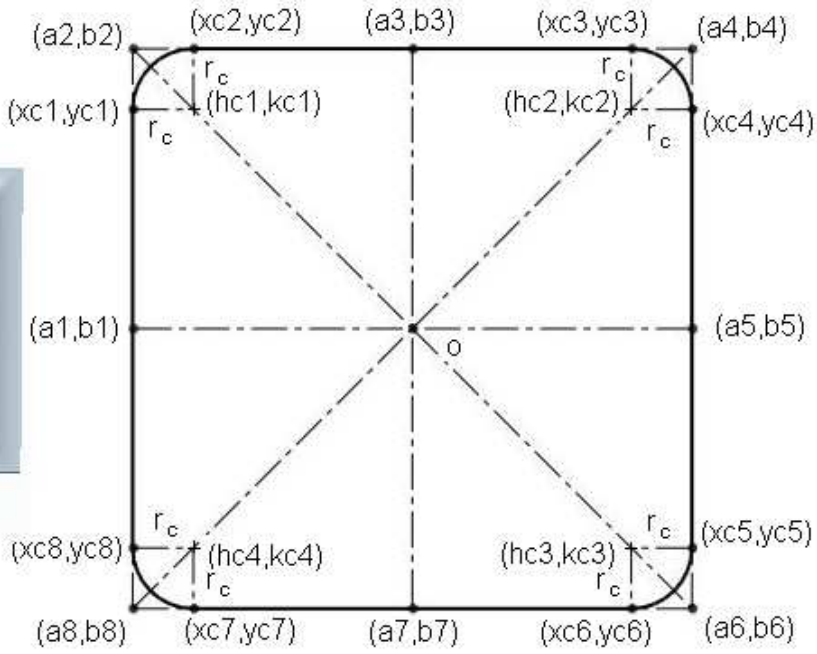

Figure 3.18: Top view of Pyramid

3.1.2.1 Calculation for top view of pyramid:

3.1.2.1.1 Determination of corners and centre point of pyramid:

Initially determine all the corner and centre coordinates of pyramid (i.e. *a1, a2, a3, a4, a5, a6, a7, a8* and *b1, b2, b3, b4, b5, b6, b7, b8*).

$$a1 = x11, b1 = 0$$
$$a2 = a1, b2 = -a1 \times \tan 45$$

Here $x11$ is determined in the same way as calculated in step 3.1.1.2.4.

In the similar way, calculate all other centre and corner coordinates of pyramid for remaining three quadrant of Pyramid.

3.1.2.1.2 Determination of start point $(xc1, yc1)$, end point $(xc2, yc2)$ and centre point $(hc1, kc1)$ of edge arc of pyramid:

$$xc1 = a1, yc1 = b2 - r_c$$
$$xc2 = a2 + r_c, yc2 = b2$$
$$hc1 = xc2, kc1 = yc1$$

Here r_C is radius of curvature at corners as shown in Figure 3.18.

Similarly calculate all other start, end and centre point coordinate of edge arc of pyramid for remaining three quadrant of Pyramid.

3.1.2.1.3 Determination of number of intermediate points moving along pyramid trajectory:

After calculating these points, calculate intermediate points by considering the number of points as input between (*a1, b1*) to (*xc1, yc1*) moving along *y* axis i.e. *x* remains constant only *y* changes, then (*xc1, yc1*) to (*xc2, yc2*) moving along an arc both *x* & *y* coordinate will change and use general equation of circle with shifting centre $(hc1, kc1)$, the equation is given by:

$$x_c = hc1 + (r_c \times \cos\theta)$$
$$y_c = kc1 + (r_c \times \sin\theta)$$

After that moving along path (*xc2, yc2*) to (*a3, b3*) only *x* changes and *y* remains constant.

Similarly, determine intermediate point for all remaining quadrant of pyramid.

Then repeat the same procedure to calculate all points on Pyramid trajectory moving in negative *z*-direction along its profile.

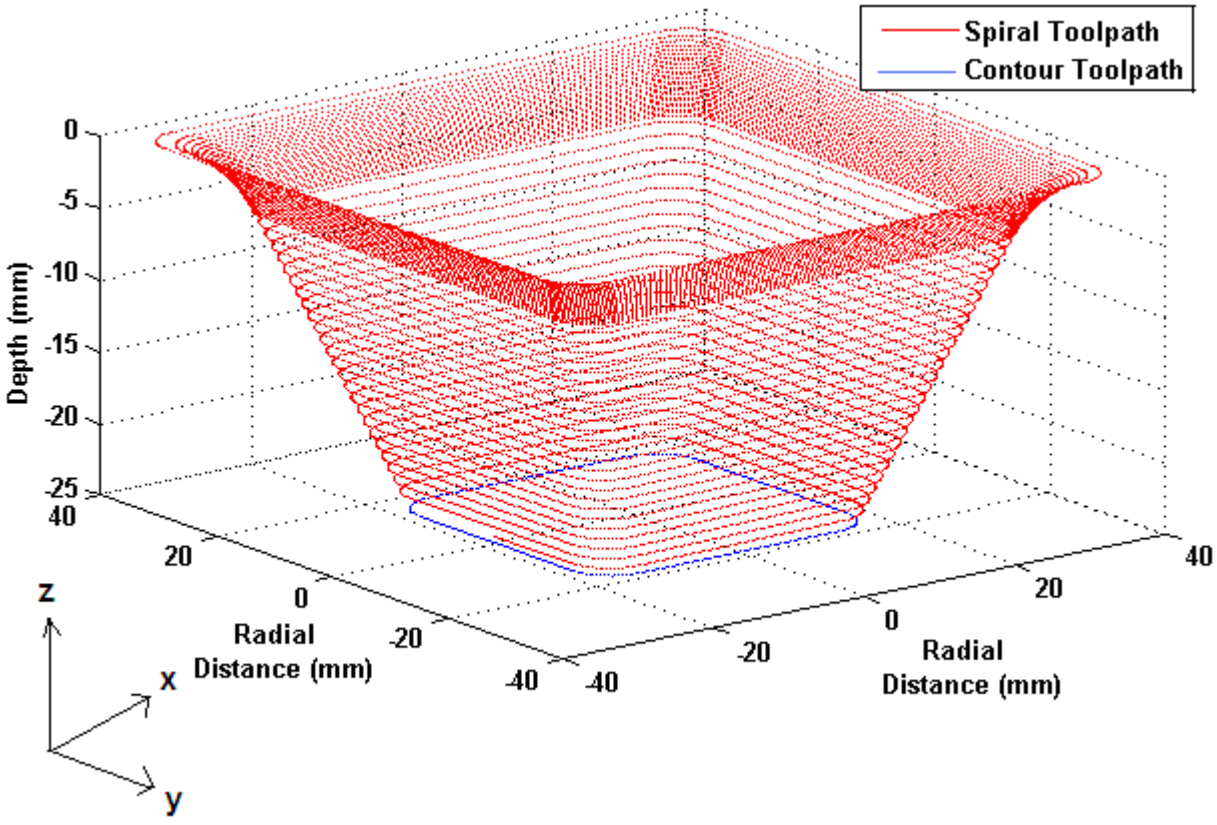

Figure 3.19: Toolpath for Top Fillet Pyramid for *OD*=70 *mm*, *TD*=8 *mm*, α =60°, *h*=25 *mm*, *dz* =0.8 *mm* and R_c =3.75 *mm*

3.1.3 Tool path generation for other axisymmetric shape (Flower):

Now deriving the methodology of other axisymmetric shape (*OAS*) and then code it in Matlab to generate the tool coordinates moving on the blank sheet in 3-axis. Side view of flower will be same as in the case of cone shown in Figure 3.14.

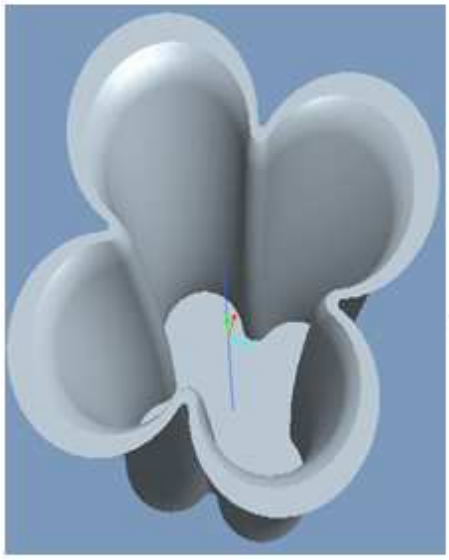

Figure 3.20: Solid model of *OAS*

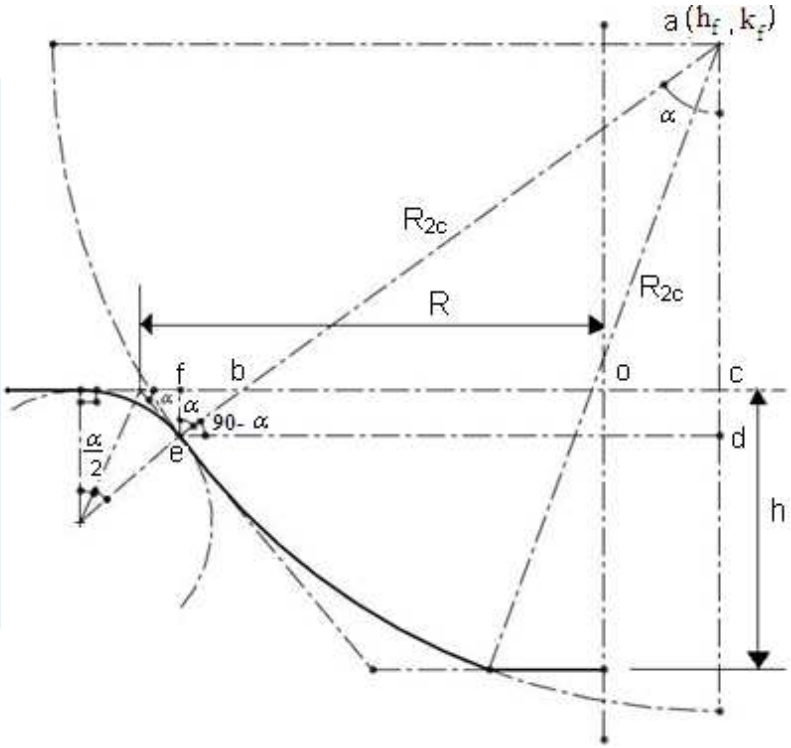

Figure 3.21: Sectional view of *OAS*

3.1.3.1 Calculation for Side view of other axisymmetric shape (flower)

Calculation for arc one used to prevent higher indentation has the same calculation as discussed in case of cone explained in step 3.1.1.3.2.1. Here discuss only the calculation for arc 2 having centre $\left(a\left(h_f, k_f\right)\right)$ and radius $\left(R_{2c}\right)$ and start point of second arc $e(x1, y1)$ that is the end point of arc 1.

3.1.3.1.1 Determination of centre point of arc $\left(h_f, k_f\right)$:

a. Determination of k_f :

In $\Delta\, aed$

$$ad = R_{2c} \times \sin(90-\alpha)$$
$$ed = R_{2c} \times \cos(90-\alpha)$$

In $\Delta\, bfe$

$$bf = ef \times \tan(\alpha)$$

Here $ef = y1$

So, $bf = y1 \times \tan(\alpha)$

In $\Delta\, abc$

$$ac = k_f = \frac{bc}{\tan(\alpha)}$$

Here from figure 3.21

$$ed = fc$$

$$bc = ed - bf$$

So, $bc = \left(R_{2c} \times \cos(90-\alpha)\right) - \left(y1 \times \tan(\alpha)\right)$

So, $k_f = \dfrac{\left(R_{2c} \times \cos(90-\alpha)\right) - \left(y1 \times \tan(\alpha)\right)}{\tan(\alpha)}$

b. Determination of h_f :

After knowing the starting point $(x1, y1)$, Radius $\left(R_{2c}\right)$ and one centre coordinate $\left(k_f\right)$ of arc. To calculate $\left(h_f\right)$, use general equation of circle as given below:

$$\left(x - h_f\right)^2 + \left(y - k_f\right)^2 = R^2$$

Put $x = x1$, $y = y1$, $R = R_{2c}$ and $\left(k_f\right)$ coordinate in above equation, then $\left(h_f\right)$ can be calculated from equation given below:

$$h_f = x1 - \sqrt{R_{2c}{}^2 - \left(y1 - k_f\right)^2}$$

3.1.3.1.2 Determination of Intermediate points on arc:

Sheet deformation occurs in the negative *z*-direction, and all *y* coordinates on arc depending upon the required height (h) and step size (dz) can be determined from equation given below:

$$y = y1 : -dz : -h$$

And *x* coordinates on arc can be calculated using general equation of circle corresponding to various *y* coordinates on arc are given as:

$$x = -\left(\sqrt{R_{2c}{}^2 - \left(y - k_f\right)^2} - h_f\right)$$

After calculating *x* & *y* coordinates on arc, apply radius compensation on each point in the same way as discussed in step 3.1.1.3.2.1.5 and 3.1.1.3.2.1.6.

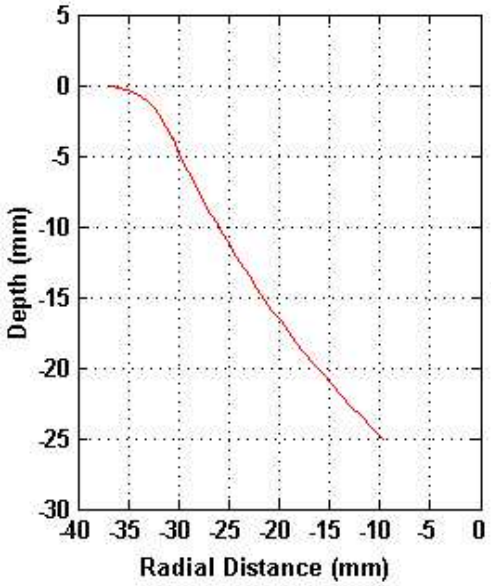

Figure 3.22: Graphical plot for sectional view of *OAS*

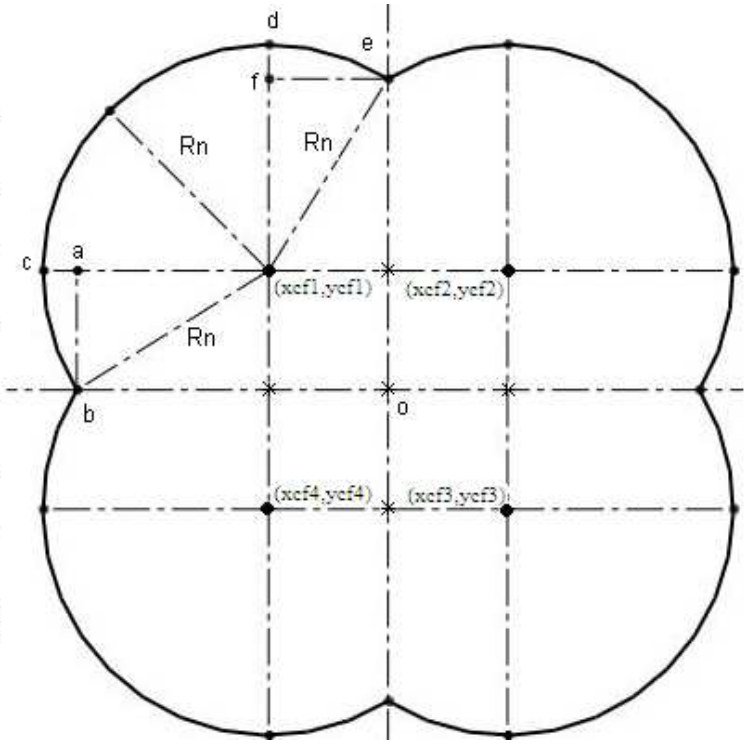

Figure 3.23: Top view of *OAS*

3.1.3.2 Determination of top view of other axisymmetric shape (flower)

3.1.3.2.1 Calculation of offsetting centre points and radius of arcs:

Here first calculate offsetting centre points $(xcf1, ycf1)$ corresponding to all points profile moving in negative *z*-direction by using relation as given below:

$$xcf1 = \frac{x11}{3}, ycf1 = -xcf1$$

$$xcf2 = -xcf1, ycf2 = ycf1$$

$$xcf3 = -xcf1, ycf2 = -ycf1$$

$$xcf4 = -xcf2, ycf4 = -ycf2$$

$$Rn = -x11 - xcf1$$

Here *x11* is the opening of the component for the different contours.

3.1.3.2.2 Calculation of number of intermediate points moving from path *b* to *c* along flower trajectory:

$$ab = ycf1$$

Consider number of points (nse) as input in between *b* and *c* in figure 3.23, then the distance between any two points along path *bc* in *y*-direction is constant and it is given by:

$$dyfc = \frac{ycf1}{nse}$$

$$yfc1 = 0 : dyfc : (yc1 - dyfc)$$

To determine *x*-coordinate along path *bc* in figure 3.23 use,

$$xfc1 = -\left(\sqrt{Rn^2 - \left(yfc1 - yc1\right)^2} - xc1\right)$$

And *z*-coordinate is given as:

$$zfc1 = y11$$

3.1.3.2.3 Calculation of number of intermediate points moving from path *c* to *d* along flower trajectory:

Consider number of points (nsf) as input in between *c* and *d* in figure 3.23, first determine angle between any two points along path *d* is given as:

$$\theta = \frac{90}{nsf}$$

To calculate *x* & *y* coordinate along path *c* to *d* in figure 3.23, use general circle parametric equations with offsetting centre $\left(xci, yci\right)$,moving from one point to another point along path *c* to *d* by increasing angle 0 degree to 90 degree is given as

$$xsc1 = xc1 + \left(Rn \times \cos\theta\right)$$
$$ysc1 = yc1 + \left(Rn \times \sin\theta\right)$$
$$zsc1 = y11$$

3.1.3.2.4 Calculation of number of intermediate points moving from path *d* to *e* along flower trajectory:

$$fe = xc1$$

Consider number of points (nse) as input in between *d* and *e* in figure 3.23, then the distance between any two points along path de in *x*-direction is constant and it is given by:

$$dxtc = \frac{xc1}{nse}$$

$$xtc1 = xc1 + dxtc : dxtc : -dxtc$$

To determine *y*-coordinate along path *ac* in figure 3.23 use,

$$ytc1 = \left(\sqrt{Rn^2 - \left(xtc1 - xc1\right)^2} + yc1\right)$$

And *z*-coordinate is given as:

$$ztc1 = y11$$

In the similar way, determine all point for remaining quadrant of Flower.

Then repeat the same procedure to calculate all points on flower trajectory moving in negative *z*-direction along its profile.

After that check minimum opening of flower should be greater than 1.5 times of tool diameter, otherwise change input parameters like draw angle, height and tool radius etc.

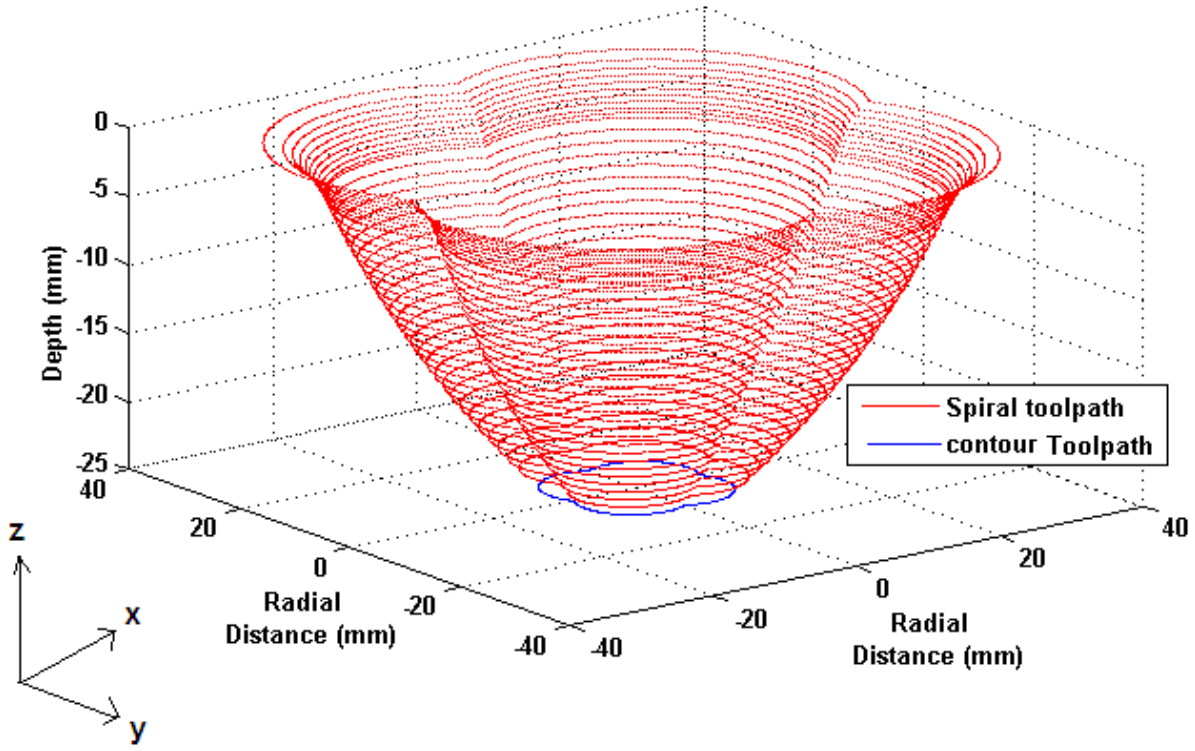

Figure 3.24: Toolpath for other axisymmetric shape (flower shape) for *OD*=70 *mm*, *TD*=8 *mm*, *max* α =60°, *h*=25 *mm*, *dz* =0.8 *mm*, R_c =4.0 *mm* and $R_{2c} = 80$ *mm*

3.1.4 Tool path generation for two-step deformation strategy

In Two-step deformation strategy**,** two kinds of toolpaths are used. When the tool motion is from the periphery of the sheet towards the centre of the sheet, and moving in the negative *Z* direction, the toolpath is called outer-to-inner (*O-to-I*) and when the tool motion is from the centre of the sheet towards the periphery, moving in the positive *Z* direction, the toolpath is called inner-to-outer (*I-to-O*) tool movement. Following steps has to be performed for this type of toolpath strategy:

Step 1: First tool is moving from outer-to-inner path by generating an intermediate profile whose opening diameter should be less than the required object opening diameter and its depth either less or equal to the depth of required object.

Step 2: After generating intermediate profile, tool will move only downwards up to the required object height only in that case, when height of intermediate profile is less than the required object height. If depth of intermediate profile is equal to the height of desired object then don't need to perform this step.

Step 3: Now tool will move along *x*-axis to reach last *x*-coordinate of required object at constant depth.

Step 4: Finally tool will move in positive *z* direction (i.e. from downward to upwards) to perform inner-to-outer operation and obtaining the desired geometry of object.

In two-step deformation strategy, different type of intermediate profiles, like straight cone, bottom fillet cone, parabola, fillet parabola etc has been studied.

3.1.4.1 Straight cone type Intermediate profile

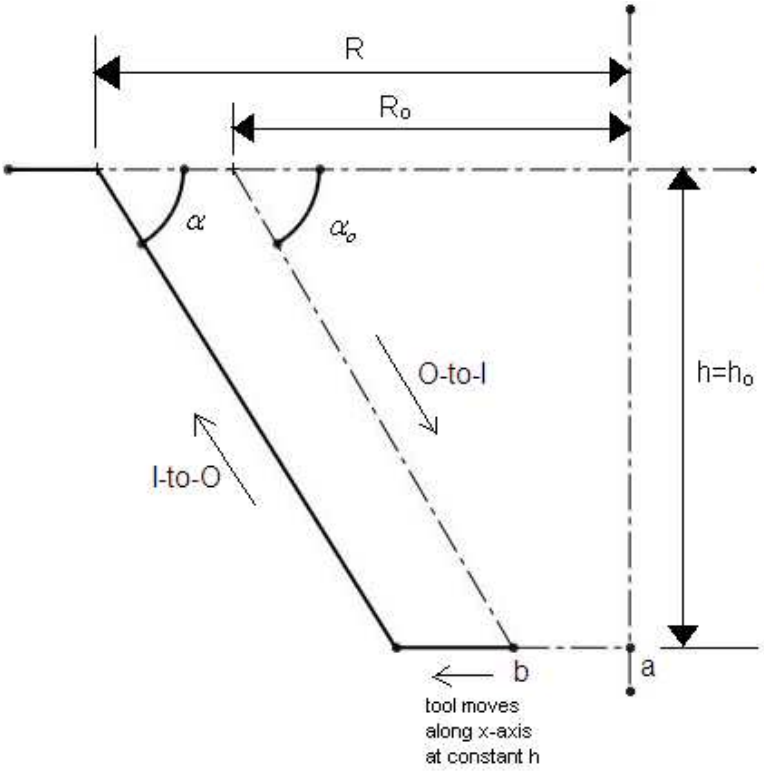

Figure 3.25: Sectional view to show *O-to-I* and *I-to-O* Toolpath for straight cone type intermediate profile

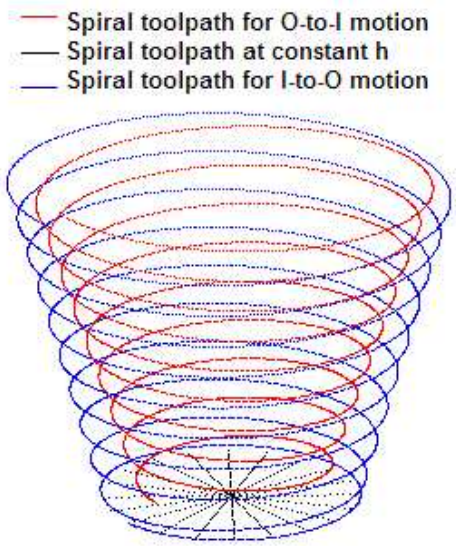

Figure 3.26: Compensated toolpath for straight cone type intermediate profile

In this case, intermediate straight cone has draw angle (α_o) and height (h_o) is same as the height of desired cone (h) but intermediate cone has opening Radius (R_o) should be less than the required cone opening radius (R).

Initially tool will move along the profile of intermediate cone i.e. tool will perform outer to inner operation, then tool move along *x*-axis at constant height and finally tool will move along the desired trajectory of cone from downward to upward direction i.e. tool will perform Inner to outer operation.

Tool Coordinates are determined in the same way as discussed in the previous cases, except that in the previous cases there is only one way movement of tool (i.e. outer-to-inner), but here tool has two way movement (i.e. *O-to-I* and *I-to-O*) once in negative *z*-direction and second in positive *z*-direction.

Disadvantages:

1. The portion *a* to *b* in figure 3.25 remains undeformed.
2. There is a maximum chance of fracture of sheet at bottom corner, because very small portion of sheet at bottom corner of intermediate cone is stretched along *x*-axis to base of required cone.

3.1.4.2 Bottom fillet cone type Intermediate profile

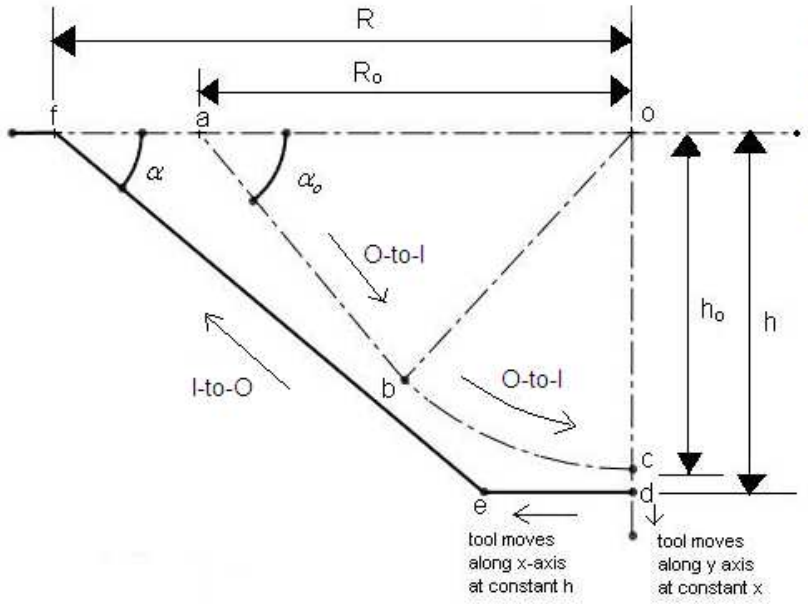

Figure 3.27: Sectional view to show *O-to-I* and *I-to-O* Toolpath for bottom fillet cone type intermediate profile

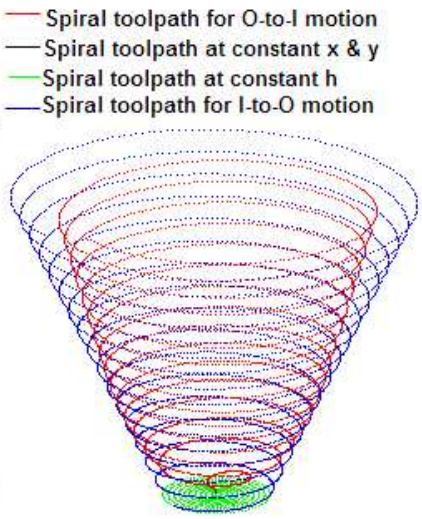

Figure 3.28: Compensated toolpath for bottom fillet cone type intermediate profile

Here tool will start to move from point *a* along the path (*ab*) to point *b* as shown in figure 3.27, after that tool will move along curved path (bc) having centre at o and radius is equal to the height of intermediate cone (h_o),then tool will move along path (cd) parallel to *y*-axis and after that tool will move along path (de) parallel to x-axis at constant required height, finally tool will move along the desired trajectory of cone from downward to upward direction i.e. tool will perform Inner-to-outer operation.

Advantages:

1. Chances of fracture at the bottom corner of sheet have been reduced, because large part of curved path (bc) has been stretched into part (de).
2. There is no undeformed region in the intermediate profile as in step 3.1.4.1, so obtain better result for thickness.

Disadvantages:

Thickness Distribution along the side walls of cone is more non uniform (Figure 3.28) than thickness distribution along the side walls of cone in step 3.1.4.1.

3.1.4.3 Parabola type intermediate profile

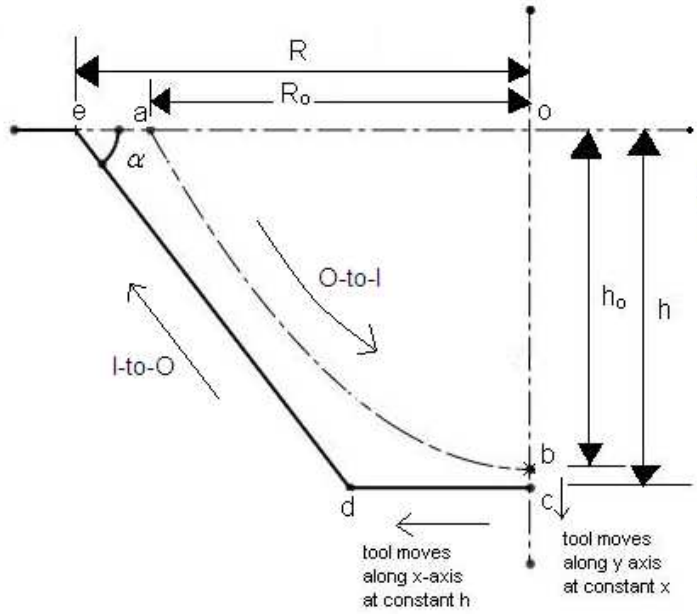

Figure 3.29: Sectional view to show *O-to-I* and *I-to-O* Toolpath for parabola type intermediate profile

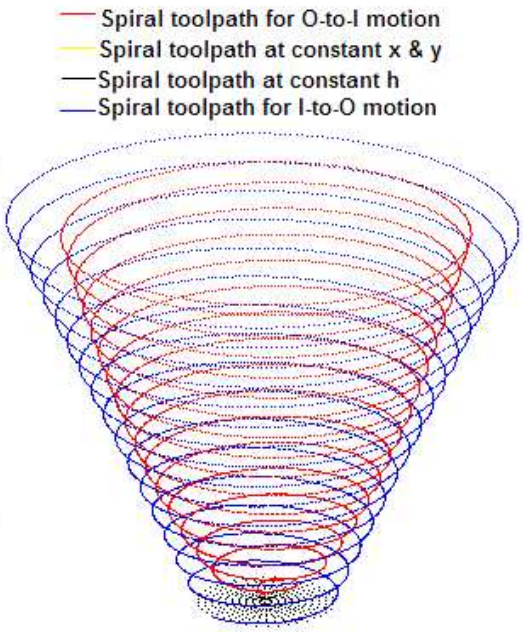

Figure 3.30: Compensated toolpath for parabola type intermediate profile

Here tool will start to move from point *a* along the parabolic trajectory to point *b*, after that tool will move along path (*bc*) parallel to *y*-axis and then tool will move along path (c*d*) parallel to *x*-axis at constant required height, finally tool will move along the desired trajectory of cone from *d* to *e* as shown in figure 3.29.

Advantages:

1. Chances of fracture at the bottom corner of sheet have been reduced with parabolic type intermediate profile.
2. Better result for thickness can be obtained for both side walls and base of desired component.

Disadvantage:

While forming the second pass when the tool motion is from the centre of the sheet towards the periphery, (i.e. moving in the positive *Z* direction), the solution does not converged. The mode of failure was a 'fold-over' type of failure. While forming the second pass, a lip formed where the wall of the initial pass met the forming tool. This lip became sharp and eventually folded over, resulting in a failure at this location explained in step 4.4.2.2.

3.1.4.3.1 Tool path generation for parabola profile

The general equation of parabola is given as:

$$y_p = a_p x_p^{\,2} + b_p x_p + c_p$$

Here $b_p = c_p = 0$, because there is not a shifting of centre point and origin of parabola. So, equation becomes:

$$y_p = a_p x_p^{\,2}$$

In above equation, the *y* coordinates along the parabola profile depending on the height (h_o) and step size can be determined using following equation as given by

$$y_p = -h_o : dz : 0$$

The constant (a_p) in the parabolic equation depends upon the opening of parabola (R_O) and its height (h_O) and is given by:

$$a_p = \frac{h_O}{R_O^{\,2}}$$

By using parabolic equation, the x-coordinate along the parabolic profile depending upon the constant (a_p) and y-coordinate can be determined and is given by an equation as:

$$x_p = \sqrt{\frac{y + h_o}{a_p}}$$

After knowing *x & y* coordinate on the profile of parabola, and then apply radius compensation in the same way as discussed in the 3.1.1.3.2.1.5.

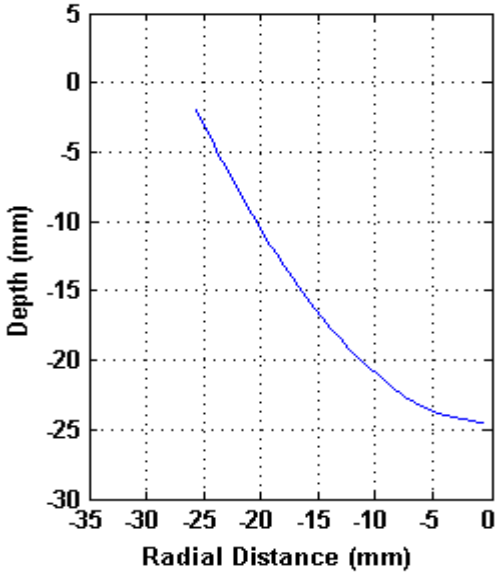

Figure 3.31: Sectional side view of parabolic profile for *OD*=60 *mm*, *TD*=8 *mm*, *max* α =60°, *h*=24.6 *mm*, *dz* =0.8 *mm*

3.1.4.4 Top fillet parabola type Intermediate profile

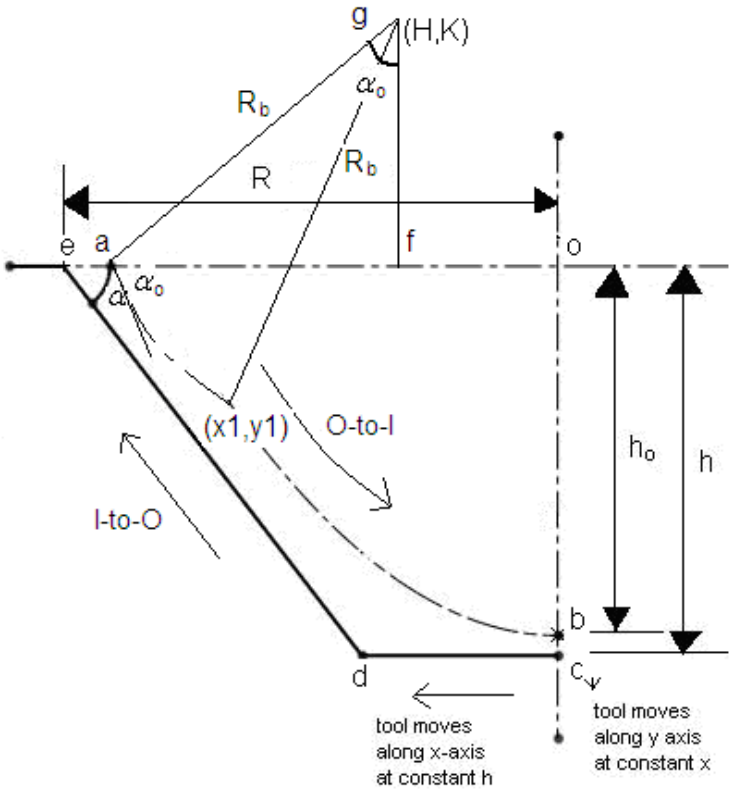

Figure 3.32: Sectional view to show *O-to-I* and *I-to-O* toolpath for top fillet Parabola type intermediate profile

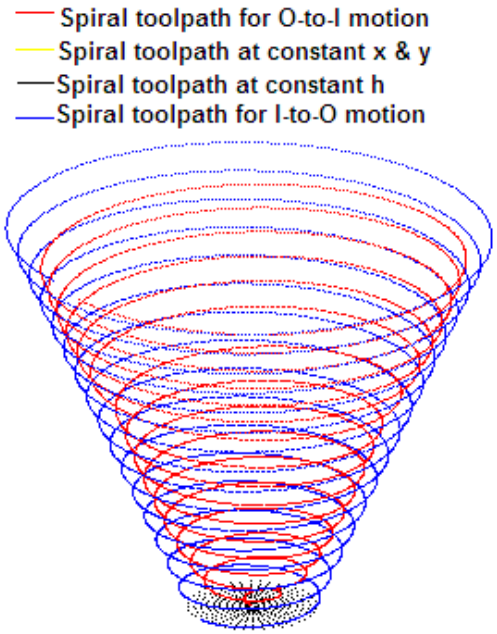

Figure 3.33: Compensated toolpath for top fillet Parabola type intermediate profile

This type of intermediate profile is used to overcome the problem of fold-over comes in step 3.1.4.3. Here intermediate profile is containing two curves one is parabolic and second is arc with centre *(H, K)* and radius of R_b as shown in Figure 3.32. The Calculation of parabolic profile is same as discussed in step 3.1.4.3.1. Here top Curvature calculation is discussed only.

In Δagf

$$K = R_b \times \cos\alpha_o$$

$$H = \sqrt{R_b{}^2 - \left(K - y1^2\right)} + x1$$

After knowing the centre point of arc and starting point of parabola *(x1, y1)* then calculate the number of intermediate points on first arc 1 by using re

lation as given below:

$$Y = y1 : dz : 0$$

$$X = \sqrt{R_b{}^2 - (y1 - K)^2}$$

3.2 SIMULATION METHODOLOGY

There are number of steps to be performed for the analysis in Abaqus. These steps explained as below:

3.2.1 Sheet modeling and selection of its geometrical properties:

1. Create a new part and describe its name as sheet.
2. The modeling space used for sheet is *3D.*
3. The type of nature for sheet is deformable and its shape of shell planar type is used.

3.2.2 Tool modeling and selection of its geometrical properties:

1. Create new *3D* part and describe its name as a tool.
2. Type of tool: Analytical rigid
3. Basic feature: Revolved shell.
4. Select the reference point at the bottom of tool.

3.2.3 Assign material to sheet and its material properties:

Material of sheet: *Al* 5052

Elastic properties of *Al* 5052:

1. Young's Modulus *(E)* = $70000\left(N/mm^2\right)$
2. Poison ratio = 0.33

Plastic properties of *Al* 5052:

1. Equivalent stress $\left(MPa\right)$
2. Equivalent strain

Table 6: Plastic properties of material

Equivalent strain	Equivalent stress $\left(MPa\right)$
0	89.6
0.01	191.00
0.1	252.00
0.15	264.00
0.2	274.00
0.3	287.00
0.4	297.00
0.5	306.00
1	332.00

For increased value of strain, the Equivalent stress can be obtained using power formula as given below:

$$\sigma_{eq} = 332 \times \varepsilon_{eq}^{0.12}$$

Here σ_{eq} = Equivalent stress (MPa)

ε_{eq} = Equivalent Plastic strain

By putting any value of strain, yield stress can be calculated.

The power formula is obtained from table 6, by plotting equivalent stress against equivalent strain in excel and then using trend line option and tick to display the power formula as shown in figure 3.34.

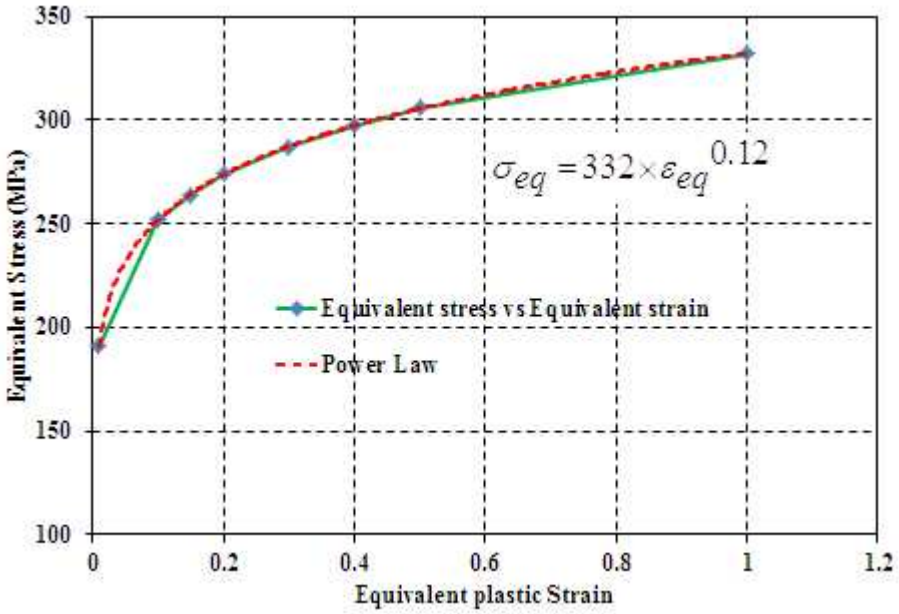

Figure 3.34: Graph to determine power formula between Equivalent stress and strain

3.2.4 Assign section to sheet

Section type: Shell / Continuum shell, homogenous

Section thickness: 0.5

Thickness integration rule: Simpson and use 5 thickness integration points

3.2.5 Create mesh to sheet

It is need to create meshing only for sheet part, no need to create meshing for tool part because tool is a analytical rigid part.

The steps to create mesh for sheet as defined below:

1. Select sheet for meshing.
2. Mesh control:

   Element shape: Quad-dominated

Element library: Standard Geometric order: Linear

Element Name: S4R→ 4-node doubly curved thin or thick shell, reduced integration, hourglass control, finite membrane strains.

3. Seed part: Seed edge by number; using mesh size of 1x1 *mm*, for each element.
4. For sheet size 75x75 *mm*, the total number of elements = 5625

3.2.6 Creation of Assembly and interaction properties:

1. Keep 0.1 *mm* gap between tool and sheet during assembly.
2. Contact type: Surface to surface contact
3. Master surface: tool
4. Slave surface: sheet
5. Interaction Properties: Mechanical properties
    a. Tangential behavior: friction formulation is frictionless
    b. Normal behavior

Pressure $\left(N/mm^2\right)$	Clearance
500	0
0	0.1

3.2.7 Define tool path coordinates for tool motion on sheet (Amplitude):

Tool moves on the sheet with respect to the entered tool coordinates. Tool coordinates are defined with respect to the reference point of tool. Three different amplitude files are defined for tool motion in *XYZ* direction with respect to step time.

3.2.8 Define number of steps for tool movement on the sheet:

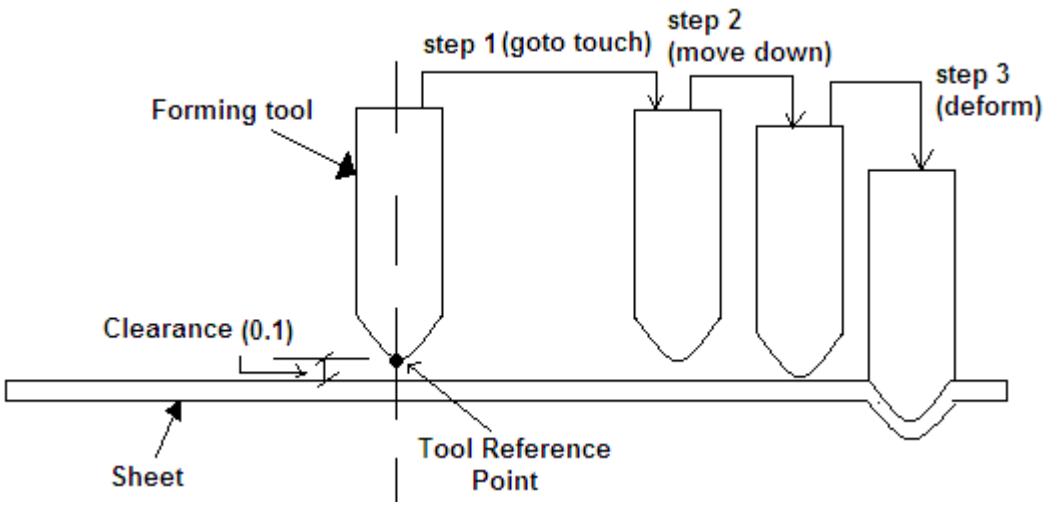

Figure 3.35: Sheet tool assembly and steps for tool motion on sheet

In Figure 3.35, step 2 (move down) and step 3 (deform) are performed at the same location of step 1. For more clarity, it is shown at different location in Figure 3.35.

Step 1 (go to touch): First move the tool in air at the starting x, y coordinate, where deformation starts.

Step 2 (move down): Tool moves in negative *z*-direction by the clearance taken during assembly, so that tool becomes in contact with sheet and further deformation can be start.

Step 3 (Deform): *XYZ* tool movement occurs on sheet as per the *XYZ* displacement defined in step 3.2.7.

In all steps, it needs to define total time period, selection of Nlgeom, and maximum number of increments must be defined.

3.2.9 Define boundary conditions:

Define the boundary conditions for all the steps have explained in step 3.2.8. It was also need to define the boundary condition for blank sheet whose all edges should be as shown in figure 3.36. To fix all edges of sheet, use Symmetry/Antisymmetry/Encastre type feature for this boundary condition.

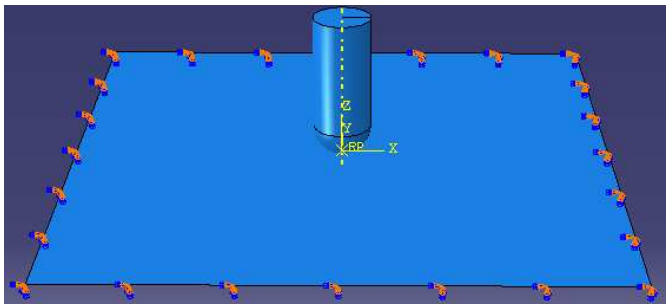

Figure 3.36: Boundary condition to fix all edges of sheet

Second boundary condition is for step 1 (goto touch) explained in 3.2.8. Here tool reference point (*RP*) as shown in figure 3.36 is selected for displacement and rotation type feature, and enter *x* and *y* displacement of translational type and remaining will be blocked.

Third boundary condition is for step 2 (move down) explained in 3.2.8. Here tool reference point (*RP*) as shown in figure 3.36 is selected of displacement and rotation type feature, and enter only *z* displacement of translational type and remaining will be blocked.

Fourth boundary condition is for step 3 (deform) explained in 3.2.8. Here 3 different boundary conditions need to define for entered tool displacement coordinates in step 3.2.7. For all three boundary conditions, tool reference point (*RP*) as shown in figure 3.36 is selected of displacement and rotation type feature, and finally select *x, y, & z* displacement from the amplitude option corresponding to boundary condition in *x, y, & z* direction of step deform. Finally submit the job.

3.3 GEOMETRIC FEATURES AND PLAN FOR SIMULATION

Table 7: Geometric features and plan for simulation

Job No.	Geometry Type	Sheet blank size (*SBS*) (mm)	Opening diameter (*mm*)	Draw angle (*degree*)	Tool Diameter (*mm*)	Height (*mm*)	Incremental Depth (*mm*)	Blank initial Thickness $(t_o)(mm)$	Top Fillet Radius (R_c) (*mm*)
1	Cone	75x75	70	60	8	25	0.8	0.5	0
2	Cone	95x95	70	60	8	25	0.8	0.5	0
3	Pyramid	75x75	70	60	8	25	0.8	0.5	0
4	Pyramid	95x95	70	60	8	25	0.8	0.5	0
5	Cone	75x75	70	45	8	25	0.8	0.5	0
6	Pyramid	75x75	70	45	8	25	0.8	0.5	0
7	Top fillet Cone	75x75	70	60	8	25	0.1 & 0.8	0.5	3.75
8	Top fillet Cone	95x95	70	60	8	25	0.1 & 0.8	0.5	3.75
9	Top fillet Pyramid	75x75	70	60	8	25	0.1 & 0.8	0.5	3.75
10	Top fillet Pyramid	95x95	70	60	8	25	0.1 & 0.8	0.5	3.75
11	Top fillet Cone	75x75	70	45	8	25	0.1 & 0.8	0.5	3.75
12	Top fillet Pyramid	75x75	70	45	8	25	0.1 & 0.8	0.5	3.75
13	Top fillet Cone	95x95	70	45	8	25	0.1 & 0.8	0.5	3.75
14	Top fillet Pyramid	75x75	70	45	8	20	0.1 & 0.8	0.8	3.75
15	Top fillet Flower	75x75	70	*Max* 60	8	25	0.1 & 0.8	0.5	4.0
16	Cone (O-to-I)	75x75	64	40	8	14.99	0.8	0.5	0
	Cone (I-to-O)	75x75	70	45	8	15	0.8	0.5	0
17	Parabola (O-to-I)	75x75	58	*Max* 60	8	24.6	0.8	0.5	0
	Cone (I-to-O)	75x75	70	45	8	25	0.8	0.5	0
18	Parabola (O-to-I)	75x75	60 and *Rb*=33	*Max* 60	8	24.99	0.8	0.5	0
	Cone (I-to-O)	75x75	70	45	8	25	0.8	0.5	0
19	Parabola (O-to-I)	95x95	60 and *Rb*=33	*Max* 60	8	24.99	0.8	0.5	0
	Cone (I-to-O)	95x95	70	45	8	25	0.8	0.5	0
20	Funnel	95x95	70	*Max* 60	8	-	0.5	0.88	-
21	Funnel	95x95	70	*Max* 60	8	-	0.2	0.88	-
22	Funnel	95x95	70	*Max* 60	12.7	-	0.5	0.88	-

CHAPTER 4

RESULTS AND DISCUSSIONS

4.1 NORMAL SIMULATION

Initially Simulation has to run in ABAQUS without taking any top fillet and height compensation effect. There are total six simulations has to run by changing geometric and process parameters as defined in Table 7 (step 3.3) from job 1 to job 6. For all these simulation, the same sheet material is *Al* 5052 having modulus of elasticity 70 *GPa* and Poison ratio 0.33 is used.

4.1.1 Job 1 for Cone with *SBS* 75x75 *mm*, *OD*=70 *mm*, α =60°, *TD*=8 *mm*, *h*=25 *mm*, *dz* =0.8 *mm*, t_o =0.5 *mm* and R_c =0

Job 1 is performed on sheet blank size of 75x75 *mm*. The geometry type for job1 is cone. Use hemi-spherical tool of diameter 8 *mm*, draw angle 60°, incremental step size in z-direction 0.8 *mm* is used. Opening diameter and height of the desired object should be 70 *mm*, 25 *mm* respectively.

The von Mises equivalent stress is the resultant of circumferential stress, meridional stress and thickness stress. There are less stresses observed in the flat and symmetrical rotational surface (green surface of figure 4.1(a)) because this surface under the plane strain stretching condition and maximum stresses are observed at the corners (red zone of figure 4.1(a)) due to biaxial stretching is occurred.

With the movement of the tool, deformation of sheet starts in the negative z-direction. Deformation occurs by stretching the sheet along the tool profile till the required depth of the desired geometry is achieved as shown in figure 4.1(b). As tool move along the required trajectory, deformation of sheet increases.

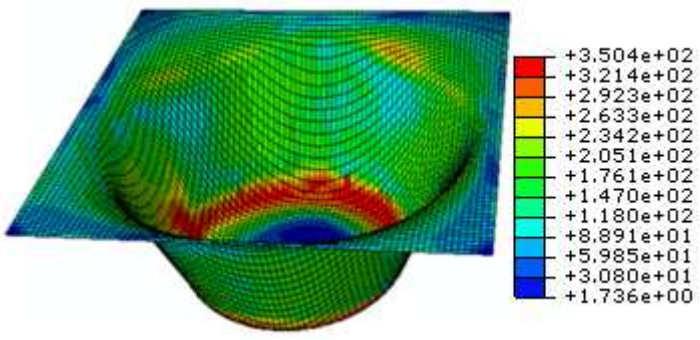

(a) Von Mises Equivalent stress (MPa)

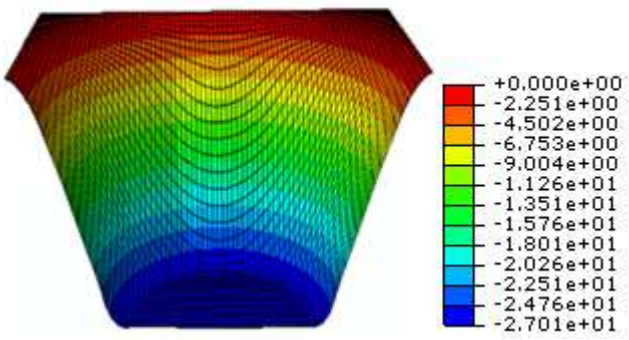

(b) Displacement/Profile (*mm*)

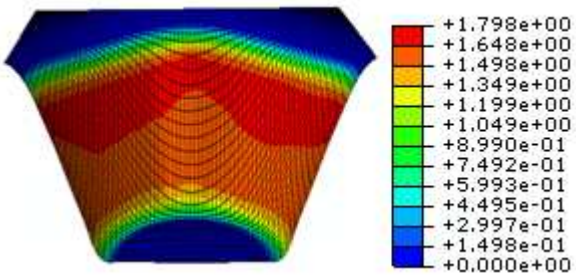

(c) Equivalent strain

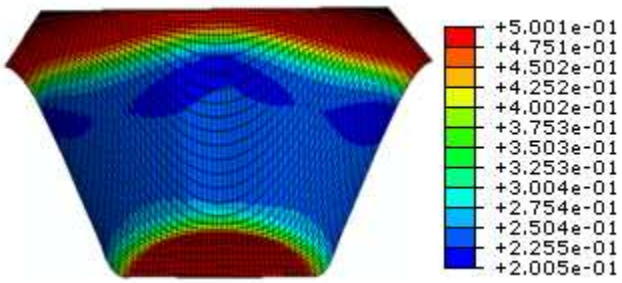

(d) Section Thickness (*mm*)

Figure 4.1: FEA simulation results of Job 1 for Cone with *SBS* 75x75 *mm*, *OD*=70 *mm*, α =60°, *TD*=8 *mm*, *h*=25*mm*, *dz* =0.8*mm*, t_o =0.5 *mm* and R_c =0

Strain increases with increase in the draw angle and decrease in incremental step size. It is depending upon circumferential, meridional and thickness strain. For the flat and symmetrical rotational surfaces, strain is more (red and orange zone of figure 4.1(c)) but it is less at the corner of the object as seen in figure 4.1(c).

Section thickness is decreases with increase in the draw angle and decrease in incremental step size. Its variation is nearly related to the strain, where strain is maximum there section thickness is minimum. This can be observed from the figure 4.1(c) and 4.1(d).

4.1.2 Job 2 for Cone with *SBS* 95x95 *mm*, *OD*=70 *mm*, α =60°, *TD*=8 *mm*, *h*=25 *mm*, *dz* =0.8 *mm*, t_o =0.5 *mm* and R_c =0

Job 2 for cone is performed on sheet blank size of 95x95 *mm*. Use of tool diameter 8 *mm*, draw angle 60°, incremental step size 0.8 *mm*, Opening diameter 70 *mm* and height 25 *mm* is used.

The von Mises equivalent stress is the resultant of circumferential stress, meridional stress and thickness stress. There are less stresses observed in the flat and symmetrical rotational surface (green surface of figure 4.2(a)) because this surface under the plane strain stretching condition and maximum stresses are observed at the corners (red zone of figure 4.2(a)) due to biaxial stretching is occurred.

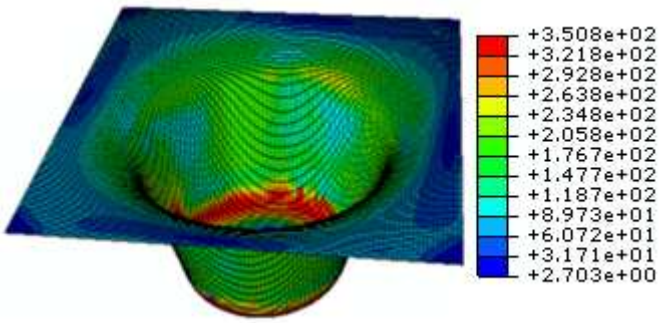

(a) Von Mises Equivalent stress (MPa)

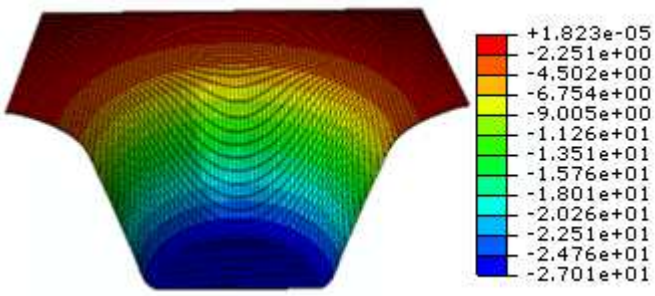

(b) Displacement/Profile (*mm*)

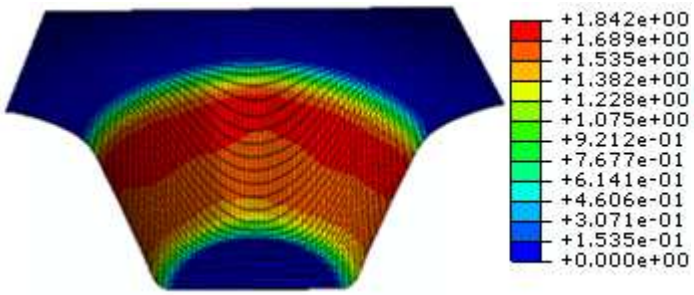

(c) Equivalent strain

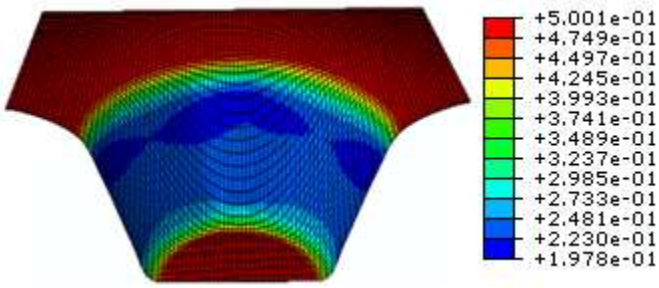

(d) Section Thickness (*mm*)

Figure 4.2: FEA simulation results of Job 2 for Cone with *SBS* 95x95 *mm*, *OD*=70 *mm*, α =60°, *TD*=8 *mm*, *h*=25*mm*, *dz* =0.8*mm*, t_o =0.5 *mm* and R_c =0

With the movement of the tool, deformation of sheet starts in the negative z-direction. Deformation occurs by stretching the sheet along the tool profile till the required depth of the desired geometry is achieved as shown in figure 4.2(b). As tool move along the required trajectory, deformation of sheet increases.

Strain increases with increase in the draw angle and decrease in incremental step size. It is depending upon circumferential, meridional and thickness strain. For the flat and symmetrical rotational surfaces, strain is more (red and orange zone of figure 4.2(c)) but it is less at the corner of the object as seen in figure 4.2(c).

Section thickness is decreases with increase in the draw angle and decrease in incremental step size. Its variation is nearly related to the strain, where strain is maximum there section thickness is minimum. This can be observed from the figure 4.2(c) and 4.2(d).

4.1.3 Job 3 for Pyramid with *SBS* 75x75 *mm*, *OD*=70 *mm*, α =60°, *TD*=8 *mm*, *h*=25 *mm*, *dz* =0.8 *mm*, t_o =0.5 *mm* and R_c =0

Job 3 is performed on sheet blank size of 75x75 *mm*. The geometry type for job 3 is Pyramid. Use hemi-spherical tool of diameter 8 mm, draw angle 60°, incremental step size in z-direction 0.8 *mm*. Opening diameter and height of the desired object should be 70 *mm*, 25 *mm* respectively.

The von Mises equivalent stress is the resultant of circumferential stress, meridional stress and thickness stress. There are less stresses observed in the flat and symmetrical rotational surface (green surface of figure 4.3(a)) because this surface under the plane strain stretching condition and maximum stresses are observed at the corners (red zone of figure 4.3(a)) due to biaxial stretching is occurred.

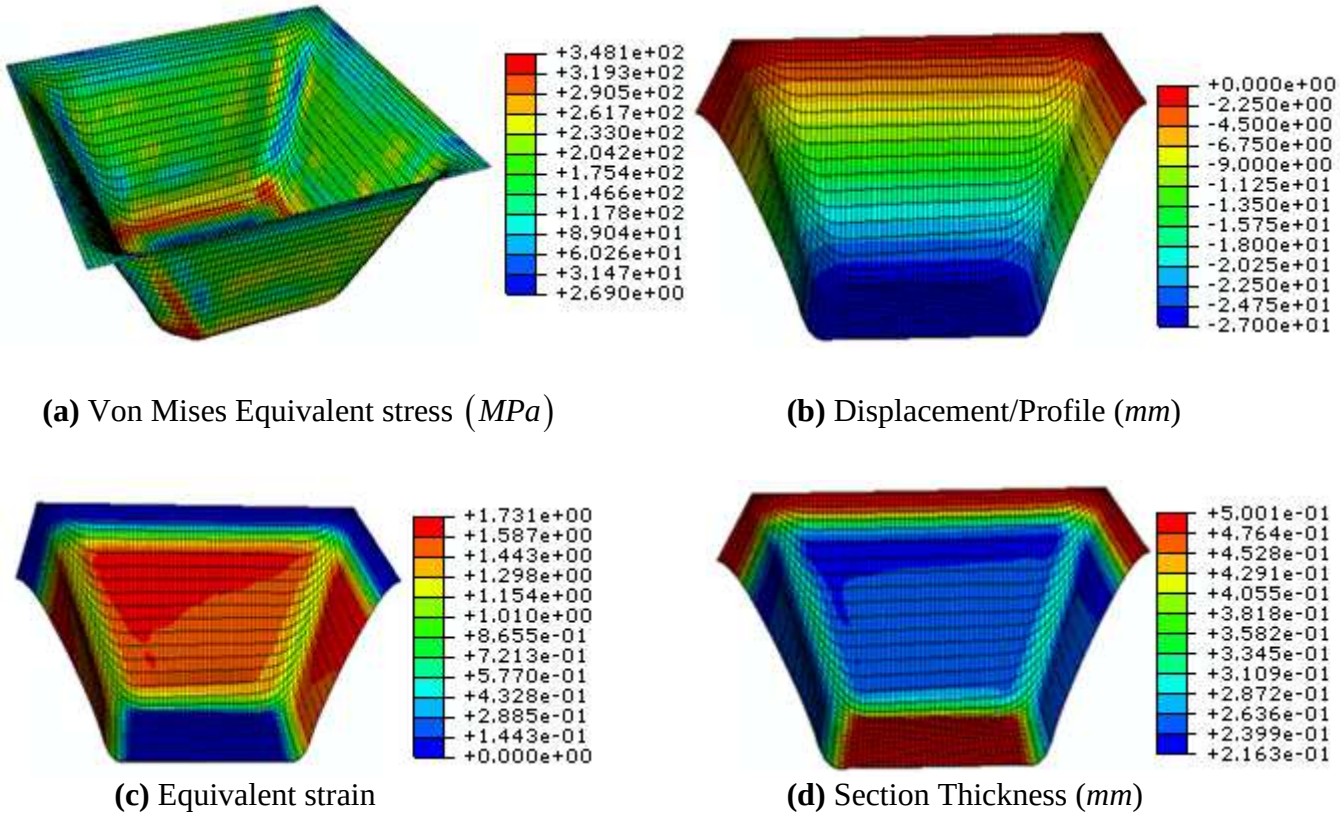

(a) Von Mises Equivalent stress (MPa) **(b)** Displacement/Profile (*mm*)

(c) Equivalent strain **(d)** Section Thickness (*mm*)

Figure 4.3: FEA simulation results of Job 3 for Pyramid with *SBS* 75x75 *mm*, *OD*=70 *mm*, α =60°, *TD*=8 *mm*, *h*=25*mm*, *dz* =0.8*mm*, t_o =0.5 *mm* and R_c =0

With the movement of the tool, deformation of sheet starts in the negative z-direction. Deformation occurs by stretching the sheet along the tool profile till the required depth of the desired geometry is achieved as shown in figure 4.3(b). As tool move along the required trajectory, deformation of sheet increases.

Strain increases with increase in the draw angle and decrease in incremental step size. It is depending upon circumferential, meridional and thickness strain. For the flat and symmetrical rotational surfaces, strain is more (red and orange zone of figure 4.3(c)) but it is less at the corner of the object as seen in figure 4.3(c).

Section thickness is decreases with increase in the draw angle and decrease in incremental step size. Its variation is nearly related to the strain, where strain is maximum there section thickness is minimum. This can be observed from the figure 4.3(c) and 4.3(d).

4.1.4 Job 4 for Pyramid with *SBS* 95x95 *mm*, *OD*=70 *mm*, α =60°, *TD*=8 *mm*, *h*=25 *mm*, *dz* =0.8 *mm*, t_o =0.5 *mm* and R_c =0

Job 4 is performed on sheet blank size of 95x95 *mm*. The geometry type for job 4 is Pyramid. Use hemi-spherical tool of diameter 8 *mm*, draw angle 60°, incremental step size in z-direction

0.8 *mm*. Opening diameter and height of the desired object should be 70 *mm*, 25 *mm* respectively. The results for equivalent stress, profile, plastic equivalent strain and section thickness obtained in the same fashion as for the jobs 1 to 3.

4.1.5 Job 5 for Cone with *SBS* 75x75 *mm*, *OD*=70 *mm*, α =45°, *TD*=8 *mm*, *h*=25 *mm*, *dz* =0.8 *mm*, t_o =0.5 *mm* and R_c =0

Job 5 is performed on sheet blank size of 75x75 *mm*. The geometry type for job 5 is Pyramid. Use hemi-spherical tool of diameter 8 *mm*, draw angle 45°, incremental step size in z-direction 0.8 *mm*. Opening diameter and height of the desired object should be 70 *mm*, 25 *mm* respectively. The results for equivalent stress, profile, plastic equivalent strain and section thickness obtained in the same fashion as for the jobs 1 to 3.

4.1.6 Job 6 for Pyramid with *SBS* 75x75 *mm*, *OD*=70 *mm*, α =45°, *TD*=8 *mm*, *h*=25 *mm*, *dz* =0.8 *mm*, t_o =0.5 *mm* and R_c =0

Job 6 is performed on sheet blank size of 75x75 *mm*. The geometry type for job 6 is pyramid. Use hemi-spherical tool of diameter 8 *mm*, draw angle 45°, incremental step size in z-direction 0.8 *mm*. Opening diameter & height of the desired object should be 70 *mm*, 25 *mm* respectively.

The von Mises equivalent stress is the resultant of circumferential stress, meridional stress and thickness stress. There are less stresses observed in the flat and symmetrical rotational surface (green surface of figure 4.4(a)) because this surface under the plane strain stretching condition and maximum stresses are observed at the corners (red zone of figure 4.4(a)) due to biaxial stretching is occurred.

With the movement of the tool, deformation of sheet starts in the negative z-direction. Deformation occurs by stretching the sheet along the tool profile till the required depth of the desired geometry is achieved as shown in figure 4.4(b). As tool move along the required trajectory, deformation of sheet increases.

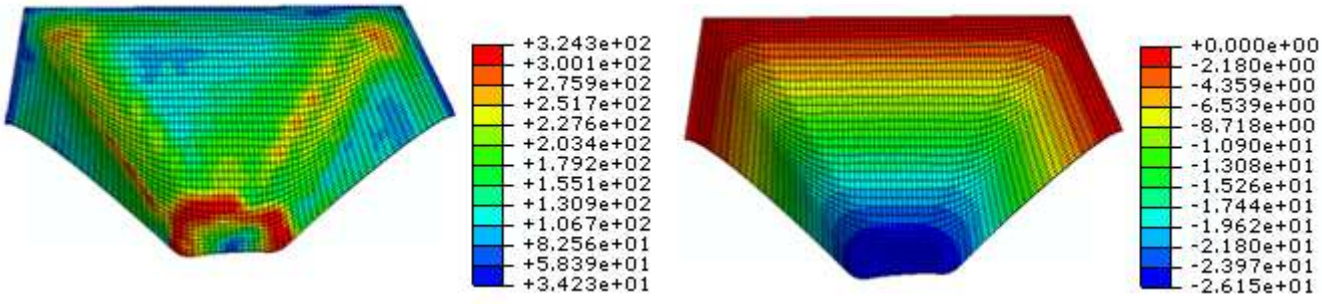

(a) Von Mises Equivalent stress (MPa) **(b)** Displacement/Profile (*mm*)

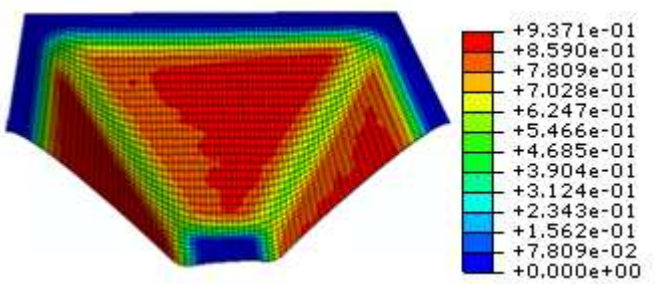

(c) Equivalent strain

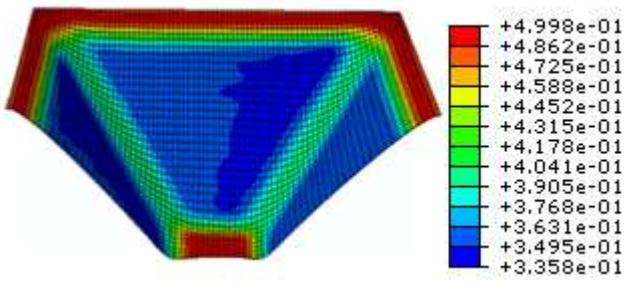

(d) Section Thickness (*mm*)

Figure 4.4: FEA simulation results of Job 6 for Pyramid with *SBS* 75x75 *mm* , *OD* =70 *mm*, α =45°, *TD*=8 *mm*, *h*=25*mm*, *dz* =0.8*mm*, t_o =0.5 *mm* and R_c =0

Strain increases with increase in the draw angle and decrease in incremental step size. It is depending upon circumferential, meridional and thickness strain. For the flat and symmetrical rotational surfaces, strain is more (red and orange zone of figure 4.4(c)) but it is less at the corner of the object as seen in figure 4.4(c).

Section thickness is decreases with increase in the draw angle and decrease in incremental step size. Its variation is nearly related to the strain, where strain is maximum there section thickness is minimum. This can be observed from the figure 4.4(c) and 4.4(d).

4.2 STUDY THE EFFECT OF BACK UP SIZE IN BENDING AND COMPONENT GEOMETRIC ACCURACY

There is no back up size plate is used in normal simulation as discussed in step 4.1 from job 1 to job 6, which results in bending at start of the component deformation. There is also some problem in component required height as compared with simulation result. Simulated resultant height is always greater than the required height because of tool compensation. Now discuss the effect of back up size in bending and component geometric accuracy graphically for all jobs 1 to 6 explained in step 4.1.

4.2.1 Study of FEA results and ideal geometry for component profile of job 1 for Cone with *SBS* 75x75 *mm*, *OD*=70 *mm*, α =60°, *TD*=8 *mm*, *h*=25 *mm*, *dz* =0.8 *mm*, t_o =0.5 *mm*, R_c =0

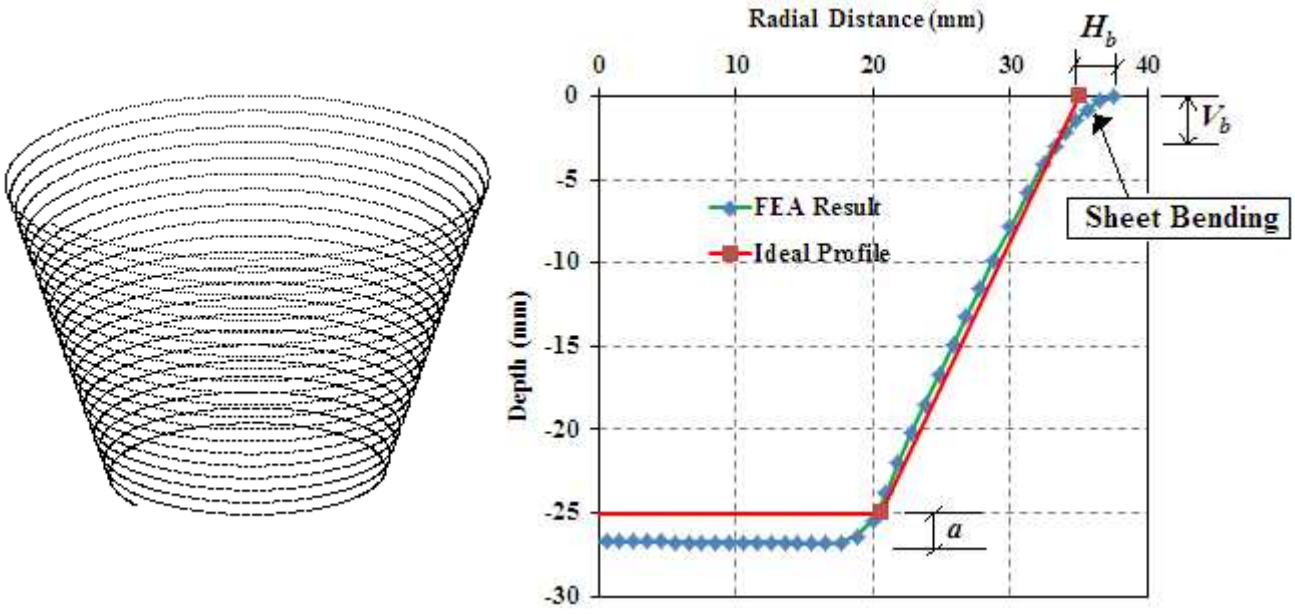

(a) Toolpath for cone **(b)** Comparison of Ideal Profile and *FEA* result

Figure 4.5: Study of Job 1 for Cone with *SBS* 75x75 *mm*, *OD*=70 *mm*, α =60°, *TD*=8 *mm*, *h*=25*mm*, *dz* =0.8*mm*, t_o =0.5 *mm* and R_c =0

Determination of (a) analytically:

Tool diameter and draw angle is known, and then (*a*), as shown in figure 4.5(b), can be determined by using the expression as derived in 3.1.1.3.1 is given by:

$$\Delta y = r \times (1 - \cos\alpha)$$

Here

$\Delta y = a$ (to be calculated)

r = tool radius = 4 mm

α = draw angle = 60°

By putting these values in the above equation, it was obtained

a = 2 *mm*

Determination of a, H_b, H_v from *FEA* results:

a = 2.01 *mm*

H_b =1.99 *mm*

V_b = 1.27 *mm*

This shows that, by using height compensation as discussed in 3.1.1.3.1, the *FEA* results (in terms of profile) can be obtained almost equal to the ideal required geometry.

4.2.2 Study of FEA results and ideal geometry for component profile of job 2 for Cone with *SBS* 95x95 *mm* , *OD*=70 *mm*, α =60°, *TD*=8 *mm*, *h*=25 *mm*, *dz* =0.8 *mm*, t_o =0.5 *mm*, R_c =0

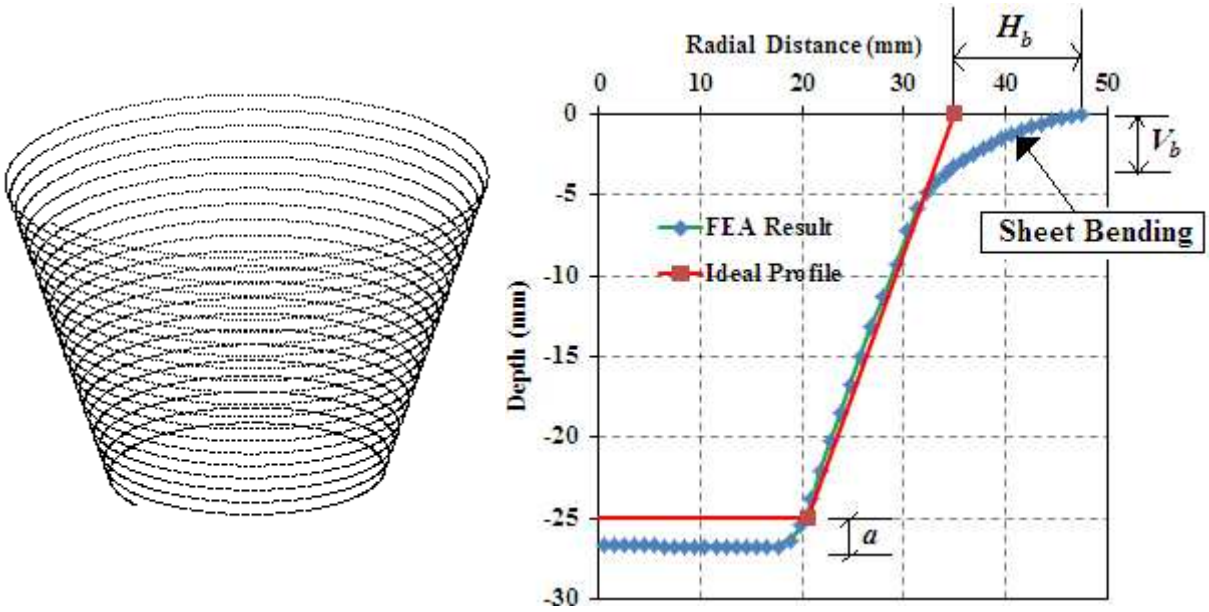

(a) Toolpath for cone **(b)** Comparison of Ideal Profile and *FEA* result

Figure 4.6: Study of Job 2 for Cone with *SBS* 95x95 *mm* , *OD*=70 *mm*, α =60°, *TD*=8 *mm*, *h*=25*mm*, *dz* =0.8*mm*, t_o =0.5 *mm* and R_c =0

Determination of (a) analytically:

Tool diameter and draw angle is known, and then (*a*), as shown in figure 4.6(b), can be determined by using the expression as derived in 3.1.1.3.1 is given by:

$$\Delta y = r \times (1 - \cos\alpha)$$

Here

$\Delta y = a$ (to be calculated)

r = tool radius = 4 *mm*

α = draw angle = 60°

By putting these values in the above equation, and get

a = 2 *mm*

Determination of a, H_b, H_v from *FEA* results:

a = 2.01 *mm*

H_b =7.56 *mm*

V_b = 3.16 *mm*

This shows that, by using height compensation as discussed in 3.1.1.3.1, the *FEA* results (in terms of profile) can be obtained almost equal to the ideal required geometry.

4.2.3 Study of FEA results and ideal geometry for component profile of job 3 for pyramid with *SBS* 75x75 *mm*, *OD*=70 *mm*, α =60°, *TD*=8 *mm*, *h*=25 *mm*, *dz* =0.8 *mm*, t_o =0.5 *mm*, R_c =0

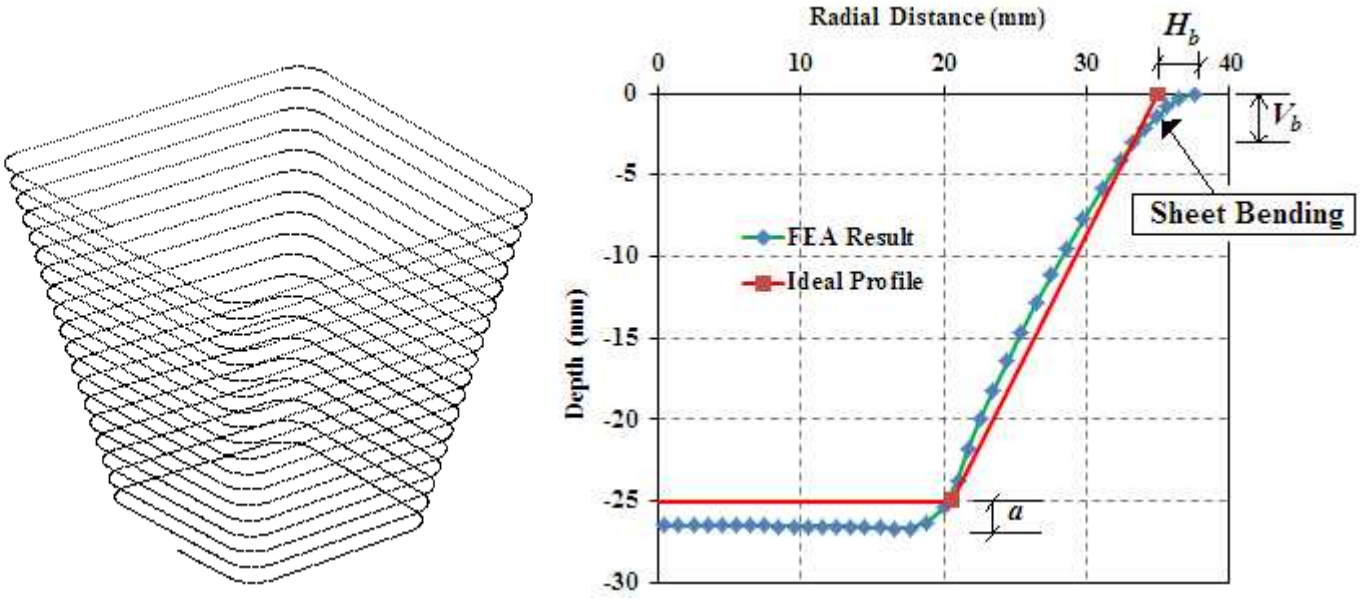

(a) Toolpath for Pyramid **(b)** Comparison of Ideal Profile and *FEA* result

Figure 4.7: Study of Job 3 for Pyramid with *SBS* 75x75 *mm*, *OD*=70 *mm*, α =60°, *TD*=8 *mm*, *h*=25*mm*, *dz* =0.8*mm*, t_o =0.5 *mm* and R_c =0

Determination of (a) analytically:

Tool diameter and draw angle is known, and then (*a*), as shown in figure 4.7(b), can be determined by using the expression as derived in 3.1.1.3.1 is given by:

$$\Delta y = r \times (1 - \cos\alpha)$$

Here

$\Delta y = a$ (to be calculated)

r = 4 *mm*, α = 60°

By putting these values in the above equation, we get

a = 2 *mm*

Determination of a, H_b, H_v from *FEA* results:

a = 2.00 *mm*

H_b =1.99 *mm*

V_b =1.33 *mm*

This shows that, by using height compensation as discussed in 3.1.1.3.1, the *FEA* results (in terms of profile) can be obtained almost equal to the ideal required geometry.

4.2.4 Study of FEA results and ideal geometry for component profile of job 4 for pyramid with *SBS* 95x95 *mm*, *OD*=70 *mm*, α =60°, *TD*=8 *mm*, *h*=25 *mm*, *dz* =0.8 *mm*, t_o =0.5 *mm* and R_c =0

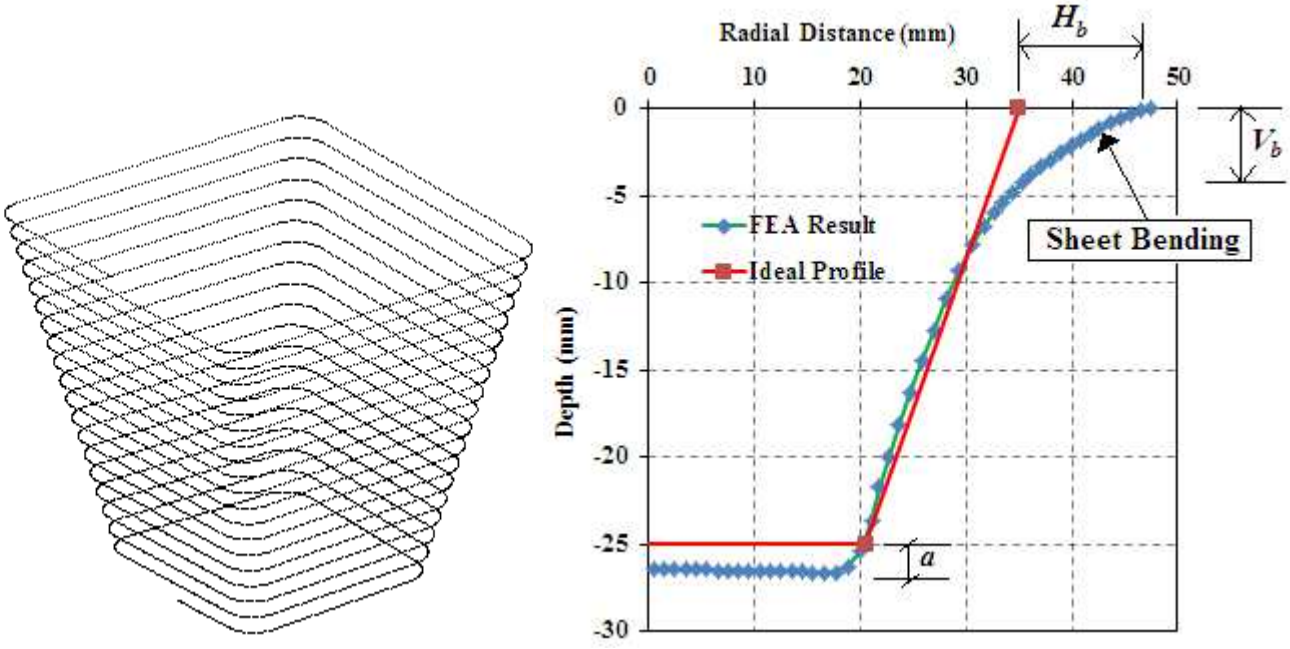

(a) Toolpath for Pyramid **(b)** Comparison of Ideal Profile and *FEA* result

Figure 4.8: Study of Job 4 for Pyramid with *SBS* 95x95 *mm*, *OD*=70 *mm*, α =60°, *TD*=8 *mm*, *h*=25*mm*, *dz* =0.8*mm*, t_o =0.5 *mm* and R_c =0

Determination of (a) analytically:

Tool diameter and draw angle is known, and then (*a*), as shown in figure 4.8(b), can be determined by using the expression as derived in 3.1.1.3.1 is given by:

$$\Delta y = r \times (1 - \cos\alpha)$$

Here

$\Delta y = a$ (to be calculated)

r = 4 *mm*, α = 60°

By putting these values in the above equation, and get

a = 2 *mm*

Determination of a, H_b, H_v from *FEA* results:

H_b =8.60 *mm*

V_b =4.56 *mm*

This shows that, by using height compensation as discussed in 3.1.1.3.1, the *FEA* results (in terms of profile) can be obtained almost equal to the ideal required geometry.

4.2.5 Study of FEA results and ideal geometry for component profile of job 5 for cone with *SBS* 75x75 *mm*, *OD*=70 *mm*, α =45°, *TD*=8 *mm*, *h*=25 *mm*, *dz* =0.8 *mm*, t_o =0.5 *mm*, R_c =0

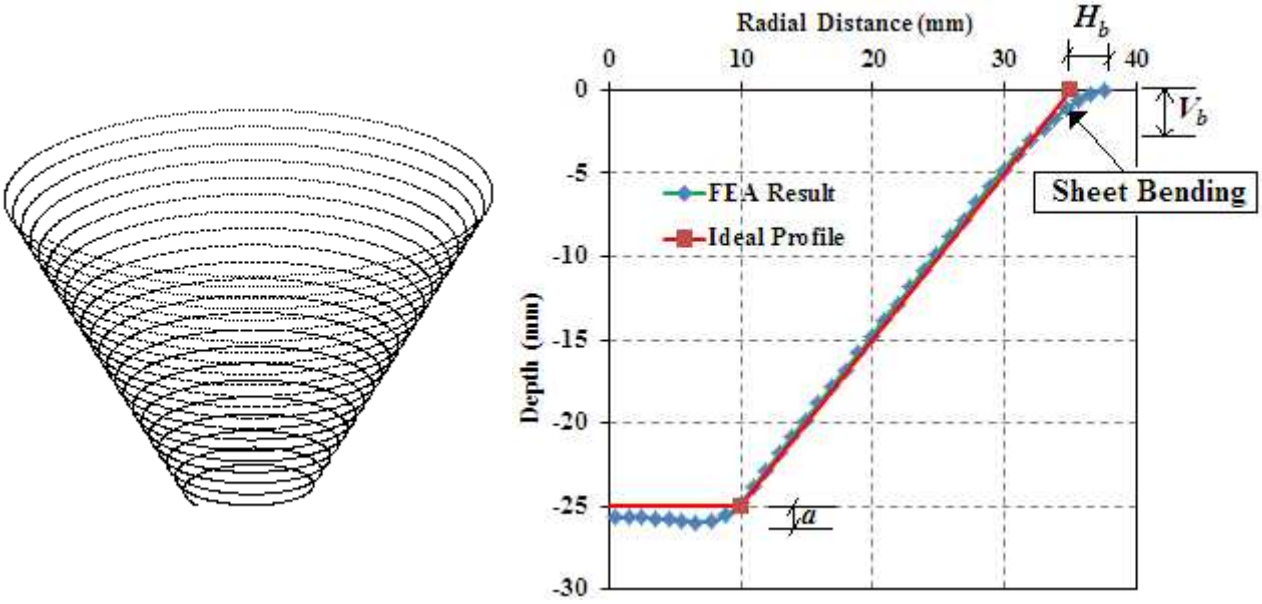

(a) Toolpath for cone **(b)** Comparison of Ideal Profile and *FEA* result

Figure 4.9: Study of Job 5 for Cone with *SBS* 75x75 *mm*, *OD*=70 *mm*, α =45°, *TD*=8 *mm*, *h*=25*mm*, *dz* =0.8*mm*, t_o =0.5 *mm* and R_c =0

Determination of (a) analytically:

Tool diameter and draw angle is known, and then (*a*), as shown in figure 4.9(b), can be determined by using the expression as derived in 3.1.1.3.1 is given by:

$$\Delta y = r \times (1 - \cos\alpha)$$

Here

$\Delta y = a$ (to be calculated)

r = 4 *mm*, α = 60°

By putting these values in the above equation, we get

a = 1.17 *mm*

Determination of a, H_b, H_v from *FEA* results:

a = 1.16 *mm*

H_b =1.98 *mm*

V_b =0.93 *mm*

This shows that, by using height compensation as discussed in 3.1.1.3.1, the *FEA* results (in terms of profile) can be obtained almost equal to the ideal required geometry.

4.2.6 Study of FEA results and ideal geometry for job 6 for pyramid with *SBS* 75x75 *mm*, *OD*=70 *mm*, α =45°, *TD*=8 *mm*, *h*=25 *mm*, *dz* =0.8 *mm*, t_o =0.5 *mm* and R_c =0

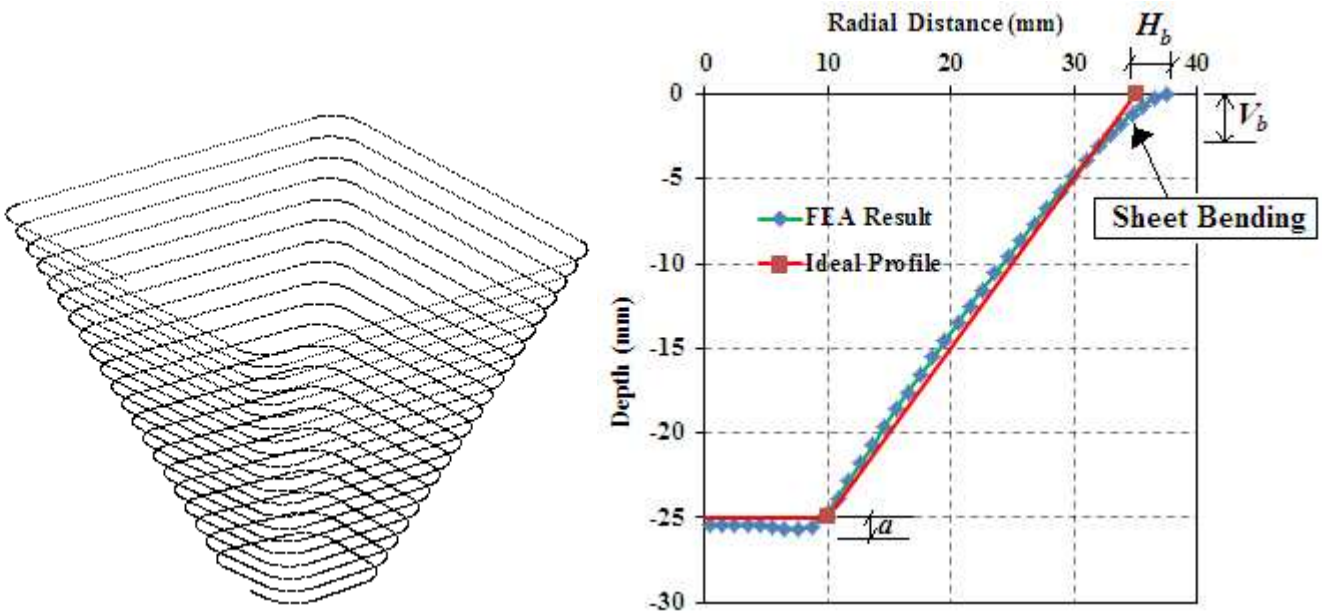

(a) Toolpath for Pyramid **(b)** Comparison of Ideal Profile and *FEA* result

Figure 4.10: Study of Job 6 for Pyramid with *SBS* 75x75 *mm*, *OD*=70 *mm*, α =45°, *TD*=8 *mm*, *h*=25*mm*, *dz* =0.8*mm*, t_o =0.5 *mm* and R_c =0

Determination of (a) analytically:

Tool diameter and draw angle is known, and then (*a*), as shown in figure 4.10(b), can be determined by using the expression as derived in 3.1.1.3.1 is given by:

$$\Delta y = r \times (1 - \cos\alpha)$$

Here

$\Delta y = a$ (to be calculated)

r = 4 *mm* and α = 45°

By putting these values in the above equation, and get

a = 1.17 *mm*

Determination of a, H_b, H_v from *FEA* results:

a = 1.15 *mm*

H_b =1.99 *mm*

V_b =1.01 *mm*

This shows that, by using height compensation as discussed in 3.1.1.3.1, the *FEA* results (in terms of profile) can be obtained almost equal to the ideal required geometry.

4.3 CHARACTERIZATION OF BENDING:

After the determination of Horizontal and vertical bending from the simulation results job 1 to job 6 in step 4.2, it can be derive the analytical expression for Horizontal bending $\left(H_b\right)$ and vertical bending $\left(V_b\right)$ using a Datafit software. These expressions are given below:

$$H_b = \left(\frac{\text{Blank size-opening diameter}}{4}\right) \times \alpha \times \frac{\Pi}{180}$$

$$V_b = \frac{H_b}{2}$$

After that calculate the Horizontal and Vertical bending using above formulas for jobs 1 to 6 and compare its value with the simulated result as given in Table 8.

Table 8: Comparison table for FEA and Calculated Horizontal and vertical bending

S. No	Geometry type	Blank size (mm)	Opening diameter (mm)	Draw angle ($degree$)	Tool dia (mm)	Simulation Result		Calculated Values	
						Horizontal bending (mm)	Vertical Bending (mm)	Horizontal bending (mm)	Vertical Bending (mm)
1	Cone	75x75	70	60	8	1.99	1.27	2.31	1.15
2	Cone	95x95	70	60	8	7.56	3.16	7.54	3.77
3	Pyramid	75x75	70	60	8	1.99	1.33	2.31	1.15
4	Pyramid	95x95	70	60	8	8.60	4.56	7.54	3.77
5	Cone	75x75	70	45	8	1.98	0.93	1.98	0.99
6	Pyramid	75x75	70	45	8	1.99	1.01	1.98	0.99

4.4 IMPROVEMENTS TO REDUCE BENDING AND GEOMETRIC DEVIATION

4.4.1 Giving top fillet irrespective of back up plate size and height Compensation for better dimensional accuracy

Six simulations has to run from job 7 to job 12 by giving top fillet irrespective of back up plate size and using height compensation for each job corresponding to the value of variable (a) obtained from first six simulation results in step 4.2. For all these simulation, the same sheet material is *Al* 5052 having modulus of elasticity 70 *GPa* and Poison ratio 0.33 is used.

4.4.1.1 Comparison of FEA results for Job 7 (Top fillet cone with *SBS* 75x75 *mm*, *OD*=70 *mm*, α =60°, *TD*=8 *mm*, *h*=25 *mm*, *dz* =0.8 *mm*, t_o =0.5 *mm* & R_c =3.75 *mm*) and Job 1 (Cone with *SBS* 75x75 *mm*, *OD*=70 *mm*, α =60°, *TD*=8 *mm*, *h*=25 *mm*, *dz* =0.8 *mm*, t_o =0.5 *mm*, R_c =0)

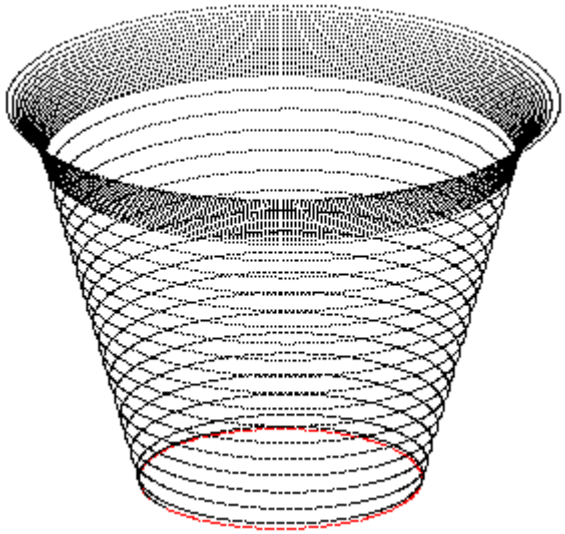

(a) Toolpath for fillet cone

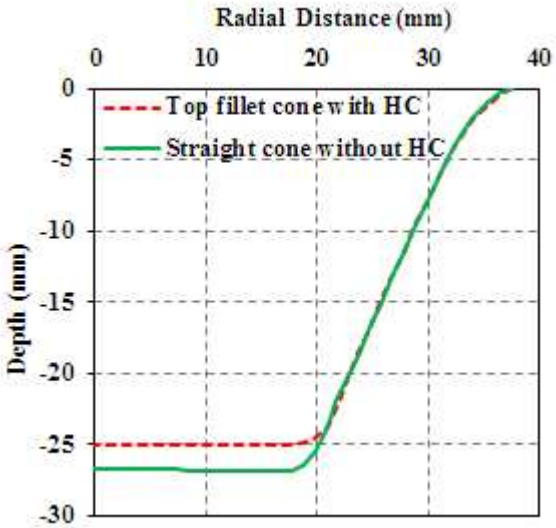

(b) Comparison of Profile

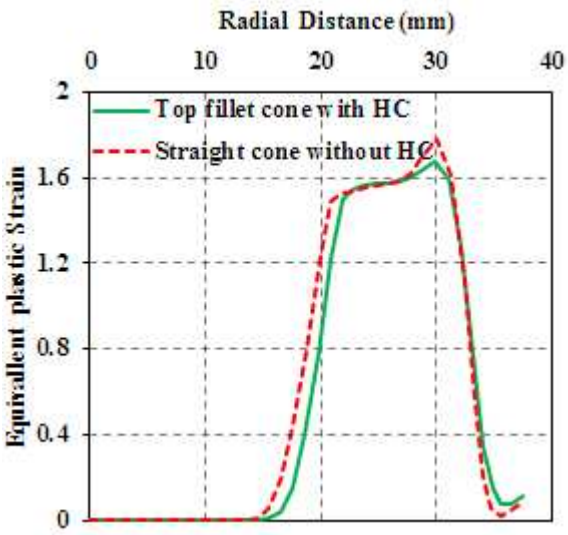

(c) Comparison of Equivalent plastic strain

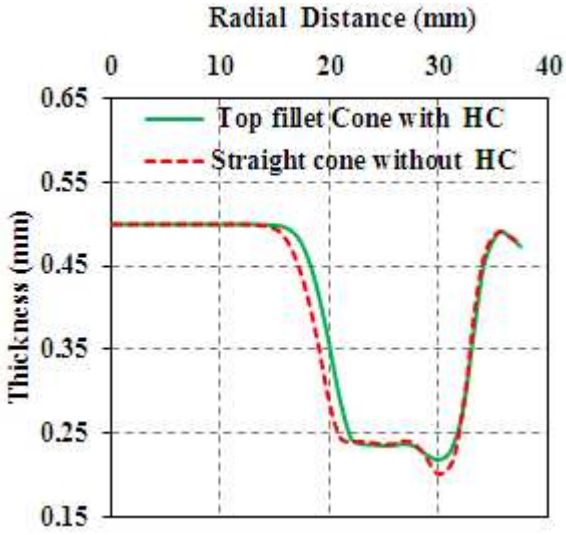

(d) Comparison of thickness

Figure 4.11: Study of FEA results for Job 7 (Top fillet cone with *SBS* 75x75 *mm*, *OD*=70 *mm*, α =60°, *TD*=8 *mm*, *h*=25*mm*, *dz* =0.8*mm*, t_o =0.5 *mm* and R_c =3.75 *mm*) and Job 1 (Cone with *SBS* 75x75 mm^2, *OD*=70 *mm*, α =60°, *TD*=8 *mm*, *h*=25*mm*, *dz* =0.8*mm*, t_o =0.5 *mm* and R_c =0)

By giving the top fillet, there is not any drastically change in the profile at the region of necking. But the problem of higher indentation due to tool compensation has been solved. It is predicted that the height of deformed component is almost equal to the required height as shown in Figure 4.11(b). When using top fillet, strain distribution along the component profile is reduced in comparison of normal simulation without use of any fillet at top as shown in Figure 4.11(c). If strain is reduced,

then better results in thickness can be obtained i.e. sheet thickness will increase. The reason is deformation takes place with gradually increase in draw angle from 0 degree to required draw angle instead of direct go with required draw angle in normal simulation.

Sheet thickness variation is nearly related to the strain, where strain is maximum there section thickness is minimum and vice-versa. With using top fillet, strain distribution along the component profile is reduced which results in increase in section thickness as shown in Figure 4.11(d) and Table 9.

Table 9: Thickness comparison for straight cone and top fillet cone (*SBS* 75x75 *mm* , α =60°)

Radial Distance (in *mm*)	Thickness Corresponding to Job 1 for cone with *SBS* 75x75 *mm* , α =60° (in *mm*)	Thickness Corresponding to Job 7 for top fillet cone with *SBS* 75x75 *mm* , α =60° (in *mm*)	% age Increase in Thickness
15.49	0.490	0.498	1.65
16.49	0.470	0.492	4.79
17.52	0.430	0.475	10.45
18.58	0.368	0.436	18.61
19.74	0.289	0.371	28.70
20.91	0.246	0.293	19.06
21.93	0.240	0.245	1.91
29.96	0.201	0.219	8.60
31.11	0.218	0.229	5.09

4.4.1.2 Comparison of FEA results for Job 8 (Top fillet cone with *SBS* 95x95 *mm* , *OD*=70 *mm*, α =60°, *TD*=8 *mm*, *h*=25 *mm*, *dz* =0.8 *mm*, t_o =0.5 *mm* & R_c =3.75 *mm*) and Job 2 (Cone with *SBS* 95x95 *mm* , *OD*=70 *mm*, α =60°, *TD*=8 *mm*, *h*=25 *mm*, *dz* =0.8 *mm*, t_o =0.5 *mm*, R_c =0)

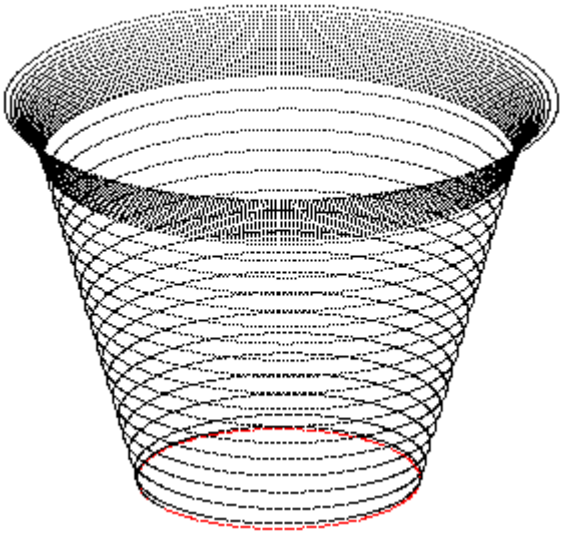

(a) Toolpath for fillet cone

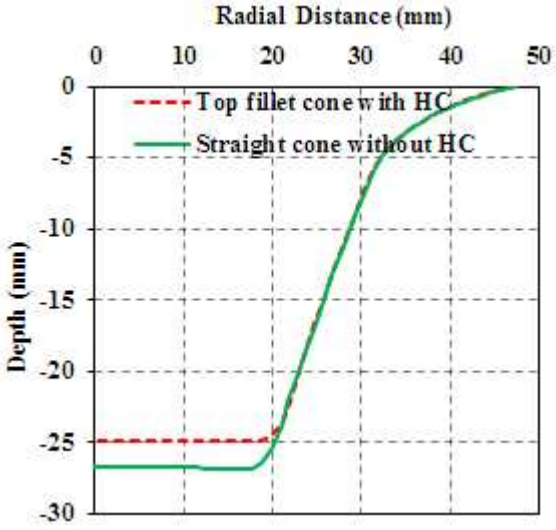

(b) Comparison of Profile

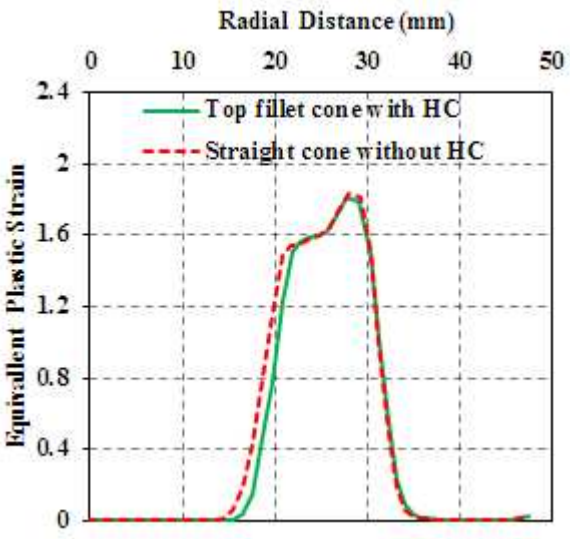

(c) Comparison of Equivalent plastic strain

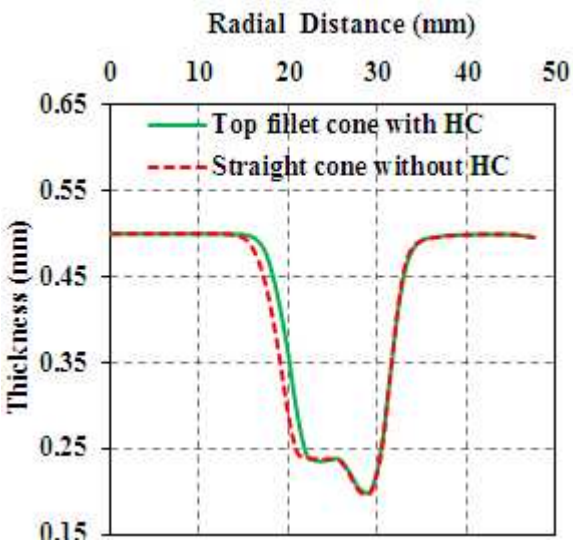

(d) Comparison of thickness

Figure 4.12: Study of FEA results for Job 8 (Top fillet cone with *SBS* 95x95 *mm* , *OD*=70 *mm*, α =60°, *TD*=8 *mm*, *h*=25*mm*, *dz* =0.8*mm*, t_o =0.5 *mm* and R_c =3.75 *mm*) and Job 2 (Cone with *SBS* 95x95 *mm* , *OD*=70 *mm*, α =60°, *TD*=8 *mm*, *h*=25*mm*, *dz* =0.8*mm*, t_o =0.5 *mm* and R_c =0)

By giving the top fillet, there is not any drastically change in the profile at the region of necking. But the problem of higher indentation due to tool compensation has been solved. It is predicted that the height of deformed component is almost equal to the required height as shown in Figure 4.12(b). When using top fillet, strain distribution along the component profile is reduced in comparison of normal simulation without use of any fillet at top as shown in Figure 4.12(c). If strain is reduced, then better results in thickness can be obtained i.e. sheet thickness will increase. The reason is deformation takes place with gradually increase in draw angle from 0 degree to required draw angle instead of direct go with required draw angle in normal simulation.

Sheet thickness variation is nearly related to the strain, where strain is maximum there section thickness is minimum and vice-versa. With using top fillet, strain distribution along the component profile is reduced which results in increase in section thickness as shown in Figure 4.12(d) and Table 10.

Table 10: Thickness comparison for straight cone and top fillet cone (*SBS* 95x95 *mm* , α =60°)

Radial Distance (in *mm*)	Thickness Corresponding to Job 2 for cone with *SBS* 95x95 *mm* , α =60° (in *mm*)	Thickness Corresponding to Job 8 for Fillet cone with *SBS* 95x95 *mm* , α =60° (in *mm*)	% age Increase in Thickness
15.48	0.490	0.498	1.57
16.49	0.471	0.493	4.55
17.51	0.433	0.476	9.91
18.57	0.369	0.437	18.52

19.75	0.291	0.374	28.36
20.93	0.247	0.293	18.94
21.96	0.239	0.244	2.20
25.72	0.236	0.237	0.67
26.73	0.221	0.224	1.45
27.87	0.200	0.204	2.29

4.4.1.3 Comparison of FEA results for Job 9 (Top fillet pyramid with *SBS* 75x75 *mm*, *OD*=70 *mm*, α =60°, *TD*=8 *mm*, *h*=25 *mm*, *dz* =0.8 *mm*, t_o =0.5 *mm* and R_c =3.75 *mm*) and Job 3 (pyramid with *SBS* 75x75 *mm*, *OD*=70 *mm*, α =60°, *TD*=8 *mm*, *h*=25 *mm*, *dz* =0.8 *mm*, t_o =0.5 *mm* and R_c =0)

By giving the top fillet, there is not any drastically change in the profile at the region of necking. But the problem of higher indentation due to tool compensation has been solved. It is predicted that the height of deformed component is almost equal to the required height as shown in Figure 4.13(b). When using top fillet, strain distribution along the component profile is reduced in comparison of normal simulation without use of any fillet at top as shown in Figure 4.13(c). If strain is reduced, then better results in thickness can be obtained i.e. sheet thickness will increase. The reason is deformation takes place with gradually increase in draw angle from 0 degree to required draw angle instead of direct go with required draw angle in normal simulation.

Sheet thickness variation is nearly related to the strain, where strain is maximum there section thickness is minimum and vice-versa. With using top fillet, strain distribution along the component profile is reduced which results in increase in section thickness as shown in Figure 4.13(d) and Table 11.

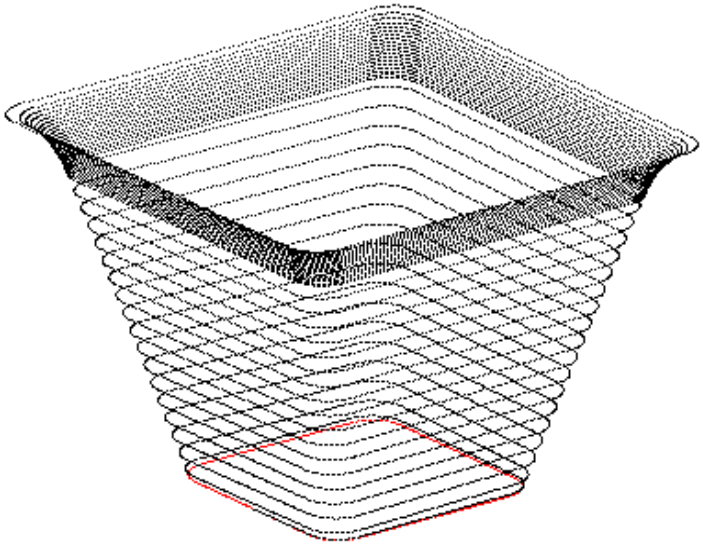

(a) Toolpath for fillet Pyramid

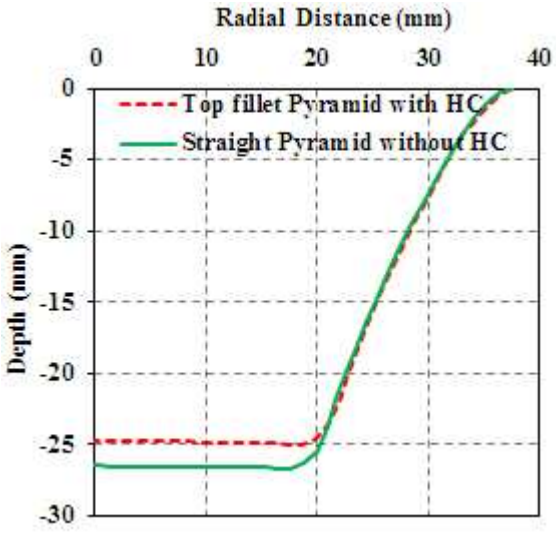

(b) Comparison of Profile

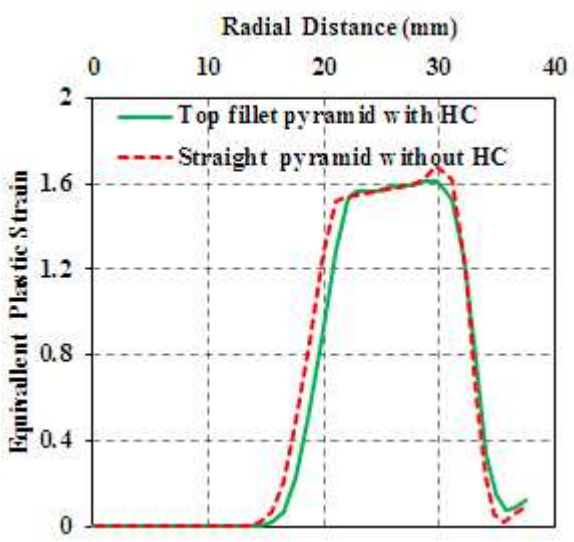

(c) Comparison of Equivalent plastic strain

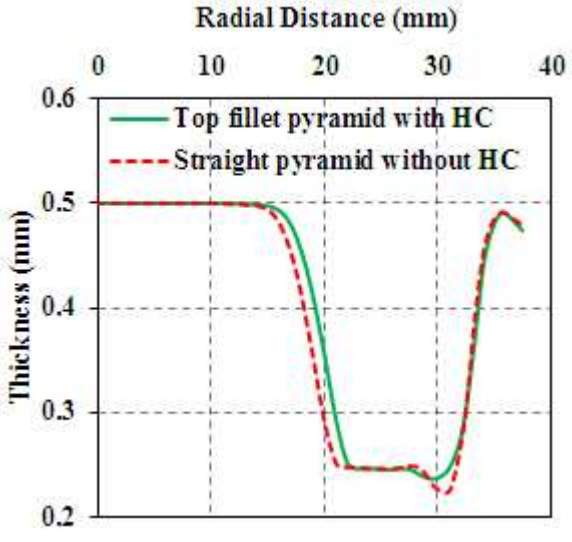

(d) Comparison of thickness

Figure 4.13: Study of FEA results for Job 9 (Top fillet Pyramid with *SBS* 75x75 *mm* , *OD*=70 *mm*, α =60°, *TD*=8 *mm*, *h*=25*mm*, *dz* =0.8*mm*, t_o =0.5 *mm* and R_c =3.75 *mm*) and Job 3 (Pyramid with *SBS* 75x75 *mm* , *OD*=70 *mm*, α =60°, *TD*=8 *mm*, *h*=25*mm*, *dz* =0.8*mm*, t_o =0.5 *mm* , R_c =0)

Table 11: Thickness comparison for straight pyramid and fillet pyramid (*SBS* 75x75 *mm* , α =60°)

Radial Distance (in *mm*)	Thickness Corresponding to Job 3 for Pyramid with *SBS* 75x75 *mm* , α =60° (in *mm*)	Thickness Corresponding to Job 9 for Top fillet Pyramid with *SBS* 75x75 *mm* , α =60° (in *mm*)	% age Increase in Thickness
14.50	0.497	0.498	0.35
15.51	0.489	0.496	1.41
16.52	0.469	0.488	4.09
17.55	0.429	0.467	8.69
18.66	0.364	0.427	17.12
19.85	0.290	0.363	25.19
21.05	0.252	0.291	15.60
22.02	0.248	0.252	1.52
29.91	0.228	0.237	3.79
31.08	0.226	0.248	9.75

4.4.1.4 Comparison of FEA results for Job 10 (Top fillet pyramid with *SBS* 95x95 *mm*, *OD*=70 *mm*, α =60°, *TD*=8 *mm*, *h*=25 *mm*, *dz* =0.8 *mm*, t_o =0.5 *mm* and R_c =3.75 *mm*) and Job 4 (pyramid with *SBS* 95x95 *mm*, *OD*=70 *mm*, α =60°, *TD*=8 *mm*, *h*=25 *mm*, *dz* =0.8 *mm*, t_o =0.5 *mm* and R_c =0)

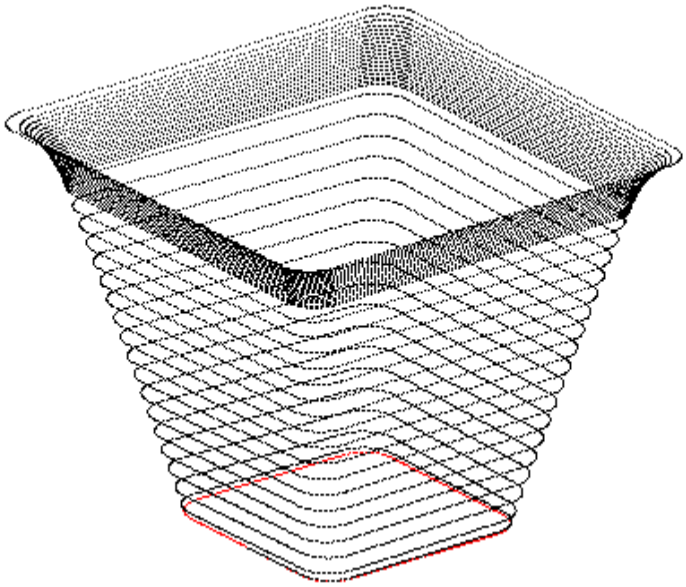

(a) Toolpath for fillet Pyramid

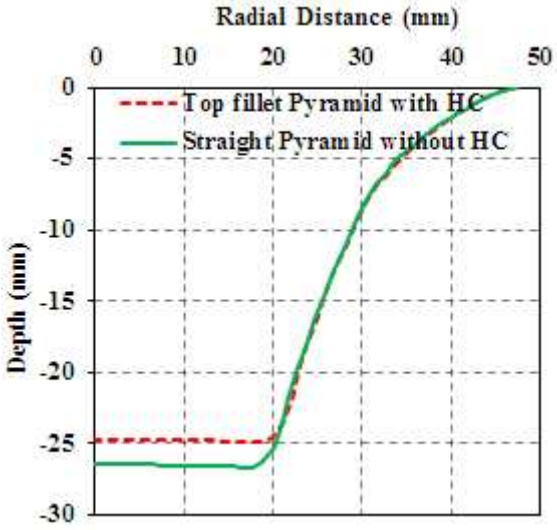

(b) Comparison of Profile

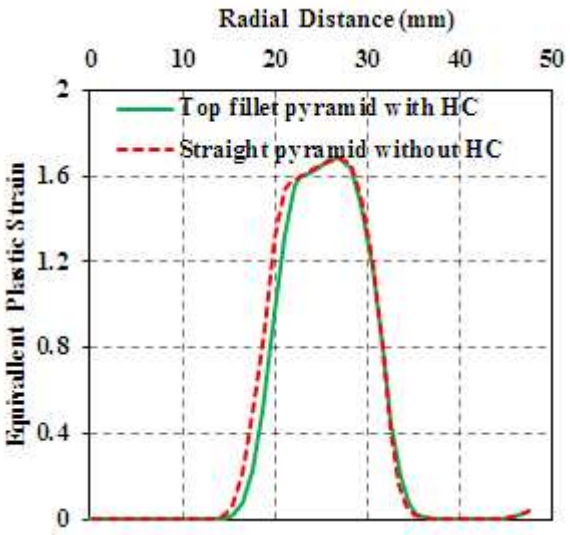

(c) Comparison of Equivalent plastic strain

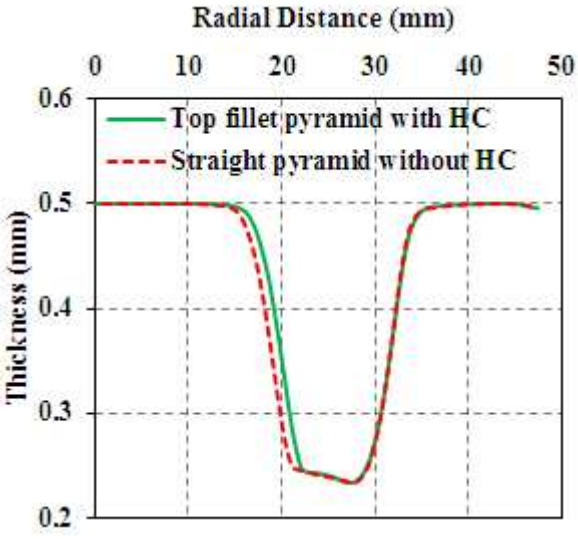

(d) Comparison of thickness

Figure 4.14: Study of FEA results for Job 10 (Top fillet Pyramid with *SBS* 95x95 *mm*, *OD*=70 *mm*, α =60°, *TD*=8 *mm*, *h*=25*mm*, *dz* =0.8*mm*, t_o =0.5 *mm* & R_c =3.75 *mm*) and Job 4 (Pyramid with *SBS* 95x95 *mm*, *OD*=70 *mm*, α =60°, *TD*=8 *mm*, *h*=25*mm*, *dz* =0.8*mm*, t_o =0.5*mm*, R_c =0)

By giving the top fillet, there is not any drastically change in the profile at the region of necking. But the problem of higher indentation due to tool compensation has been solved. It is predicted that the height of deformed component is almost equal to the required height as shown in Figure 4.14(b). When using top fillet, strain distribution along the component profile is reduced in comparison of normal simulation without use of any fillet at top as shown in Figure 4.14(c). If strain is reduced, then better results in thickness can be obtained i.e. sheet thickness will increase. The reason is deformation takes place with gradually increase in draw angle from 0 degree to required draw angle instead of direct go with required draw angle in normal simulation.

Sheet thickness variation is nearly related to the strain, where strain is maximum there section thickness is minimum and vice-versa. With using top fillet, strain distribution along the component profile is reduced which results in increase in section thickness as shown in Figure 4.14(d) and Table 12.

Table 12: Thickness comparison for straight pyramid and fillet pyramid (*SBS* 95x95 *mm* , α =60°)

Radial Distance (in *mm*)	Thickness Corresponding to Job 4 for Pyramid with *SBS* 95x95 *mm* , α =60° (in *mm*)	Thickness Corresponding to Job 10 for Top fillet Pyramid with *SBS* 95x95 *mm* , α =60° (in *mm*)	% age Increase in Thickness
15.51	0.489	0.496	1.45
16.52	0.468	0.488	4.26
17.55	0.428	0.466	9.04
18.66	0.361	0.426	18.02
19.85	0.287	0.362	25.95
21.07	0.250	0.288	15.14
29.41	0.252	0.255	1.29
30.60	0.294	0.298	1.13

4.4.1.5 Comparison of FEA results for Job 11 (Top fillet cone with *SBS* 75x75 *mm* , *OD*=70 *mm*, α =45°, *TD*=8 *mm*, *h*=25 *mm*, *dz* =0.8 *mm*, t_o =0.5 *mm* and R_c =3.75 *mm*) and Job 5 (Cone with *SBS* 75x75 *mm* , *OD*=70 *mm*, α =45°, *TD*=8 *mm*, *h*=25 *mm*, *dz* =0.8 *mm*, t_o =0.5 *mm*, R_c =0)

By giving the top fillet, there is not any drastically change in the profile at the region of necking. But the problem of higher indentation due to tool compensation has been solved. It is predicted that the height of deformed component is almost equal to the required height as shown in Figure 4.15(b). When using top fillet, strain distribution along the component profile is reduced in comparison of normal simulation without use of any fillet at top as shown in Figure 4.15(c). If strain is reduced, then better results in thickness can be obtained i.e. sheet thickness will increase. The reason is deformation takes place with gradually increase in draw angle from 0 degree to required draw angle instead of direct go with required draw angle in normal simulation.

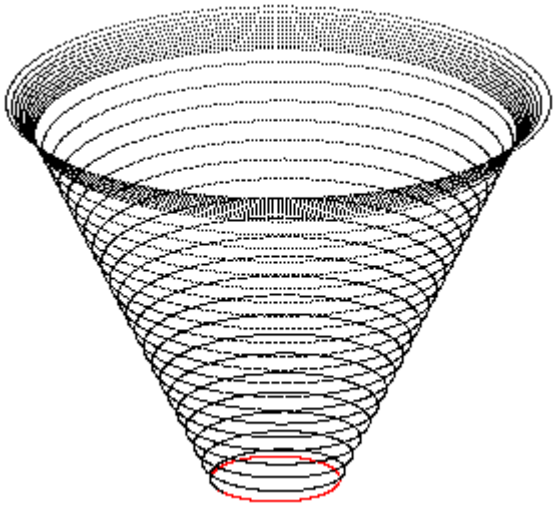

(a) Toolpath for fillet cone

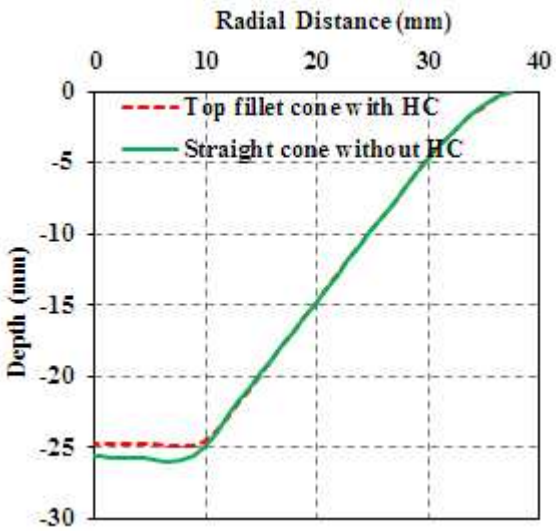

(b) Comparison of Profile

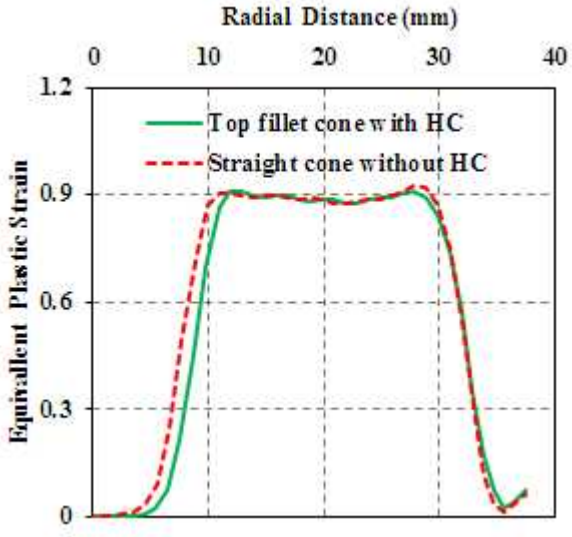

(c) Comparison of Equivalent plastic strain

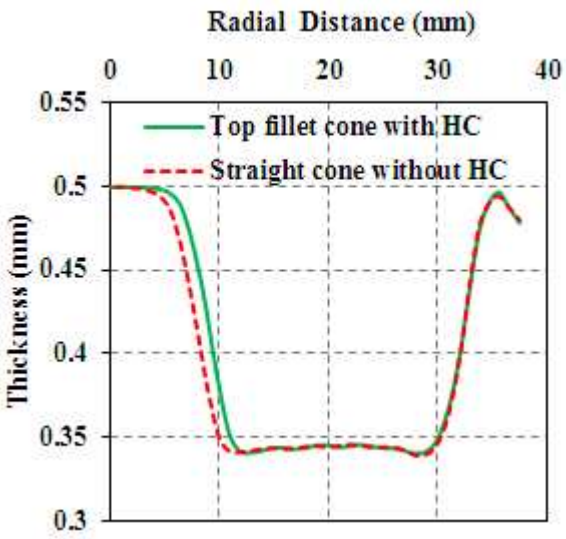

(d) Comparison of thickness

Figure 4.15: Study of FEA results for Job 11 (Top fillet Cone with *SBS* 75x75 *mm*, *OD*=70 *mm*, α =45°, *TD*=8 *mm*, *h*=25*mm*, *dz* =0.8*mm*, t_o =0.5 *mm* and R_c =3.75 *mm*) and Job 5 (Cone with *SBS* 75x75 *mm*, *OD*=70 *mm*, α =45°, *TD*=8 *mm*, *h*=25*mm*, *dz* =0.8*mm*, t_o =0.5 *mm* and R_c =0)

Sheet thickness variation is nearly related to the strain, where strain is maximum there section thickness is minimum and vice-versa. With using top fillet, strain distribution along the component profile is reduced which results in increase in section thickness as shown in Figure 4.15(d) and Table 13.

Table 13: Thickness comparison for straight cone and top fillet cone (*SBS* 75x75 *mm*, α =45°)

Radial Distance (in *mm*)	Thickness Corresponding to Job 5 for cone with *SBS* 75x75 *mm*, α =45° (in *mm*)	Thickness Corresponding to Job 11 for Top fillet cone with *SBS* 75x75 *mm*, α =45° (in *mm*)	% age Increase in Thickness
4.47	0.494	0.498	0.87
5.47	0.485	0.496	2.15
6.47	0.463	0.488	5.54
7.50	0.423	0.467	10.47
8.65	0.380	0.432	13.56
9.79	0.350	0.387	10.43
10.91	0.342	0.352	3.05

4.4.1.6 Comparison of FEA results for Job 12 (Top fillet pyramid with *SBS* 75x75 *mm*, *OD*=70 *mm*, α =45°, *TD*=8 *mm*, *h*=25 *mm*, *dz* =0.8 *mm*, t_o =0.5 *mm* and R_c =3.75 *mm*) and Job 6 (pyramid with *SBS* 75x75 *mm*, *OD*=70 *mm*, α =45°, *TD*=8 *mm*, *h*=25 *mm*, *dz* =0.8 *mm*, t_o =0.5 *mm* and R_c =0 *mm*)

By giving the top fillet, there is not any drastically change in the profile at the region of necking. But the problem of higher indentation due to tool compensation has been solved. It is predicted that the height of deformed component is almost equal to the required height as shown in Figure 4.16(b). When using top fillet, strain distribution along the component profile is reduced in comparison of normal simulation without use of any fillet at top as shown in Figure 4.16(c). If strain is reduced, then better results in thickness can be obtained i.e. sheet thickness will increase. The reason is deformation takes place with gradually increase in draw angle from 0 degree to required draw angle instead of direct go with required draw angle in normal simulation.

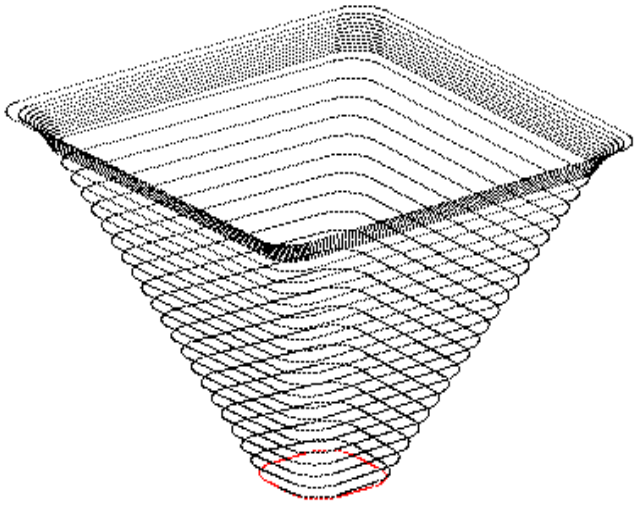

(a) Toolpath for fillet Pyramid

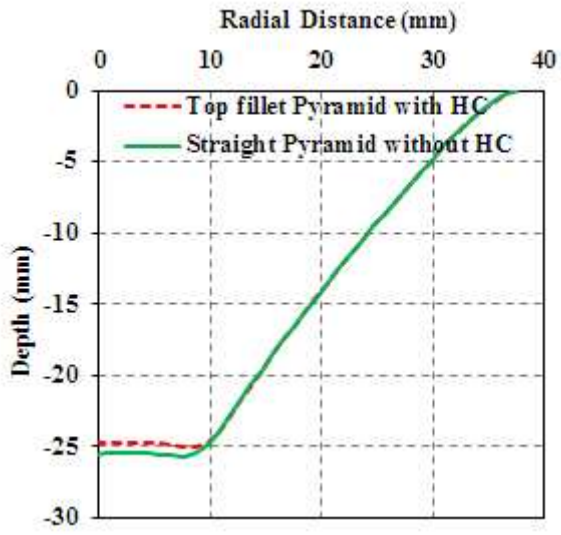

(b) Comparison of Profile

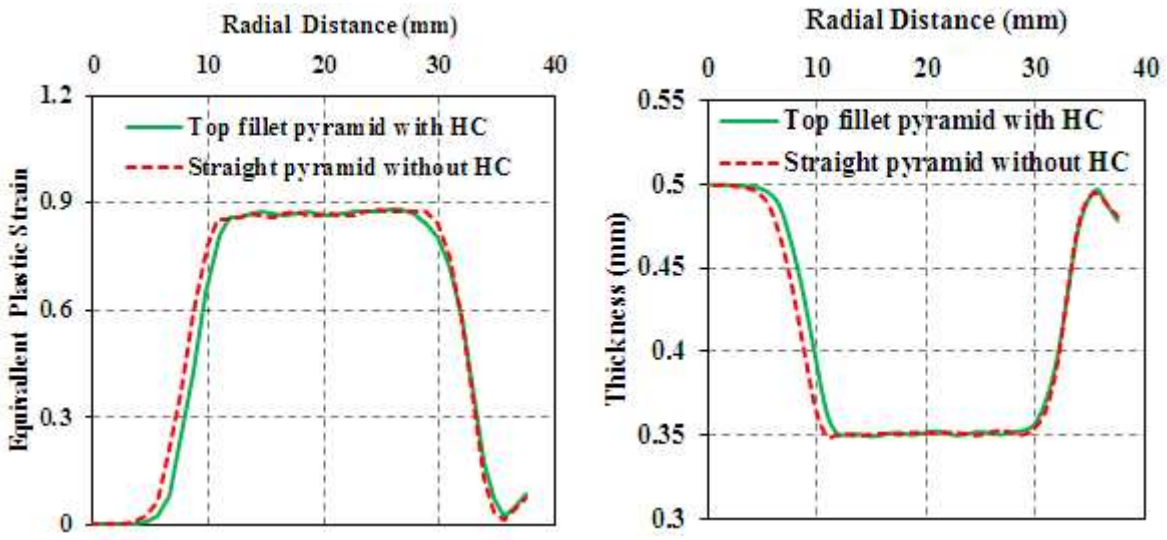

(c) Comparison of Equivalent plastic strain **(d)** Comparison of thickness

Figure 4.16: Study of FEA results for Job 12 (Top fillet Pyramid with *SBS* 75x75 *mm*, *OD*=70 *mm*, α =45°, *TD*=8 *mm*, *h*=25*mm*, *dz* =0.8*mm*, t_o =0.5 *mm* and R_c =3.75 *mm*) and Job 6 (Pyramid *SBS* 75x75 *mm*, *OD*=70 *mm*, α =45°, *TD*=8 *mm*, *h*=25*mm*, *dz* =0.8*mm*, t_o =0.5 *mm* and R_c =0)

Sheet thickness variation is nearly related to the strain, where strain is maximum there section thickness is minimum and vice-versa. With using top fillet, strain distribution along the component profile is reduced which results in increase in section thickness as shown in Figure 4.16(d) and Table 14.

Table 14: Thickness comparison for straight pyramid and fillet pyramid (*SBS* 75x75 *mm*, α =45°)

Radial Distance (in *mm*)	Thickness Corresponding to Job 6 for Pyramid with *SBS* 75x75 *mm*, α =45° (in *mm*)	Thickness Corresponding to Job 12 for Top fillet Pyramid with *SBS* 75x75 *mm*, α =45° (in *mm*)	% age Increase in Thickness
5.52	0.488	0.495	1.42
6.53	0.470	0.487	3.64
7.56	0.442	0.466	5.52
8.66	0.404	0.437	8.16
9.79	0.366	0.398	8.71
10.88	0.350	0.363	3.80
11.81	0.350	0.351	0.32
28.85	0.350	0.353	0.73
29.92	0.355	0.357	0.73
30.99	0.366	0.372	1.57

4.5 TWO-STEPS DEFORMATION STRATEGY

In two-steps deformation strategy, two kinds of toolpaths are used. When the tool motion is from the periphery of the sheet towards the centre of the sheet, and moving in the negative *Z* direction, the toolpath is called outer-to-inner (*O-to-I*) tool movement and When the tool motion is from the centre of the sheet towards the periphery, and moving in the positive *Z* direction, the toolpath is called inner-to-outer (*I-to-O*) tool movement. The need of this type of toolpath strategy is required to achieve better results for thickness distribution along the side walls and geometry control of the formed component.

4.5.1 Study of two-step Cone for Job 16 {Cone (*O-to-I*) with *SBS* 75x75 *mm*, *OD*=64 *mm*, α =40°, *TD*=8 *mm*, *h*=14.99 *mm*, *dz* =0.8 *mm*, t_o =0.5 *mm*, R_c =0} and {Cone (*I-to-O*) with *SBS* 75x75 *mm*, *OD*=70 *mm*, α =45°, *TD*=8 *mm*, *h*=15*mm*, *dz* =0.8 *mm*, t_o =0.5 *mm*, R_c =0}

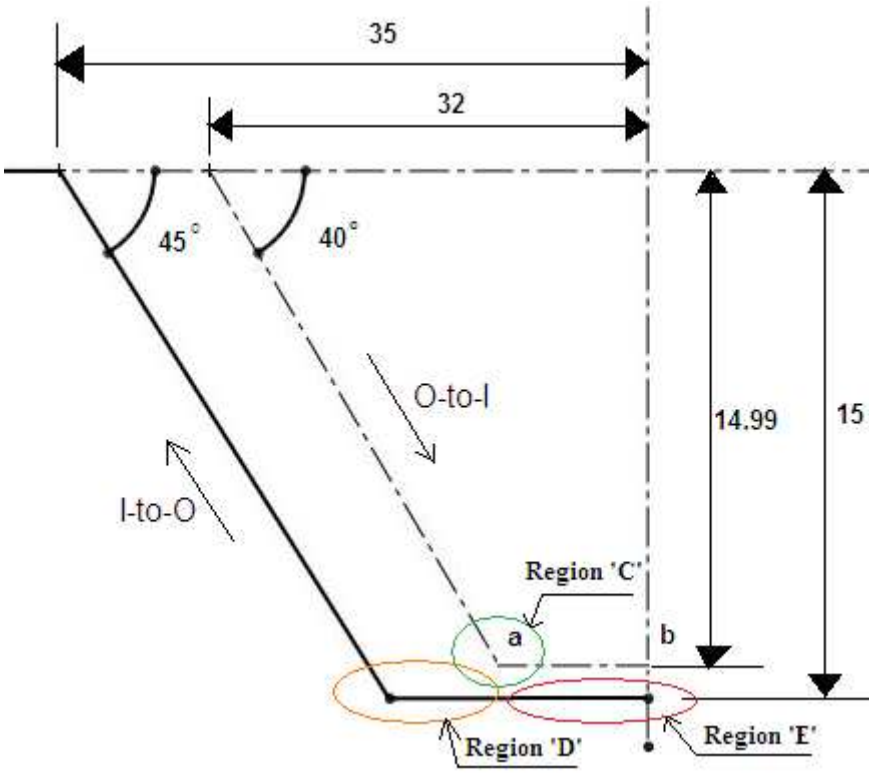

(a) Ideal Geometry

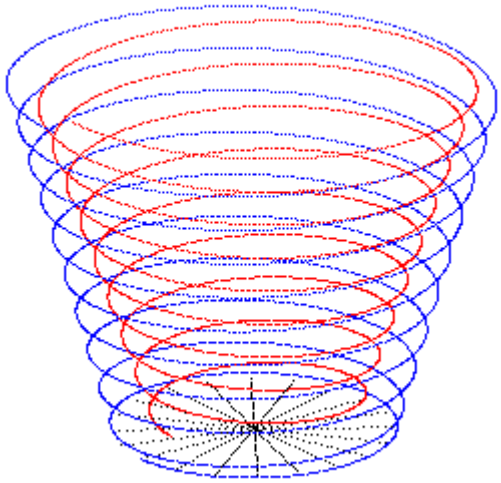

(b) Compensated Toolpath

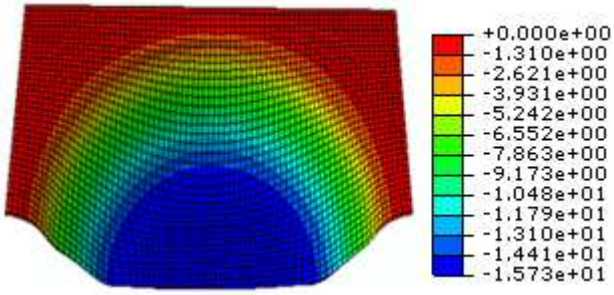

(c) FEA result for profile (*mm*)

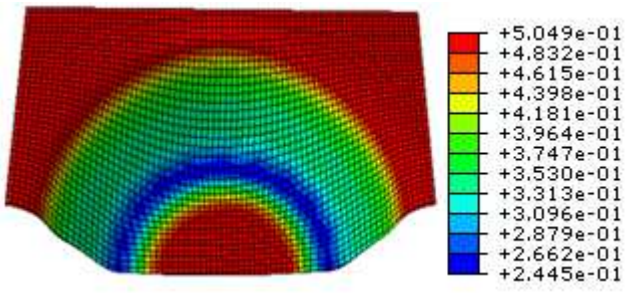

(d) FEA result for Thickness (*mm*)

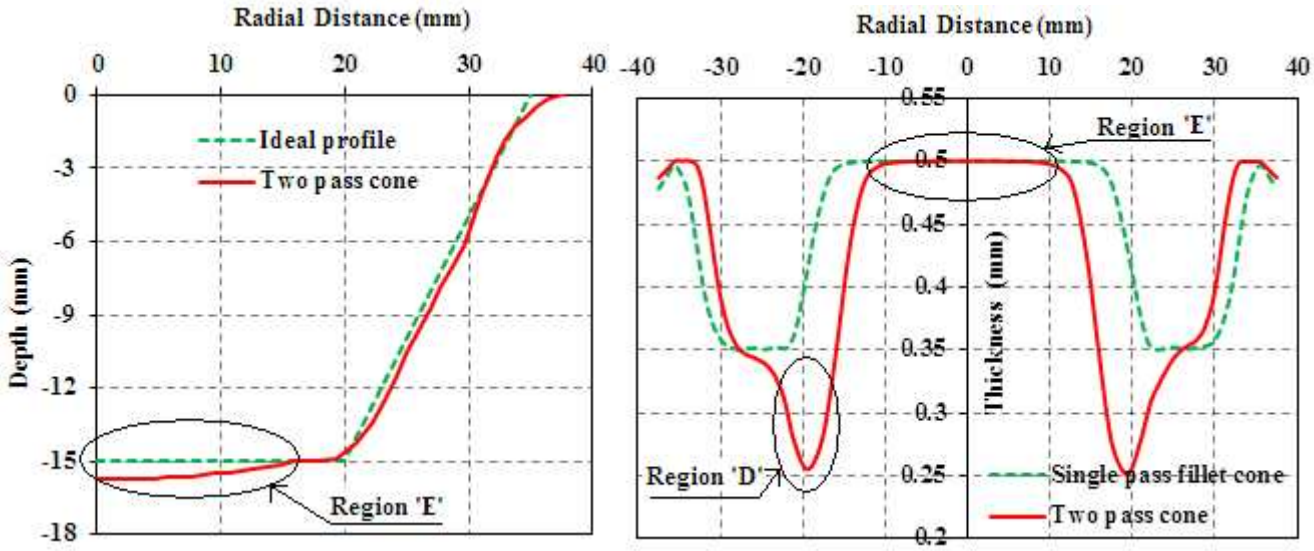

(e) Comparison for profile **(f)** Comparison for Thickness

Figure 4.17: Study of two-step Cone for Job 16 {Cone (*O-to-I*) with *SBS* 75x75 *mm* , *OD*=64 *mm*, α =40°, *TD*=8 *mm*, *h*=14.99 *mm*, dz =0.8 *mm*, t_o =0.5 *mm*, R_c =0} and {Cone (*I-to-O*) with *SBS* 75x75 *mm* , *OD*=70 *mm*, α =45°, *TD*=8 *mm*, *h*=15*mm*, dz =0.8 *mm*, t_o =0.5 *mm*, R_c =0}

When the tool motion is from the centre of the sheet towards the periphery, while moving in the positive *Z* direction (i.e. *I-to-O*), the region of the intermediate shape undergoes a rigid body translation in the negative Z direction. This rigid body translation is to cause stepped features on the final formed component as can be seen region '*E*' in Figure 4.17(e).

Disadvantages:

1. The central portion or portion *a* to *b* of Figure 4.17(a) remains undeformed and its result can be seen as region '*F*' in Figure 4.17(f).
2. There is a maximum chance to occur fracture in region '*D*' of Figure 4.17(a) and 4.17(f), because very small portion of region '*C*' (i.e. at the bottom corner of intermediate profile) is stretched to large portion of region '*D*' as shown in Figure 4.17(a). Therefore it results in reduction of thickness in that particular region '*D*' as can be shown in Figure 4.17(f).

4.5.2 Study of two-step Cone for Job 17 { Parabola (*O-to-I*) with *SBS* 75x75 *mm*, *OD*=58 *mm*, *max* α =60°, *TD*=8 *mm*, *h*=24.6 *mm*, *dz* =0.8 *mm*, t_o =0.5 *mm*, R_c =0} and {Cone (*I-to-O*) with *SBS* 75x75 *mm*, *OD*=70 *mm*, α =45°, *TD*=8 *mm*, *h*=25 *mm*, *dz* =0.8 *mm*, t_o =0.5 *mm*, R_c =0}

Job 14 is performed on sheet blank size of 75x75 *mm*. There are two types of toolpath used first from out-to-in i.e. deformation in negative *z*-direction and second one is in-to-out i.e. deformation in Positive *z*-direction and final geometry is obtained.

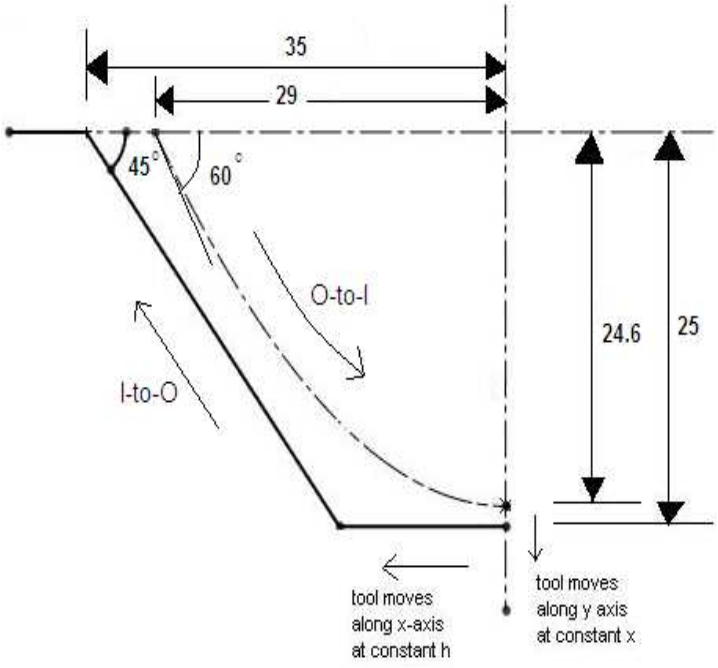

(a) Ideal Geometry

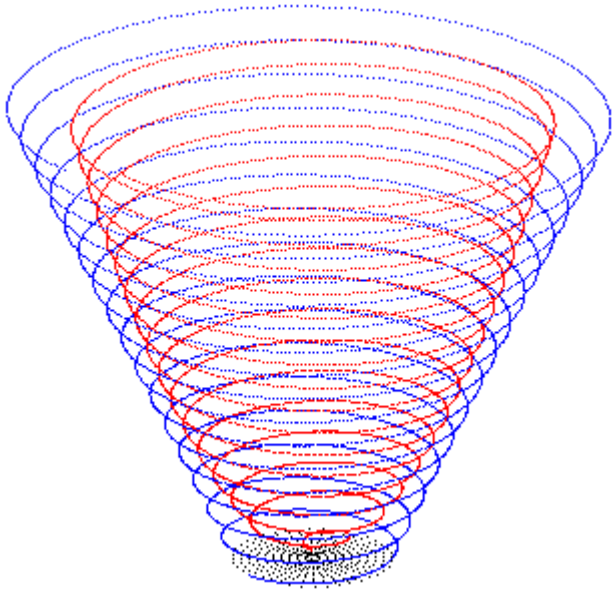

(b) Compensated Toolpath

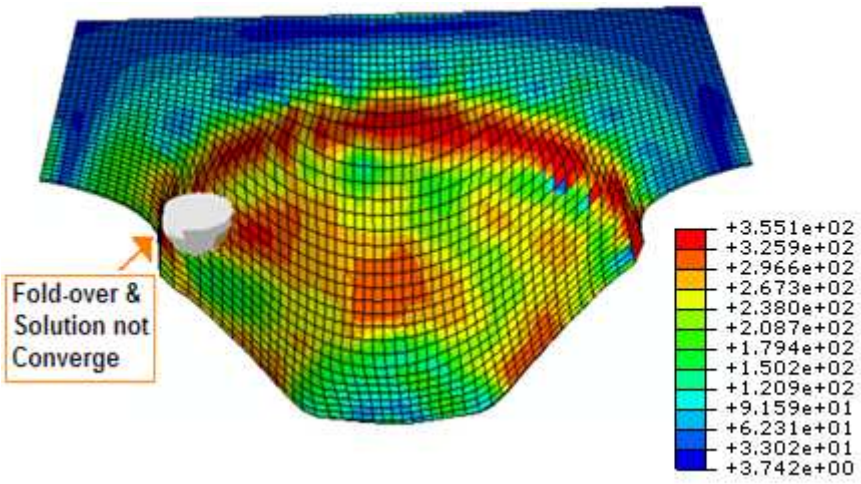

(c) FEA result for Von Mises equivalent stress (*MPa*)

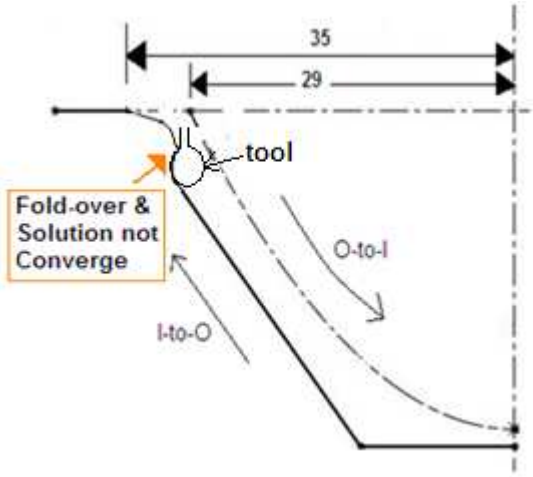

(d) Detail for Fold-over failure

Figure 4.18: Study of two-step Cone for Job 17 { Parabola (*O-to-I*) *SBS* 75x75 *mm*, *OD*=58 *mm*, *max* α =60°, *TD*=8 *mm*, *h*=24.6 *mm*, *dz* =0.8 *mm*, t_o =0.5 *mm*, R_c =0} and {Cone (*I-to-O*) *SBS* 75x75 *mm*, *OD*=70 *mm*, α =45°, *TD*=8 *mm*, *h*=25 *mm*, *dz* =0.8 *mm*, t_o =0.5 *mm*, R_c =0}

While forming the second pass when the tool motion is from the centre of the sheet towards the periphery, (i.e. moving in the positive *Z* direction), the solution does not converge and simulation stopped. The mode of failure was a 'fold-over' type of failure, as shown in Figure 4.18(c) and Figure 4.18(d). While forming the second pass, a lip formed where the wall of the initial pass met the forming tool. This lip became sharp and eventually folded over, resulting in a failure at this location.

4.5.3 Study of two-step Cone for Job 18 { Parabola (*O-to-I*) with *SBS* 75x75 *mm*, *OD*=58 *mm*, *Rb*=33 *mm*, *max* α =60°, *TD*=8 *mm*, *h*=24.99 *mm*, *dz* =0.8 *mm*, t_o =0.5 *mm* and R_c =0} and {Cone (*I-to-O*) with *SBS* 75x75 *mm*, *OD*=70 *mm*, α =45°, *TD*=8 *mm*, *h*=25 *mm*, *dz* =0.8 *mm*, t_o =0.5 *mm* and R_c =0}

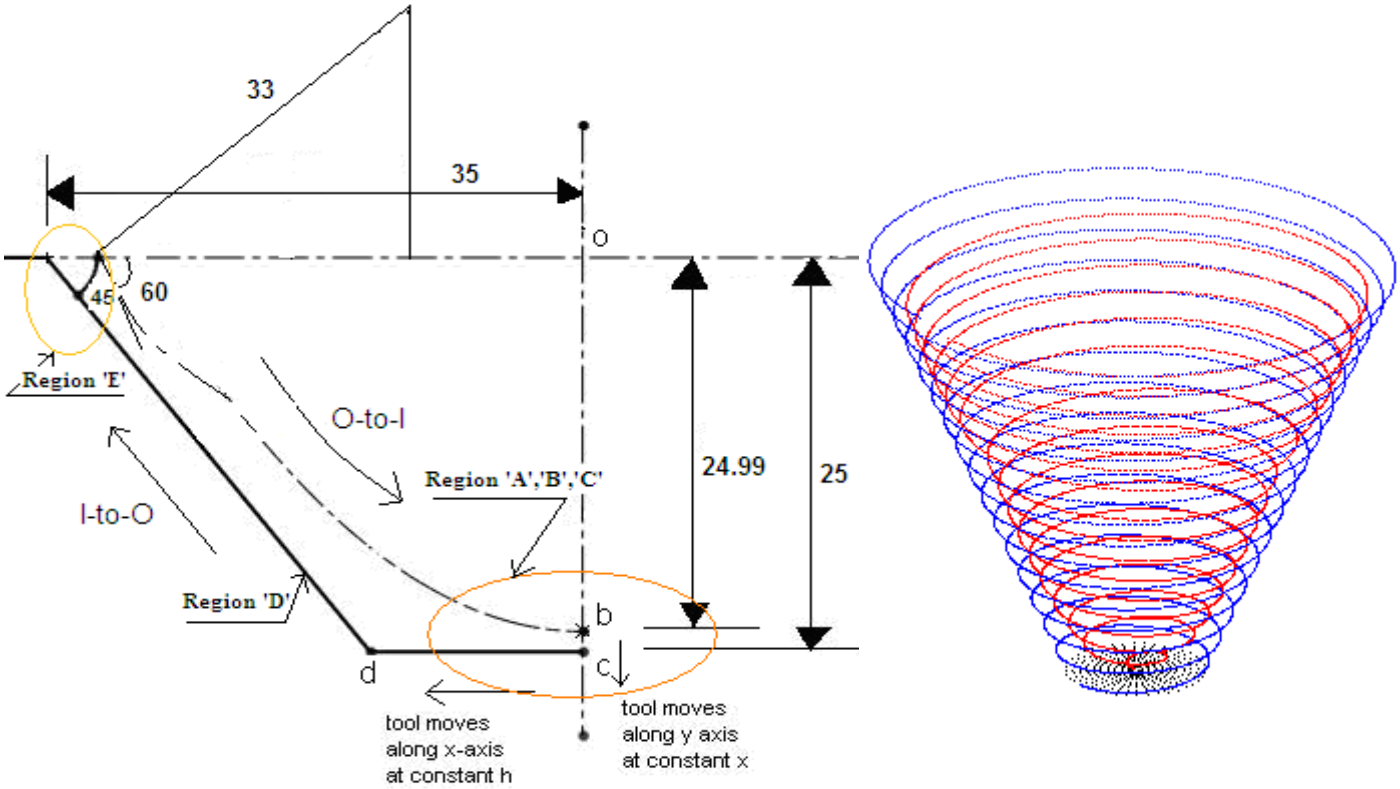

(a) Ideal Geometry **(b)** Compensated Toolpath

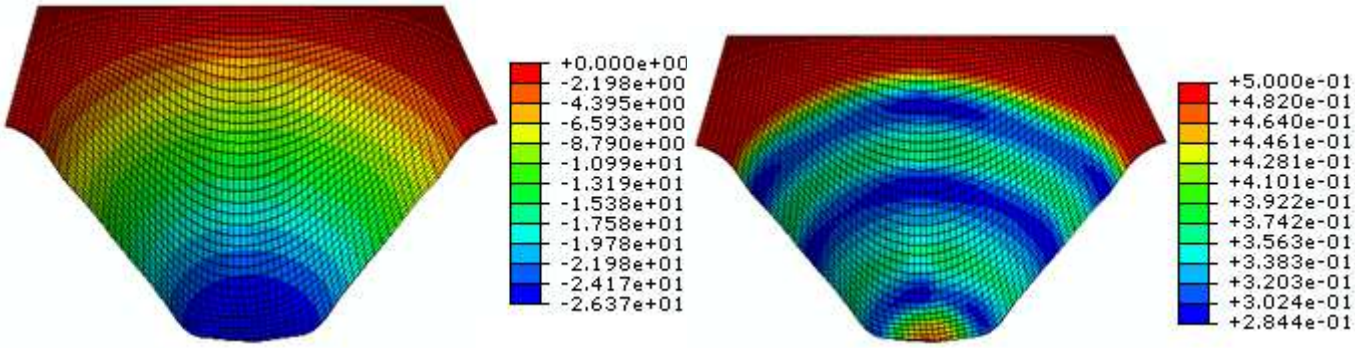

(c) FEA result for profile (*mm*) **(d)** FEA result for Thickness (*mm*)

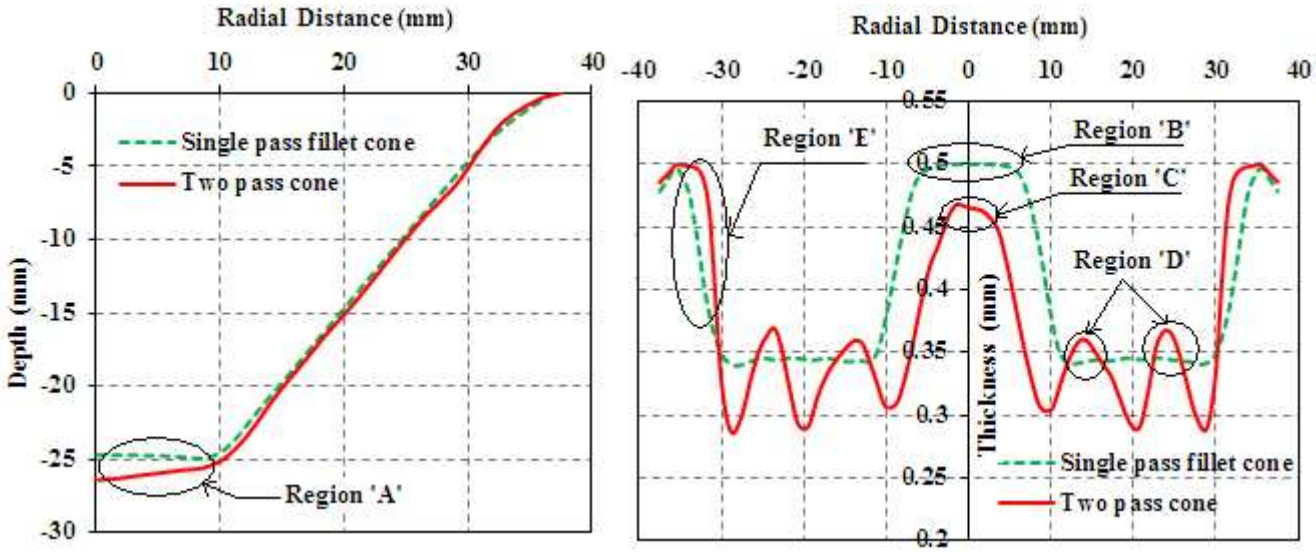

(e) Comparison for profile **(f)** Comparison for Thickness

Figure 4.19: Study of two-step Cone for Job 18 { Parabola (*O-to-I*) with *SBS* 75x75 *mm*, *OD*=58 *mm*, *Rb*=33 *mm*, *max* α =60°, *TD*=8 *mm*, *h*=24.99 *mm*, dz =0.8 *mm*, t_o =0.5 *mm* and R_c =0} and {Cone (*I-to-O*) with *SBS* 75x75 *mm*, *OD*=70 *mm*, α =45°, *TD*=8 *mm*, *h*=25 *mm*, dz =0.8 *mm*, t_o =0.5 *mm* and R_c =0}

When the tool motion is from the centre of the sheet towards the periphery, while moving in the positive *Z* direction (i.e. *I-to-O*), the Region '*A*' shown in figure 4.19(e) of the intermediate shape undergoes a rigid body translation in the negative *Z* direction. This rigid body translation is to cause stepped features on the final formed component as can be seen in Region '*A*' of figure 4.19(e).

With single step deformation strategy, then centre portion of sheet remains undeformed and it can be seen as Region '*B*' of figure 4.19(f). While two-step deformation strategy is used, then central portion of sheet can be deformed and there is some thickness distribution from central portion to the corner and side walls of the deformed object and its result can be seen as Region '*C*'and Region '*D*' of figure 4.19(f). There are some better results obtained of thickness distribution for top fillet region of the component as shown in Region '*E*' of figure 4.19(f).

4.5.4 Study of two-step Cone for Job 19 { Parabola (*O-to-I*) with *SBS* 95x95 *mm*, *OD*=58 *mm*, *Rb*=33 *mm*, *max* α =60°, *TD*=8 *mm*, *h*=24.99 *mm*, *dz* =0.8 *mm*, t_o =0.5 *mm* and R_c =0} and {Cone (*I-to-O*) with *SBS* 95x95 *mm*, *OD*=70 *mm*, α =45°, *TD*=8 *mm*, *h*=25 *mm*, *dz* =0.8 *mm*, t_o =0.5 *mm* and R_c =0}

When the tool motion is from the centre of the sheet towards the periphery, while moving in the positive *Z* direction (i.e. *I-to-O*), the Region '*A*' shown in figure 4.20(e) of the intermediate shape undergoes a rigid body translation in the negative *Z* direction. This rigid body translation is to cause stepped features on the final formed component as can be seen in Region '*A*' of figure 4.20(e).

The better results are observed in reduction of vertical and horizontal bending in two-step deformation strategy in comparison of single step deformation strategy as can be seen in Region '*B*' of figure 4.20(e).

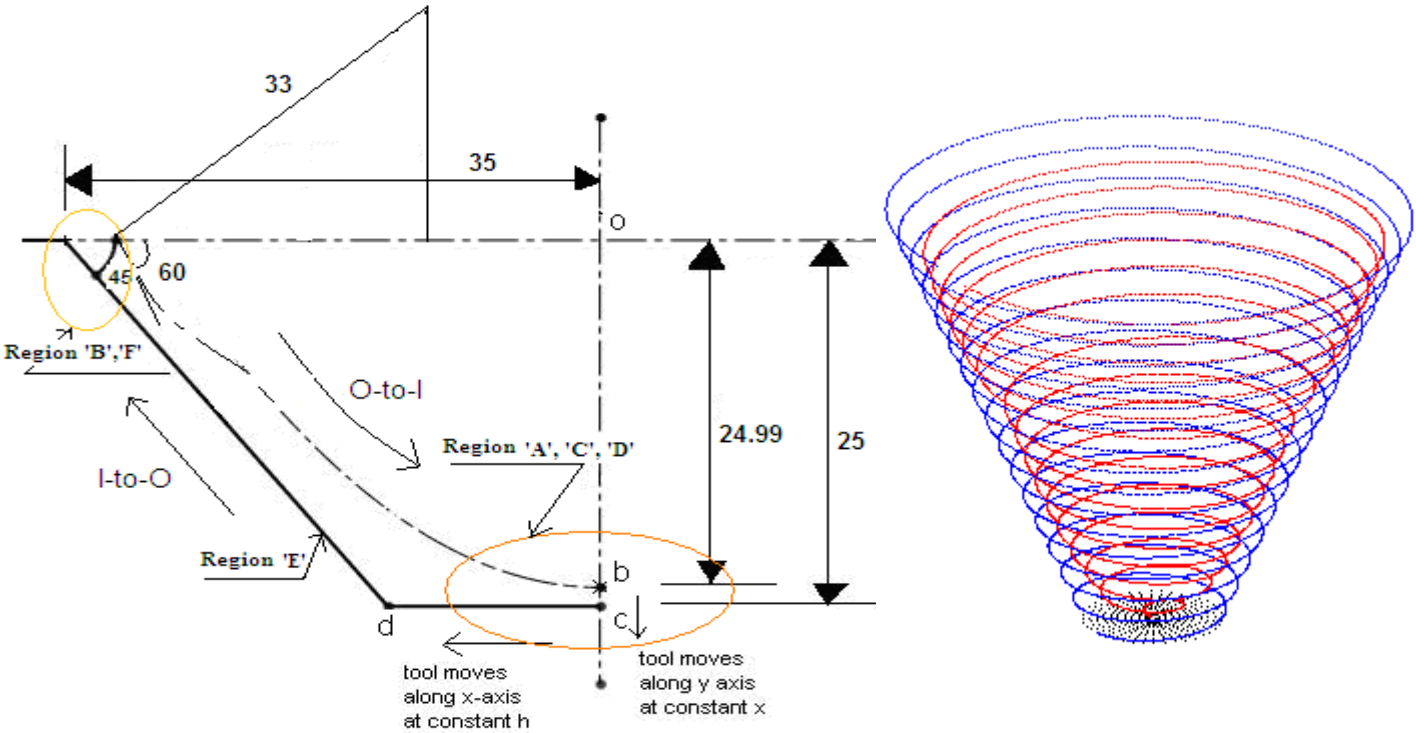

(a) Ideal Geometry **(b)** Compensated Toolpath

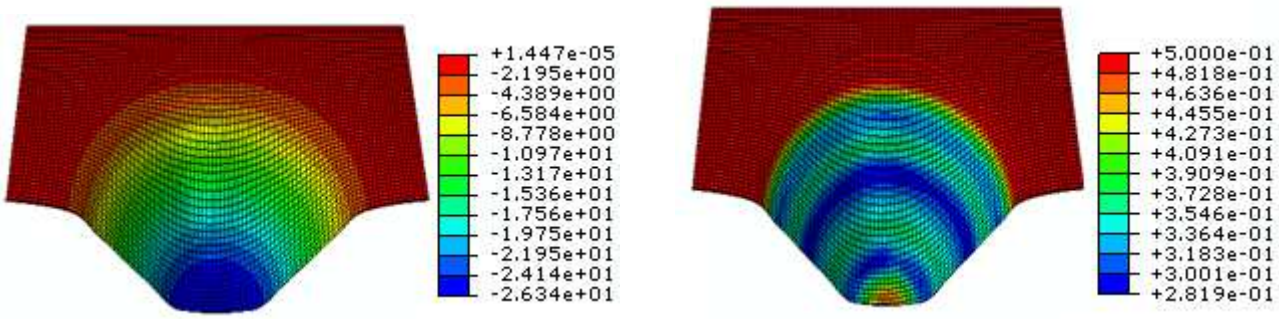

(c) FEA result for profile (*mm*) **(d)** FEA result for Thickness (*mm*)

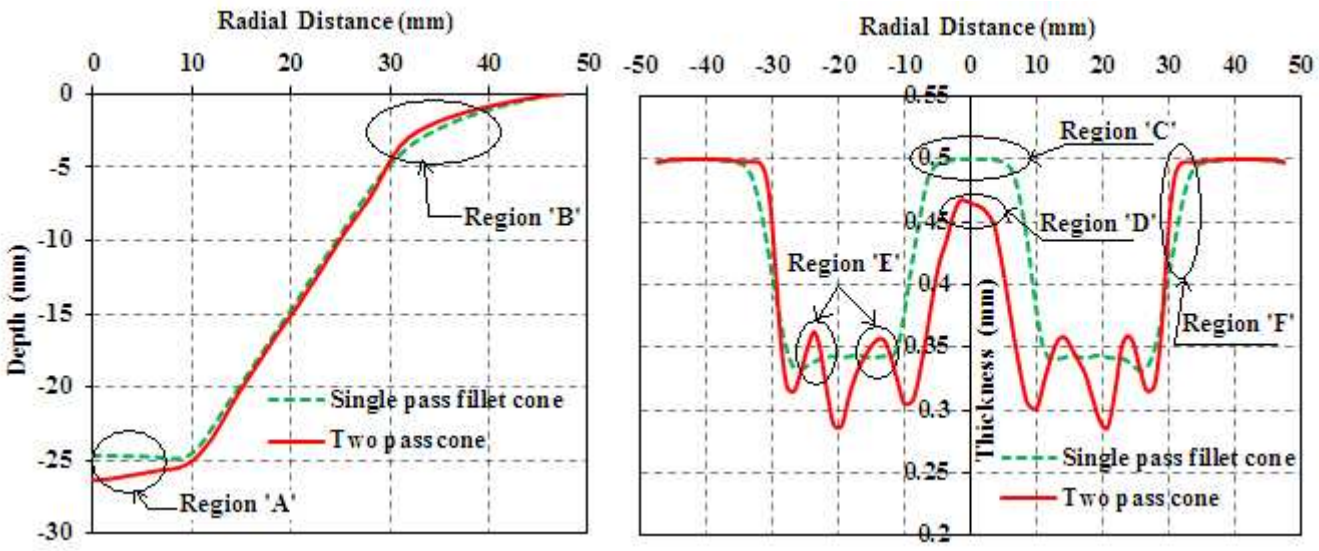

(e) Comparison for profile **(f)** Comparison for Thickness

Figure 4.20: Study of two-step Cone for Job 19 { Parabola (*O-to-I*) with *SBS* 95x95 *mm*, *OD*=58 *mm*, *Rb*=33 *mm*, *max* α =60°, *TD*=8 *mm*, *h*=24.99 *mm*, dz =0.8 *mm*, t_o =0.5 *mm* and R_c =0} and {Cone (*I-to-O*) with *SBS* 95x95 *mm*, *OD*=70 *mm*, α =45°, *TD*=8 *mm*, *h*=25 *mm*, dz =0.8 *mm*, t_o =0.5 *mm* and R_c =0}

With single step deformation strategy, then centre portion of sheet remains undeformed and it can be seen as Region '*C*' of figure 4.20 (f). While two-step deformation strategy is used, then central portion of sheet can be deformed and there is some thickness distribution from central portion to the corner and side walls of the deformed object and its result can be seen as Region '*D*'and Region '*E*' of figure 4.20(f). There are some better results obtained of thickness distribution for top fillet region of the component as shown in Region '*F*' of figure 4.20(f). Thus, better result for thickness distribution can be achieved with two step deformation strategy.

4.5.5 Guidelines for intermediate profile selection:

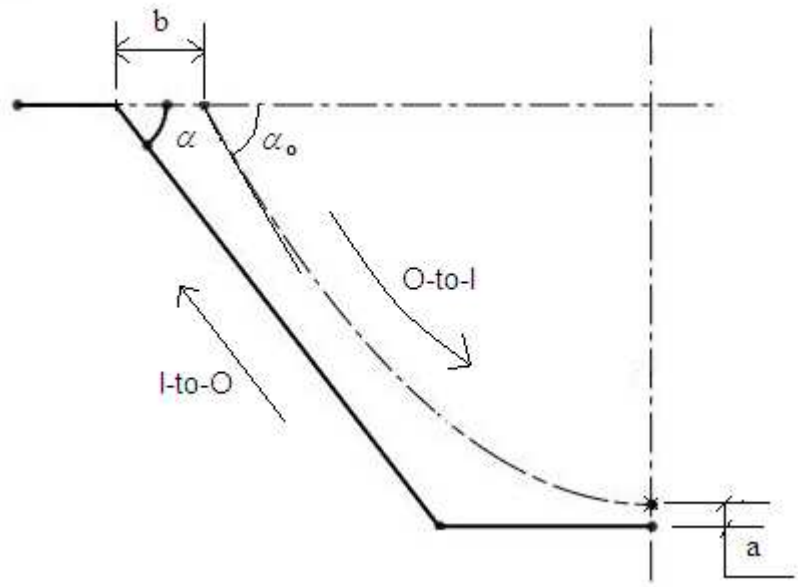

Figure 4.21: Sectional view of cone with intermediate profile of parabola

1. The distance *a* as shown in figure 4.21 should be kept minimum, so that indentation at the base of the deformed component can be reduced.

2. The intermediate profile draw angle (α_o) should be greater than the desired profile draw angle (α) to reduce deflection at the side walls of the deformed component.

3. The distance *b* as shown in figure 4.21 should be minimum, if this distance is more, then problem of fold over will create and simulation does not converge the solution as discussed in step 4.5.2.

4. Avoid to use sharp edges at the bottom corner of intermediate profile, otherwise thickness at the corner of desired profile will be reduced or sometimes fracture at the corner may be occur as discussed in step 4.5.2. It is a good practice to use fillet or curvature at the bottom corner of intermediate profile as shown in figure 4.21.

4.6 STRAIN HISTORY AND DISTRIBUTION

4.6.1 Single pass deformation

4.6.1.1 Strain history of Job 9 for Top fillet pyramid with *SBS* 75x75 *mm*, *OD*=70 *mm*, α =60°, *TD*=8 *mm*, *h*=25 *mm*, dz =0.8 *mm*, t_o =0.5 *mm* and R_c =3.75 *mm*

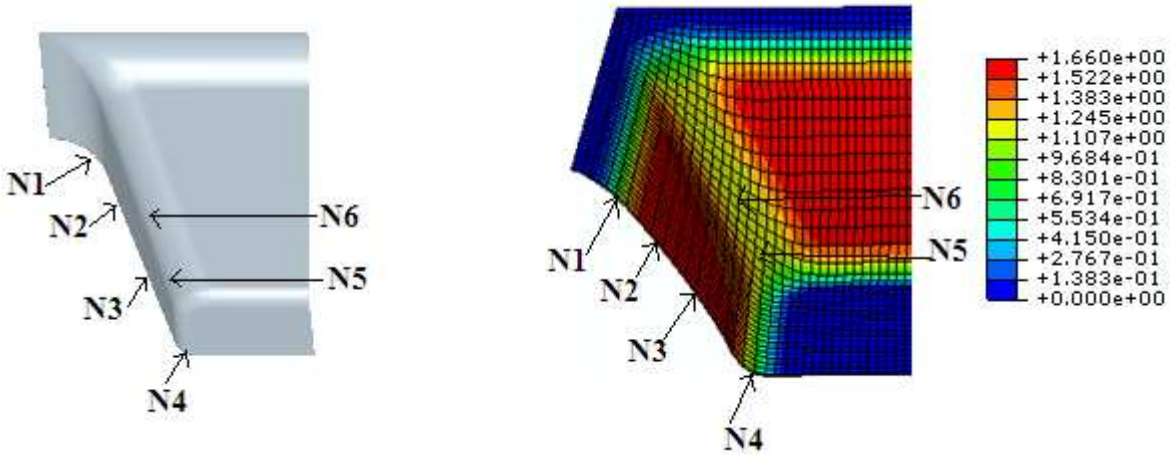

(a) *N1* to *N6* nodes on blank sheet **(b)** *N1* to *N6* nodes on FEA equivalent strain contour

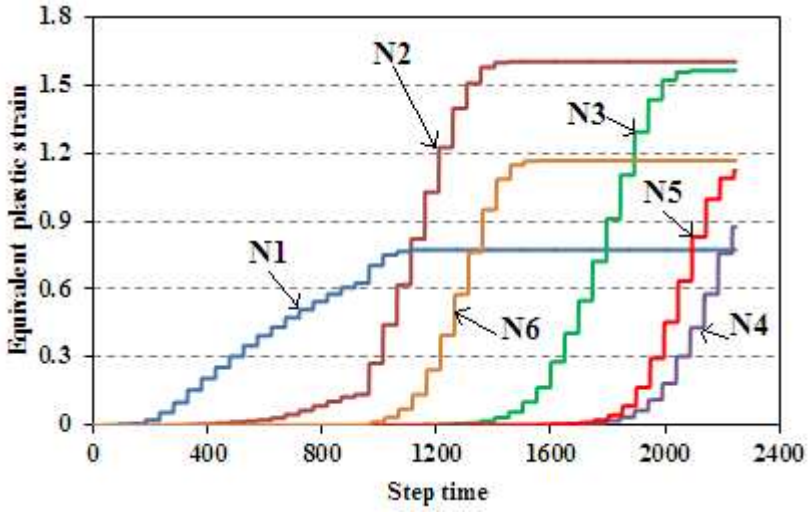

(c) Strain history for nodes *N1* to *N6*

Figure 4.22: Study of Strain history for Job 9 of Top fillet Pyramid with *SBS* 75x75 *mm*, *OD*=70 *mm*, α =60°, *TD*=8 *mm*, *h*=25 *mm*, dz =0.8 *mm*, t_o =0.5 *mm* and R_c =3.75 *mm*

The strain path is analyzed for the nodes *N1* to *N6* indicated in figure 4.22(a) and 4.22(b) for the top fillet pyramid. During the simulation, these six nodes are subsequently affected by the movement of the tool. It is observed that strain paths are characterized by a typical step-trend and each strain increment is directly due to the action of the tool as it passes the particular node. The description of nodes *N1* to *N6* is given below:

Node 1 (*N1*), which is close to the blank edge, is the former node to undergo deformation, but it

reaches just a limited strain since it undergoes the tool action just for a few contours and a wall angle in the region of node 1 (*N1*) is less.

Node 2 (*N2*), and Node 3 (*N3*) lying in between the blank, therefore *N2* and *N3* undergoes a tool action for the maximum number of contours. The maximum value of strain for *N2* and *N3* is 1.60 and 1.56 has been reached due to the maximum wall angle (α =60°) for *N2* and *N3*.

Node 4 (*N4*) and Node 5 (*N5*), which is close to the centre of the blank, is not affected by the tool in the initial contours and the deformation takes place later in the process. As a result, the deformation reaches a limited level before the process finishes.

Node *6* lying in between the pyramid edge corner and less strain is observed as compared to the Node *2* and Node *3*.

4.6.1.2 Strain history of Job 11 for Top fillet cone with *SBS* 75x75 *mm*, *OD*=70 *mm*, α =45°, *TD*=8 *mm*, *h*=25 *mm*, *dz* =0.8 *mm*, t_o =0.5 *mm* and R_c =3.75 *mm*

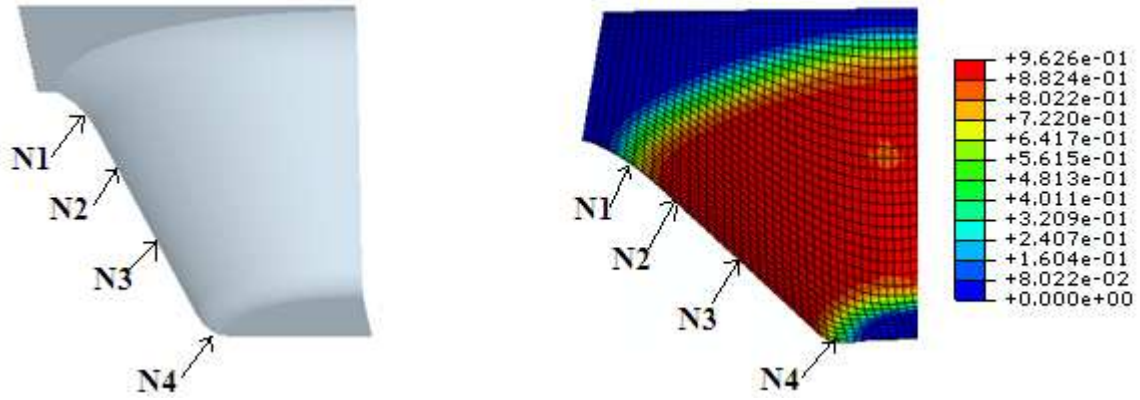

(a) *N1* to *N4* nodes on blank sheet **(b)** *N1* to *N4* nodes on FEA equivalent strain contour

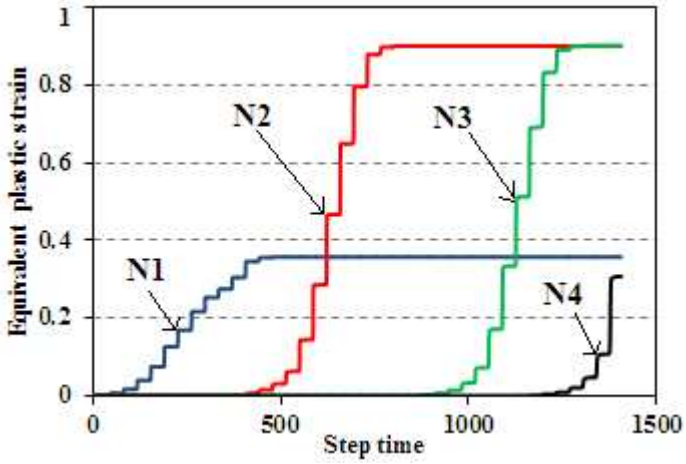

(c) Strain history for nodes *N1* to *N4*

Figure 4.23: Study of Strain history for Job 11 of Top fillet cone with *SBS* 75x75 *mm*, *OD*=70 *mm*, α =45°, *TD*=8 *mm*, *h*=25 *mm*, *dz* =0.8 *mm*, t_o =0.5 *mm* and R_c =3.75 *mm*

The strain path is analyzed for the nodes *N1* to *N4* indicated in figure 4.23(a) and 4.23(b) for the top fillet cone. During the simulation, these four nodes are subsequently affected by the movement of the tool. It is observed that strain paths are characterized by a typical step-trend and each strain increment is directly due to the action of the tool as it passes the particular node. The description of nodes *N1* to *N4* is given below:

Node 1 (*N1*), which is close to the blank edge, is the former node to undergo deformation, but it reaches just a limited strain since it undergoes the tool action just for a few contours and a wall angle in the region of node 1 (*N1*) is less.

Node 2 (*N2*), and Node 3 (*N3*) lying in between the blank, therefore *N2* and *N3* undergoes a tool action for the maximum number of contours. The maximum value of strain for *N2* and *N3* is 0.90 has been reached due to the maximum wall angle (α =45°) for *N2* and *N3*. The maximum value of strain in the top fillet cone is less as compared to the top fillet pyramid (step 4.6.1.1) because of change in draw angle (α) from 60° to 45° in case of top fillet cone. Thus strain increases with increase in the draw angle.

Node 4 (*N4*), which is close to the centre of the blank, is not affected by the tool in the initial contours and the deformation takes place later in the process. As a result, the deformation reaches a limited level before the process finishes.

4.6.1.3 Strain history of Job 15 for top fillet flower with *SBS* 75x75 *mm*, *OD*=70 *mm*, *max* α =60°, *TD*=8 *mm*, *h*=25 *mm*, *dz* =0.8 *mm*, t_o =0.5 *mm* and R_c =4.0 *mm*

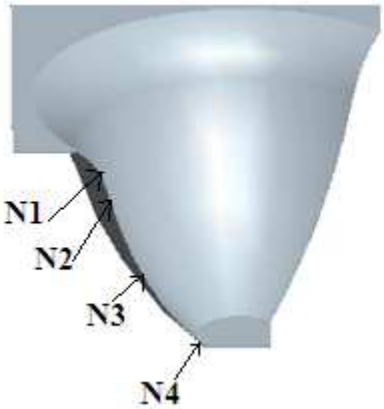

(a) *N1* to *N4* nodes on blank sheet

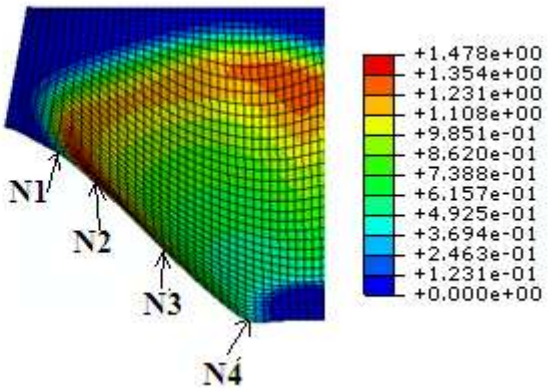

(b) *N1* to *N4* nodes on FEA equivalent strain contour

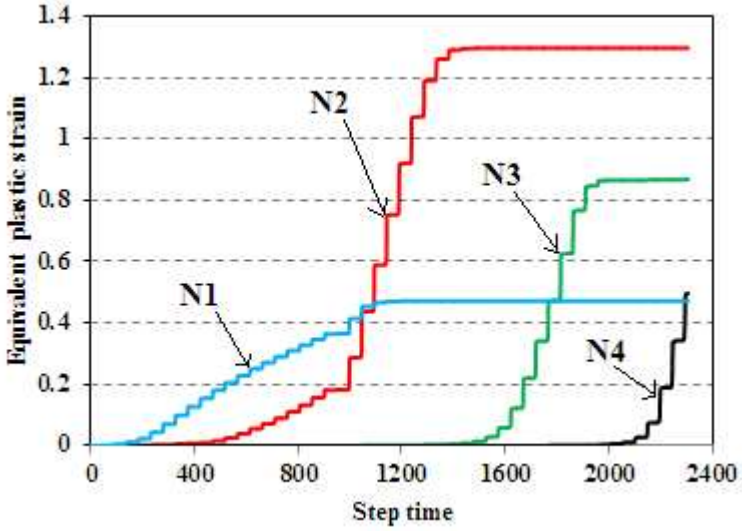

(c) Strain history for nodes *N1* to *N4*

Figure 4.24: Study of Strain history for Job 15 of Top fillet flower with *SBS* 75x75 *mm* , *OD*=70 *mm*, *max* α =60°, *TD*=8 *mm*, *h*=25 *mm*, *dz* =0.8 *mm*, t_o =0.5 *mm* and R_c =4.0 *mm*

The strain path is analyzed for the nodes *N1* to *N4* indicated in figure 4.24(a) and 4.24(b) for the top fillet flower. During the simulation, these four nodes are subsequently affected by the movement of the tool. It is observed that strain paths are characterized by a typical step-trend and each strain increment is directly due to the action of the tool as it passes the particular node. The description of nodes *N1* to *N4* is given below:

Node 1 (*N1*), which is close to the blank edge, is the former node to undergo deformation, but it reaches just a limited strain since it undergoes the tool action just for a few contours and a wall angle in the region of node 1 (*N1*) is less.

Node 2 (*N2*), and Node 3 (*N3*) lying in between the blank, therefore *N2* and *N3* undergoes a tool action for the maximum number of contours. The maximum value of strain for *N2* is 1.29 has been reached due to the maximum wall angle for *N2*. The maximum value of strain for *N3* is 0.88 and is less than the strain value of *N2*, because of decrease in the draw angle due to the curved path of flower. Thus strain decreases with decrease in the draw angle.

Node 4 (*N4*), which is close to the centre of the blank, is not affected by the tool in the initial contours and the deformation takes place later in the process. As a result, the deformation reaches a limited level before the process finishes.

4.6.2 Two pass deformation

4.6.2.1 Strain history of Job 18 for two-step Cone { Parabola (*O-to-I*) with *SBS* 75x75 *mm*, *OD*=58 *mm*, *Rb*=33 *mm*, *max* α =60°, *TD*=8 *mm*, *h*=24.99 *mm*, *dz* =0.8 *mm*, t_o =0.5 *mm* and R_c =0} and {Cone (*I-to-O*) with *SBS* 75x75 mm^2, *OD*=70 *mm*, α =45°, *TD*=8 *mm*, *h*=25 *mm*, *dz* =0.8 *mm*, t_o =0.5 *mm* and R_c =0}

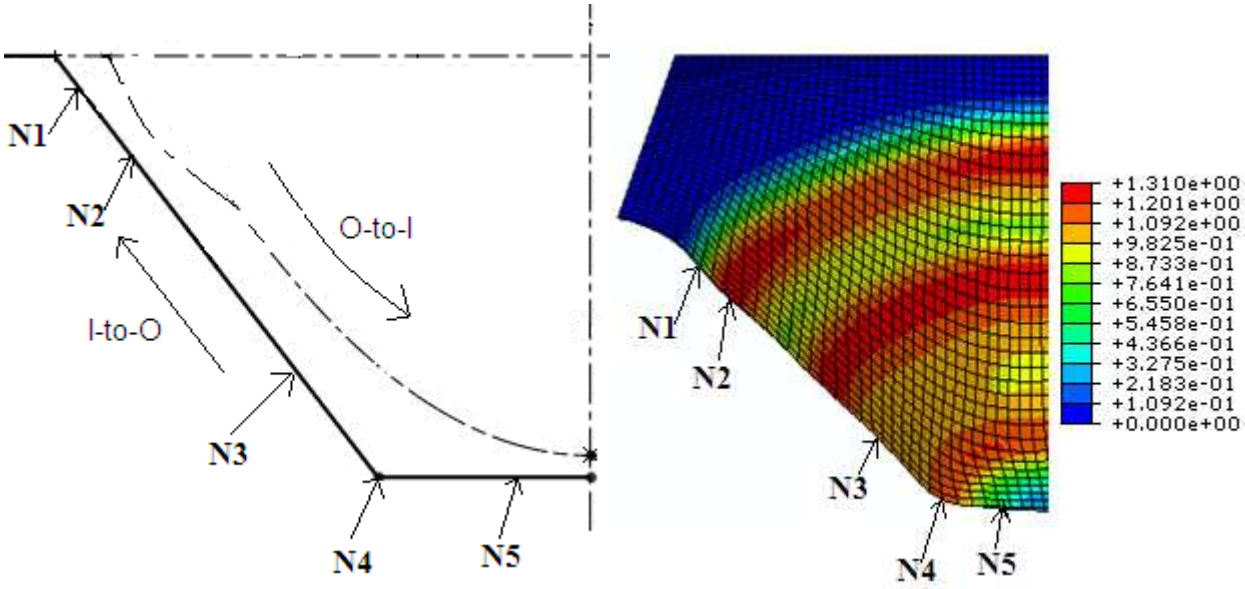

(a) *N1* to *N5* nodes on blank sheet **(b)** *N1* to *N5* nodes on FEA equivalent strain contour

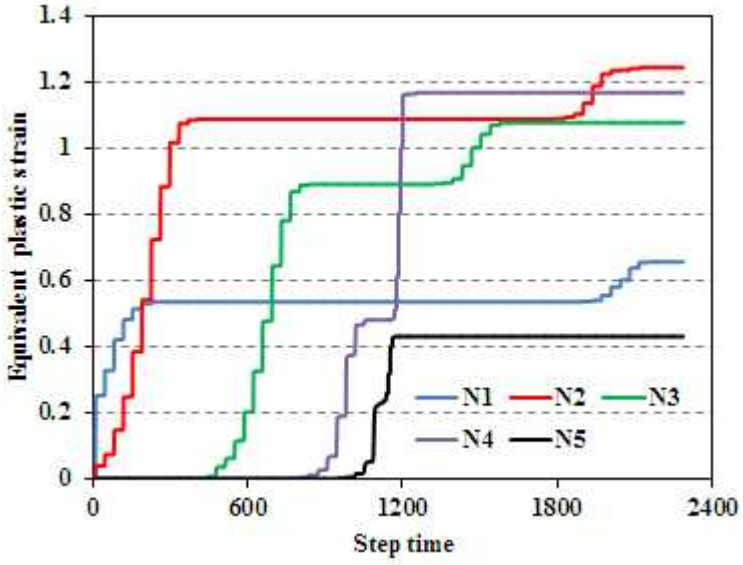

(c) Strain history for nodes *N1* to *N5*

Figure 4.25: Study of Strain history for two-step Cone for Job 18 { Parabola (*O-to-I*) with *SBS* 75x75 *mm*, *OD*=58 *mm*, *Rb*=33 *mm*, *max* α =60°, *TD*=8 *mm*, *h*=24.99 *mm*, *dz* =0.8 *mm*, t_o =0.5 *mm* and R_c =0} and {Cone (*I-to-O*) with *SBS* 75x75 *mm*, *OD*=70 *mm*, α =45°, *TD*=8 *mm*, *h*=25 *mm*, *dz* =0.8 *mm*, t_o =0.5 *mm* and R_c =0}

The strain path is analyzed for the nodes *N1* to *N5* indicated in figure 4.25(a) for the two step cone. During the simulation, these five nodes are subsequently affected twice by the movement of the tool once tool motion from *O-to-I* and second from *I-to-O* as can be seen in figure 4.25(b). It is observed that strain paths are characterized by a typical step-trend and each strain increment is directly due to the action of the tool as it passes the particular node. The description of nodes *N1* to *N5* is given below:

Node 1 (*N1*), which is close to the blank edge, is the former node in *O-to-I* toolpath undergoes deformation, initially it reaches just a limited strain since it undergoes the tool action just for a few contours and finally it becomes later node in *I-to-O* toolpath and again undergoes deformation to a limited value of strain and the final value of strain has increased.

Similarly nodes *N2, N3* and *N4* undergo deformation twice, once in *O-to-I* toolpath and second in *I-to-O* toolpath. Therefore, strain values for these node increases as compared to single step deformation.

Node (*N5*) lying very close to the centre of blank, also undergoes deformation and limited value of strain has been reached as can be seen in figure 4.25(b). Therefore, the centre portion of the blank contributes thickness to the corner and side wall of the deformed component and obtain better results for thickness which is not possible in single pass toolpath.

4.7 TOOL REACTION FORCES (*TRF*)

4.7.1 Single pass deformation

4.7.1.1 Tool Reaction forces for Job 14 of Pyramid with *SBS* 75x75 *mm*, *OD*=70 *mm*, α =60°, *TD*=8 *mm*, *h*=20 *mm*, *dz* =0.1 & 0.8 *mm*, t_o =0.8 *mm* and R_c =3.75 *mm*

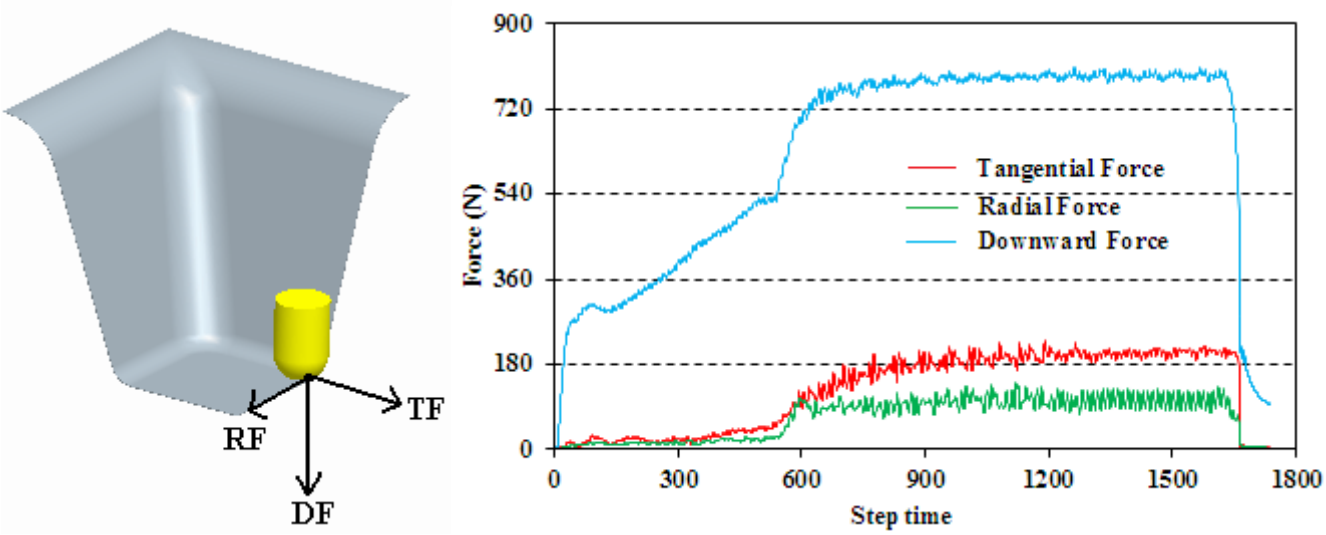

(a) Model to represent direction of Force components **(b)** Graphical representation of *TRF*

Figure 4.26: Graphical representation of Tool reaction forces for Job 14 of Top fillet Pyramid with *SBS* 75x75 *mm*, *OD*=70 *mm*, α =60°, *TD*=8 *mm*, *h*=20 *mm*, *dz* =0.1 & 0.8 *mm*, t_o =0.8 *mm* and R_c =3.75 *mm*

For the part geometry pyramid and single pass toolpath, forces are measured in three directions corresponding to a cylindrical coordinate system. These three force components are Tangential force (*TF*), Radial force (*RF*) and downward force (*DF*) as shown in figure 4.26. The downward force which is along the axis of tool has more importance as compared to other two components of forces because downward force component is responsible for sheet stretching. Therefore magnitude of downward force is more as compared to other two forces. The forming forces are mainly affected by the three process parameters: incremental step size (dz), sheet thickness (t_o) and draw angle (α).

4.7.1.2 Tool Reaction forces for Job 20 for funnel with *SBS* 95x95 *mm*, *OD*=70 *mm*, *max* α =60°, *TD*=8 *mm*, *dz* =0.5 *mm*, t_o =0.88 *mm*

For the part geometry type funnel and single pass toolpath, forces are measured in three directions corresponding to a cylindrical coordinate system. These three force components are Tangential force (*TF*), Radial force (*RF*) and downward force (*DF*) as shown in figure 4.27. For

the geometry type funnel, draw angle (α) changes gradually along the wall of the component. For the present study it increases from 15° to 60° along the component wall, therefore tangential component of force increases with increase in the wall angle as can be seen in the figure 4.27. As a result, change in draw angle has more impact on tangential force rather than the downward force and radial force component.

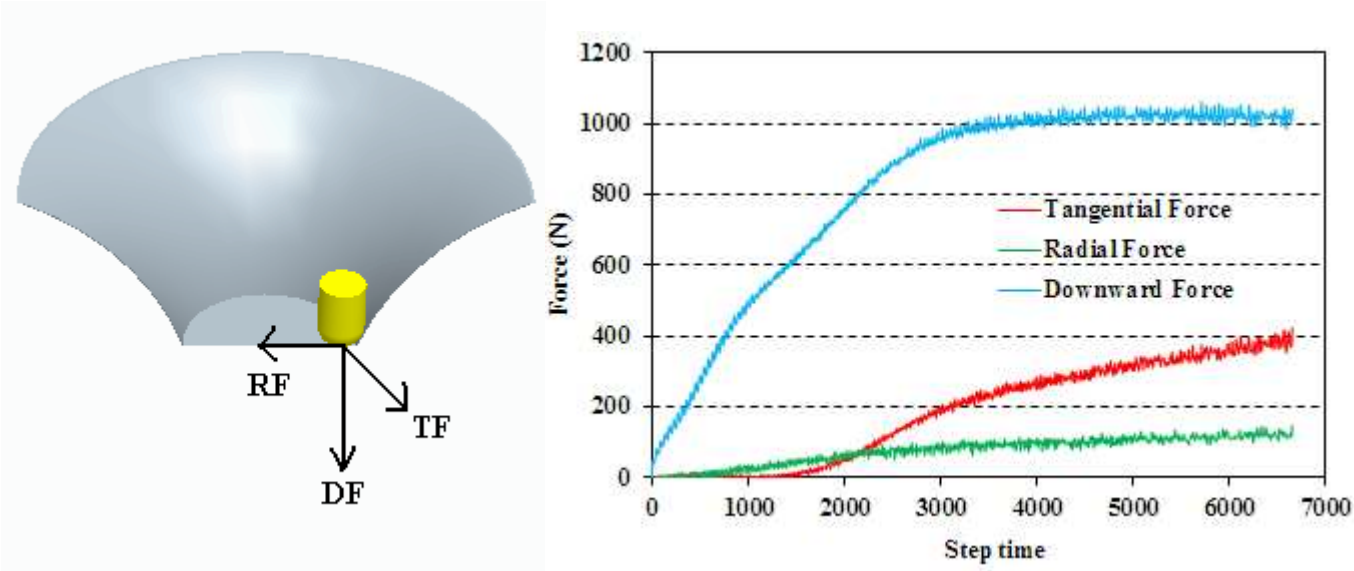

(a) Model to represent direction of Force components **(b)** Graphical representation of *TRF*

Figure 4.27: Graphical representation of Tool reaction forces for Job 20 of funnel with *SBS* 95x95 *mm*, *OD*=70 *mm*, *max* α =60°, *TD*=8 *mm*, dz =0.5 *mm*, t_o =0.88 *mm*

4.7.1.3 Tool Reaction force curves for varying incremental step size for job 20 (funnel with *SBS* 95x95 *mm*, *OD*=70 *mm*, *max* α =60°, *TD*=8 *mm*, dz =0.5 *mm*, t_o =0.88 *mm*) & job 21 (funnel with *SBS* 95x95 *mm*, *OD*=70 *mm*, *max* α =60°, *TD*=8 *mm*, dz =0.2 *mm*, t_o =0.88 *mm*)

Figure 4.28 show results for tool reaction forces for two different vertical step size (dz) 0.5 mm and 0.2 mm. As a result with increase in vertical step size, tool reaction forces increased. Therefore the magnitude of tool reaction forces is directly proportional to the depth of vertical step between two consecutive contours. It can also be noticed that change in vertical step size has more impact on the magnitude of downward force rather than other two components of tool reaction forces.

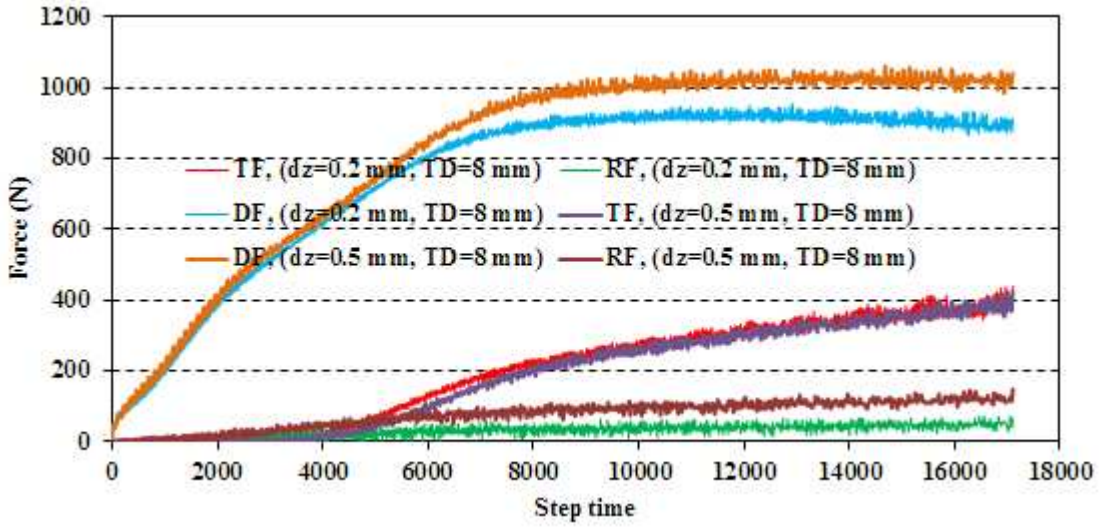

Figure 4.28: Graphical comparison of Tool reaction forces for varying step size for Job 20 (funnel with *SBS* 95x95 mm^2 , *OD*=70 *mm*, *max* α =60°, *TD*=8 *mm*, *dz* =0.5 *mm*, t_o =0.88 *mm*) & job 21 (funnel with *SBS* 95x95 *mm* , *OD*=70 *mm*, *max* α =60°, *TD*=8 *mm*, *dz* =0.2 *mm*, t_o =0.88 *mm*)

4.7.1.4 Tool Reaction force curves for varying Tool diameter for job 20 (funnel with *SBS* 95x95 *mm* , *OD*=70 *mm*, *max* α =60°, *TD*=8 *mm*, *dz* =0.5 *mm*, t_o =0.88 *mm*) & job 22 (funnel with *SBS* 95x95 *mm* , *OD*=70 *mm*, *max* α =60°, *TD*=12.7 *mm*, *dz* =0.5 *mm*, t_o =0.88 *mm*)

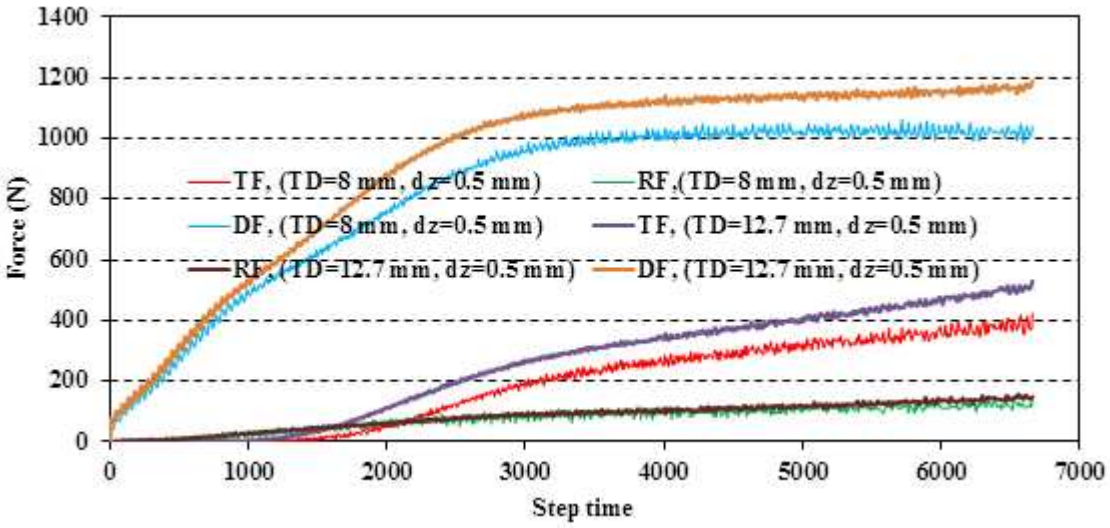

Figure 4.29: Graphical comparison of Tool reaction forces for tool diameter for Job 20 (funnel with *SBS* 95x95 *mm* , *OD*=70 *mm*, *max* α =60°, *TD*=8 *mm*, *dz* =0.5 *mm*, t_o =0.88 *mm*) & job 22 (funnel *SBS* 95x95 *mm* , *OD*=70 *mm*, *max* α =60°, *TD*=12.7 *mm*, *dz* =0.5 *mm*, t_o =0.88 *mm*)

Figure 4.29 show results for tool reaction forces for two different tool diameters (*TD)* 8 mm and 12.7 mm. As a result with increase in tool diameter, tool reaction forces increased. Therefore the magnitude of tool reaction forces is also directly proportional to the tool diameter used. It can also

be noticed that change in tool diameter has more impact on the magnitude of downward force and tangential force and less impact on radial force.

4.7.2 Two pass deformation

4.7.2.1 Tool reaction forces for two-step Cone for Job 19 { Parabola (*O-to-I*) with *SBS* 95x95 *mm*, *OD*=58 *mm*, *Rb*=33 *mm*, *max* α =60°, *TD*=8 *mm*, *h*=24.99 *mm*, *dz* =0.8 *mm*, t_o =0.5 *mm* and R_c =0} and {Cone (*I-to-O*) with *SBS* 95x95 *mm*, *OD*=70 *mm*, α =45°, *TD*=8 *mm*, *h*=25 *mm*, *dz* =0.8 *mm*, t_o =0.5 *mm* and R_c =0}

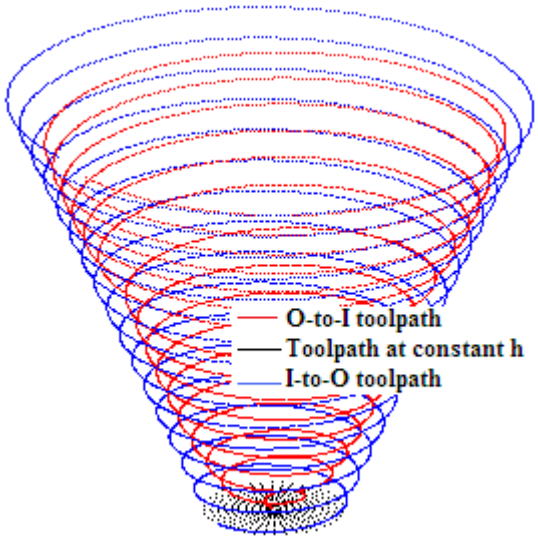

(a) Compensated Toolpath

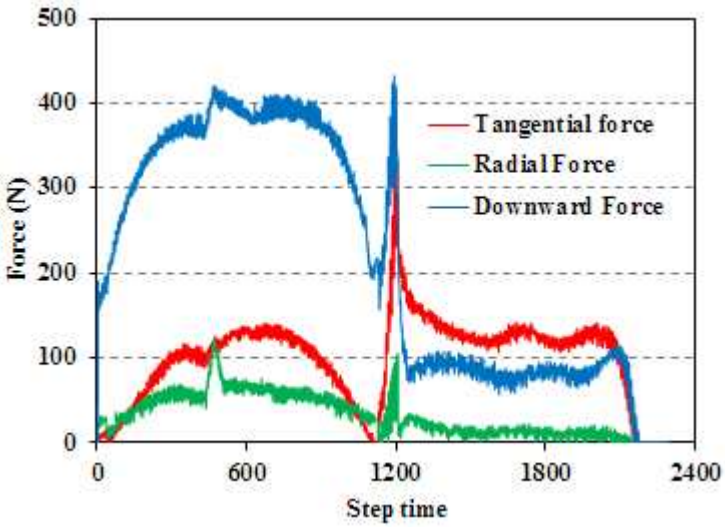

(b) Reaction Forces (RF)

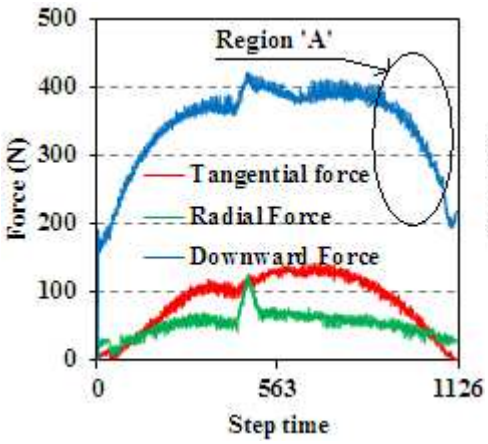

(c) RF for O-to-I toolpath

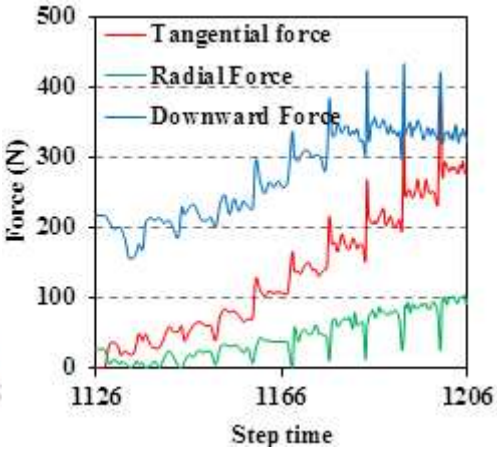

(d) RF for toolpath at constant *h*

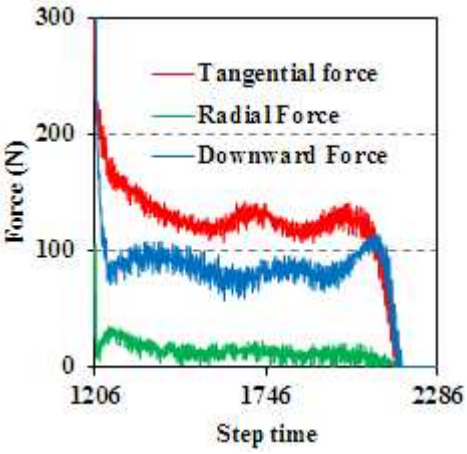

(e) RF for I-to-O toolpath

Figure 4.30: Study of tool reaction forces for two-step Cone for Job 19 { Parabola (*O-to-I*) with *SBS* 95x95 *mm*, *OD*=58 *mm*, *Rb*=33 *mm*, *max* α =60°, *TD*=8 *mm*, *h*=24.99 *mm*, *dz* =0.8 *mm*, t_o =0.5 *mm* and R_c =0} and {Cone (*I-to-O*) with *SBS* 95x95 *mm*, *OD*=70 *mm*, α =45°, *TD*=8 *mm*, *h*=25 *mm*, *dz* =0.8 *mm*, t_o =0.5 *mm* and R_c =0}

For the part geometry cone and two pass toolpath, forces are measured in three directions corresponding to a cylindrical coordinate system. These three force components are Tangential force, Radial force and vertical downward force as shown in figure 4.30(b).

Figure 4.30(c) represents the tool reaction forces for *O-to-I* toolpath having intermediate profile of parabola. Here sheet is more stretched in downward direction, therefore magnitude of downward force is more as compared to other two forces. The draw angle decreases along the parabolic profile, therefore magnitude of downward force also decreased as shown in region '*A*' of figure 4.30(c).

Figure 4.30(d) represents the tool reaction forces for toolpath at constant height. Here magnitude of tangential and downward force increases due to sheet is pushed in both tangential and vertical downward direction simultaneously.

Figure 4.30(e) represents the tool reaction forces for *I-to-O* toolpath having outer profile of cone. Here sheet is more pushed in tangential direction rather than downward direction. Therefore magnitude of tangential force is more as compared to magnitude of downward force for *I-to-O* toolpath as shown in figure 4.30(e).

Table 15: Further study for the influence of process parameters on tool reaction forces

S. No.	Geometry type	dz (mm)	t_o (mm)	α	Force Component	Graphical Comparison	Conclusion
1	Pyramid	0.8	0.5	45°	Tangential Force	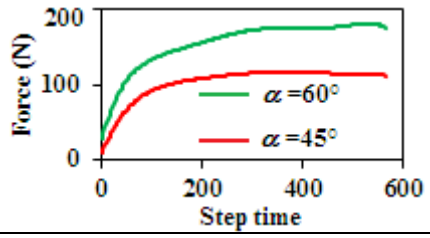	Tangential force increase with increase in the draw angle.
	Pyramid	0.8	0.5	60°			
2	Pyramid	0.2	0.5	60°	Downward Force	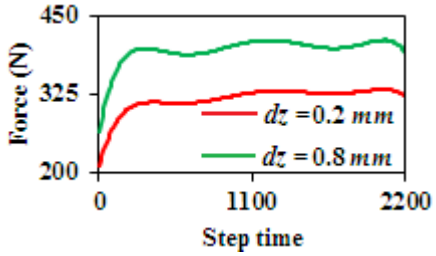	Downward force increase with increase in the step size.
	Pyramid	0.8	0.5	60°			
3	Pyramid	0.8	0.5	60°	Downward Force	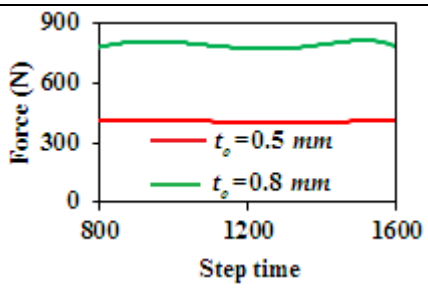	Downward force increase with increase in the sheet thickness.
	Pyramid	0.8	0.8	60°			

CHAPTER 5
CONCLUSION AND FUTURE SCOPE

5.1 CONCLUSION

It has been observed that incremental sheet metal forming process is a very promising manufacturing process which still requires further optimization. The dimensional accuracy and geometrical errors in the single point incremental forming process is discussed and analyzed by using FEA techniques and highlighting very relevant discrepancies between the designed geometry and obtained ones.

1. The effect of back up size irrespective to sheet bending at the major base of component has been studied. The equation for horizontal and vertical bending is derived analytically.
2. Use top fillet irrespective of the backup plate size to reduce bending and higher indentation at major base of component. Higher indentation occurs due to the tool compensation. But by giving some fillet at major base of component, draw angle increases gradually from zero to required geometry angle and indentation can be controlled.
3. After giving tool compensation, the inaccurate results about the height of the component are obtained. To reduce over travel of the tool, the height compensation is used.
4. Two-step deformation strategy has been proposed and it was found to be an effective method of avoiding excessive thinning in specific areas like corner of the deformed component. With single step deformation strategy, central portion of the blank remains undeformed but this is not happen with two-step deformation strategy and there is some thickness distribution from central portion to the corner and side walls of the deformed object. Therefore better results for homogenous thickness distribution along the side walls and corners can be achieved.
5. It is observed that strain paths are characterized by a typical step-trend and each strain increment is directly due to the action of the tool as it passes the particular node. There is no strain increment occurs, when the tool continues its path along the same contour far away from the particular node. This confirms the localized deformation that characterizes single point incremental forming process. With increase in the value of draw angle, equivalent strain will increase and sheet thickness will decrease.
6. Tool reaction forces are measured in 3 directions for single pass and two pass deformation strategy. It was observed that when tool motion from O-to-I profile, then impact of downward force is more as compared to other two forces while tool motion from I-to-O profile, then tangential force has more impact. The influence of incremental step size, draw angle, tool

diameter and sheet thickness on the tool reaction forces has been studied. With increasing any one of the above parameters, will increase the tool reaction force components.

5.2 SCOPE OF FUTURE WORK

1. To reduce the occurrence of stepped feature at the base of the final deformed component in two-step deformation strategy is in the future scope.
2. The effect of Local spring back and global spring back were not taken into consideration in dimensional and geometric accuracy of final deformed component. However, the proposed model can be further enhanced to include these limitations.
3. Analytical prediction of sheet thickness, tool reaction forces, equivalent stress and equivalent plastic strain to reduce computational cost and time is also in the future scope.

REFERENCES

1. Jeswiet.J, F. Micari.F, Hirt.G, Bramley.A, Duflou.J, Allwood.J, (2005), Asymmetric single point Incremental Forming of sheet metal, CIRP Annals- Manufacturing Technology, Volume 54, page 88-114.
2. http://www.custompartnet.com/wu/sheet-metal-forming
3. www.mech.northwestern.edu/ampl/index.html
4. Ham.M, Jeswiet.J, (2008), Dimensional accuracy of single point Incremental Forming, International Journal of material forming, Volume 1, page 1171-1174.
5. Verbert.J, Belkassem.B, Henrard.C, Habraken.A.M, Gu.J, Sol.H, Lauwers.B, Duflou.J.R, (2008), Multi step toolpath approach to overcome forming limitations in single point incremental forming, International Journal of material forming, Volume 1, page 1203-1206.
6. Skjoedt.M, Bay.N, Endelt.B, Ingarao.G, (2008), Multi stage strategies for single point incremental forming of a cup, International Journal of material forming, Volume 1, page 1199-1202.
7. Bhattacharya.A, Malhotra.R, Kumar.A, Reddy.N.V, Cao.J, (2011), A new methodology for multi-pass single point incremental forming with mixed toolpaths, CIRP Annals-Manufacturing Technology, Volume 60, page 323-326.
8. Bambach.M, (2010), A geometrical model of the kinematics of incremental sheet forming for the prediction of membrane strains and sheet thickness, Journal of materials processing technology, Volume 210, page 1562-1573.
9. Durante.M, Formisano.A, Langella.A, Minutolo.M.C, (2009), The influence of tool rotation on an incremental forming process, Journal of materials processing technology, Volume 209, Issue 9, page 4621-4626.
10. Silva.M,B, Skjoedt.M, Atkins.A.G, Bay.N, Martins.P.A.F, (2008), Single point Incremental Forming and formability failure diagrams, Journal of Strain Analysis for Engineering design, Volume 43, page 15-35.
11. Ambrogio.G, Filice.L, Gagliardi.F, Micari.F, (2005), Sheet thinning prediction in single point Incremental Forming, Journal of Advanced materials research, Volume 6-8, page 479-486.
12. Ambrogio.G, Costantino.I, Napoli.L.De, Filice.L, Fratini.L, Muzzupappaa.M, (2004), Influence of some relevant process parameters on the dimensional accuracy in incremental forming, Journal of materials Processing Technology, Volume 153-154,

page 501-507.

13. Young.D, Jeswiet.J, (2004), Wall thickness variations in single-point incremental forming, Journal of Engineering Manufacture, Volume 218, page 1453-1459.
14. Taleb Araghi.B, Manco.G.L, Bambach.M, Hirt.G, (2009), Investigation into a new hybrid forming process: Incremental sheet forming combined with stretch forming, CIRP Annals- Manufacturing Technology, Volume 58, page 225-228.
15. Cerro, Maidagan.E, Arana.J, Riveroa.A, Rodrıguez.P.P, (2006), Theoretical and experimental analysis of the dieless incremental sheet forming process, Journal of materials processing technology, Volume 177, page 404-408.
16. Micari.F, Ambrogio.G, Filice.L, (2007), Shape and dimensional accuracy in Single Point Incremental Forming: State of the art and future trends, Journal of materials processing technology, Volume 191, page 390-395.
17. http://www.lcmp.eng.cam.ac.uk/wellformed/incremental-sheet-forming.
18. Duflou.J.R, Verbert.J, Belkassem.B, Gu.J,Sol.H, HenrardC, Habraken.A.M (2008), Process window enhancement for single point incremental forming through multi-step toolpaths, CIRP Annals- Manufacturing Technology, Volume 57, page 253-256.
19. Ambrogio.G, Filice.L, Napoli.L.De, Muzzupappaa.M, (2005), A simple approach for reducing profile diverting in a single point incremental forming process, Journal of Engineering manufacturing (Part B), Volume 219, page 823-830.
20. Ambrogio.G, Filice.L, Micari.F, (2006), A force measuring based strategy for failure prevention in incremental forming, Journal of materials Processing Technology, Volume 177, page 413-416.
21. Ambrogio.G, Cozza.V, Filice.L, Micari.F, (2007), An analytical model for improving precision in single point incremental forming, Journal of materials Processing Technology, Volume 191, page 92-95.
22. Filice.L, Fratini.L, Micari.F, (2002), Analysis of Material formability in incremental forming, CIRP Annals- Manufacturing Technology, Volume 51, page 199-202.
23. Filice.L, (2006), A phenomenology-based approach for modeling Material thinning and formability in incremental forming of cylindrical parts, Journal of Engineering manufacturing (Part B), Volume 220, page 1449-1455.
24. Henrard.C, Habraken.A.M, Szekeres.A, Duflou.J.R, He.S, Van Bael.A, Van Houtte.P (2005), Comparison of FEM Simulations for the Incremental Forming Process, Journal of Advanced materials research, Volume 6-8, page 533-542.
25. Kim.Y.H, Park.J.J, (2002), Effect of process parameters on formability in incremental

forming of sheet metal, Journal of materials Processing Technology, Volume 130-131, page 42-46.

26. Hirt.G, Ames.J, Bambach.M, Kopp.R, (2004), Forming strategies and Process modeling for CNC incremental sheet forming, CIRP Annals- Manufacturing Technology, Volume 53, page 203-206.

27. Park.Jong-Jin, Kim.Yung-Ho, (2003), Fundamental studies on the incremental sheet metal forming technique, Journal of materials Processing Technology, Volume 140, page 447-453.